DEVELOPING A CELL-LIKE SUBSTRATE TO INVESTIGATE THE MECHANOSENSITIVITY OF CELL-TO-CELL JUNCTIONS

by

Kent D. Shilts

A Dissertation

Submitted to the Faculty of Purdue University

In Partial Fulfillment of the Requirements for the degree of

Doctor of Philosophy

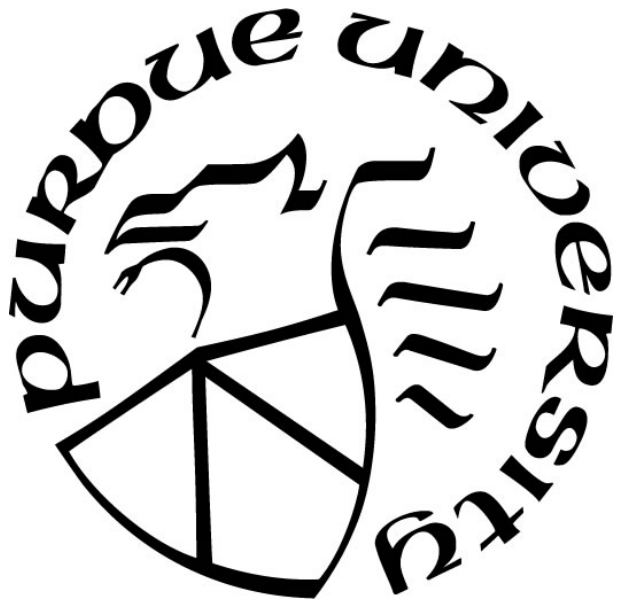

Department of Chemistry and Chemical Biology at IUPUI

Indianapolis, Indiana

August 2020

THE PURDUE UNIVERSITY GRADUATE SCHOOL
STATEMENT OF COMMITTEE APPROVAL

Dr. Christoph Naumann, Chair

Department of Chemistry and Chemical Biology

Dr. Eric C. Long

Department of Chemistry and Chemical Biology

Dr. Chien-Chi Lin

Department of Biomedical Engineering

Dr. Frédérique Deiss

Department of Chemistry and Chemical Biology

Approved by:

Dr. Eric C. Long

ACKNOWLEDGMENTS

This cumulative work has been a long journey in the making, and as it comes to a close, I want to bring recognition to those who I benefitted greatly from working and living alongside. First, thank you Christoph for seeing me through, being a guide, teacher, boss, and scholar. I have learned about biophysics, biomaterials, artificial lipid membranes, and I hope my work adds an interesting subset of materials made in the Naumann group. Next, I would like to thank Yifan Ge, colleague and friend, for her continued efforts to show me how to do FCS, run the microscopes, and be a scientist who works consistently and achieves many things. To Corey Lin, I thank you for your efforts in showing me how to fabricate artificial lipid membranes by LB/LS and vesicle methods.

To former members of the Naumann lab Amanda Siegel and Dan Minner, I owe you both greatly and I appreciated your continued efforts in science and scholarship. Amanda, thank you for the many lunch time talks, for sharing your thoughts, and for caring about how I was doing. Dan, you are a very helpful person, creative and fun, your energy was greatly appreciated, and I know things went more smoothly in the lab because of your continued efforts. Kridnut Chuduang, Krit, thanks for being a companion in the final stretch of my work, best of luck and carry on the research with joy. Partha Basu, chair of the Chemistry and Chemical Biology Department, I thank you for looking out for me and supporting me in several ways that I greatly benefitted from.

To friends and colleagues that made life at IUPUI much better, thank you. Mark Woollam, you are a great friend and an inspiration in work ethic. Alex Latta, thanks for sharing graduate school experiences and the many talks in the hallway. I also want to thank the high school students and undergraduate students who spent time doing research in the Naumann lab, these experiences benefitted me and always gave me energy to keep going.

Finally, I want to thank the people that surrounded me, encouraged me, and loved me through my life, and certainly this graduate school adventure. To all who supported Emily and I through these years, thank you and we love and appreciate you. To my family, we all share in the accomplishments of one another because our achievements are tied to all of us, much love to Mom and Dad, Papo, Mamo, Mema, Pepa, and the rest of my beautiful, crazy family. To my wife, Emily, you give me such great energy and encouragement, I would not be the person I am today with out

you. Thank you for believing in me and pushing me to reach my potential, I love you. I dedicate this work to Jesus Christ, who came to serve and to give his life as a ransom for many (Matthew 20:28), teach me to serve and love.

TABLE OF CONTENTS

LIST OF FIGURES

LIST OF TABLES

LIST OF ABBREVIATIONS

AFM	Atomic force microscopy
APS	Ammonium persulfate
ATCS	Allyltrichlorosilane
Biotin-PE	1,2-dioleoyl-sn-glycero-3-phosphoethanolamine-N-biotinyl Na+ salt
CDF	Cumulative Distribution Function
D	Diffusion coefficient
DGS-NTA	1,2-dioleoyl-sn-glycero-3-[(N-(5-amino-1-carboxypentyl)iminodiacetic acid)succinyl] Ni2+ salt
DMEM	Dulbecco's Modification of Eagle's Media
DOPC	1,2-dioleoyl-sn-glycero-3-phosphocholine
DPTE	1,2-dipalmitoyl-sn-glycero-3-phosphothioethanol Na+ salt
E	Young's modulus
ECM	Extracellular matrix
EDC	1-Ethyl-3-(3-dimethylaminopropyl)carbodiimide
ERK	Extracellular signal-related kinase
FA	Focal adhesion
FCS	Fluorescence correlation spectroscopy
FN	Fibronectin
FRAP	Fluorescence recovery after photobleaching
G'	Elastic modulus
G''	Viscous modulus
GUV	Giant Unilamellar vesicle
LB	Langmuir-Blodgett
LS	Langmuir Schaeffer
LSCM	Laser scanning confocal microscope
MTFM	Molecular tension force microscopy
NBD-PE	(N-(7-nitrobenz-2-oxa-1,3-diazol-4-yl)-1,2-dihexadecanoyl-sn-glycero-3-phosphoethanolamine, triethylammonium salt
NHS	N-hydroxysuccinimide
PBS	Phosphate buffer solution
PEG	Polyethyleneglycol
POPC	1-palmitoyl-2-oleoyl-sn-glycero-3-phosphocholine
PTLB	Polymer-tethered lipid bilayer
RGD	Arginine-glycine-aspartic acid peptide sequence
r_m	Measured bleach radius
r_u	User defined bleach radius
SDS	Sodium dodecyl sulfate
SEM	Scanning electron microscopy
SFA	Surface forces apparatus
SLB	Supported lipid bilayer

SMFM	Single molecule fluorescence microscopy
sulfo-GMBS	N-(γ-maleimidobutyryloxy)sulfosuccinimide ester
sulfo-NHS-LC-biotin	Sulfosuccinimidyl-6-[biotin-amido]hexanoate
sulfo-SANPAH	Sulfosuccinimidyl-6-[4'-azido-2'-nitrophenylamino]hexanoate
SUV	Small Unilamellar vesicle
$t_{1/2}$	One-half recovery time
TEMED	Tetramethylethylenediamine
TRITC-DHPE	(N-(6-tetramethylrhodaminethiocarbamoyl)-1,2-dihexadecanoyl-sn-glycero-3-phosphoethanolamine, triethylammonium salt
VF	Vesicle fusion
w	Bleaching spot radius

ABSTRACT

The role of mechanical forces in the fate and function of adherent cells has been revealed to be a pivotal factor in understanding cell biology. Cells require certain physical cues to be present in their microenvironment or the cell will begin apoptosis. Mechanical signals from the environment are interpreted at the cellular level and biochemical responses are made due to the information from outside the cell, this process is known as mechanotransduction. Misinterpretation of physical cues has been indicated in many disease states, including heart disease and asthma. When a cell is bound to the ECM, proteins such as integrins are engaged at static and stable adhesion sites. These tight and static anchoring points found at the ECM exist in stark contrast to the dynamic conditions seen at intercellular junctions. Intercellular junctions, such as gap and adherens junctions, are formed between cells to act as a mechanism to relay information and exchange material. Due to the important role intercellular junctions play in processes of wound healing, epithelial-mesenchymal transition and cancer metastasis developing more sophisticated levels of understanding of these mechanisms would provide valuable insight.

Complex biological processes, including immune cell signaling and cellular ECM adhesions, have been effectively replicated in model systems. These model systems have included the use of solid supported lipid bilayers and polymeric hydrogels that display cell adhesion molecules. Studies of cellular mechanotransduction at ECM adhesion sites has also been completed with covalently functionalized polymeric substrates of adjustable elasticity. However, developing model systems that allow the accurate reproduction of properties seen at intercellular junctions, while also allowing the investigation of cellular mechanosensitivity has proven to be a difficult task. Previous work has shown that polymer-tethered lipid bilayers (PTLBs) are a viable material to allow the replication of the dynamics and adhesion seen at intercellular junctions. Although efforts have been made to produce PTLBs with different mechanical properties, there is currently not a material with sufficient tunable elastic properties for the study of cellular mechanotransduction.

To establish a system that allows the study of stiffness effects across a biologically relevant range (~0.50 – 40 kPa) while maintaining the dynamic properties seen at cell-to-cell junctions, polymer gel-tethered bilayers (PGTBs) were developed. A fabrication strategy was established to allow the incorporation of a hydrogel support with easily tunable stiffness and a tethered lipid

bilayer coating, which produced a powerful platform to study the effects of stiffness at intercellular junctions. Careful attention was given to maintain the beneficial properties of membrane diffusion, and it was shown that on different linking architectures lipid bilayers could be established and diffusion was preserved. Microscopy-based FCS and FRAP methodology were utilized to measure lipid diffusion in these systems, while confocal microscopy was used to analyze cell spreading and adhesion. Three distinct architectures to link the lipid membrane to the underlying polyacrylamide hydrogel were pursued in this work, a non-covalent biotin-streptavidin system, a covalently linked design with fibronectin, and a direct covalent linkage utilizing crosslinker chemistry. In this work, it was shown that cells were able to spread and adhere on these substrates, with cell adhesion zones visualized under plated cells that demonstrate the capability of the cell to rearrange the presented linkers, while maintaining a stable material. Also confirmed is the tunability of the polymer hydrogel across a wide range of stiffness, this was shown by quantitative changes in cell spreading area in response to polymer properties.

CHAPTER 1. INTRODUCTION

1.1 Rationale

Adherent cells are able to sense and react to the mechanical properties of their local environment, even to the point of stem cell differentiation being directed based on the elasticity of the environment [1]. Due to the critical nature of the mechanics of the environment, much effort has gone into understanding the cellular processes and mechanisms that allow cells to interpret their environment. Adherent cells, such as epithelial, muscle, or bone cells, have the machinery to probe their local environment and the mechanical information is interpreted at the cell level in a process called mechanotransduction. When the signals from the mechanical information have been interpreted and biochemical processes have been adjusted there is a cellular response, which leads to global cell changes, such as apoptosis. Issues with mechanotransduction have been identified in many disease states, including cancer metastasis, wound healing, epithelial-mesenchymal transition.

In the field of mechanobiology, much progress has been made in identifying the myriad of components and proteins and signaling cascades involved in mechanotransduction; however, where there remain open questions is in regard to how these larger processes work together to direct cellular fate and function. Regarding mechanotransduction, two distinct situations are seen at the cellular level, one being cell adhesions to extracellular matrix and the second being cell-to-cell adhesions. When a cell makes a connection to an extracellular protein, such as laminin or fibronectin, the formed adhesion is static and unmoving. If the cell pulls harder at an established adhesion, the adhesion will grow, but will not move as the cell migrates.

The situation at extracellular matrix junctions is in sharp contrast to cell-to-cell adhesions, called adherens junctions, where adherens junctions are known to move the entire length of the cell. Specific patterns of adherens junction movement have even been identified, which exemplifies the dynamic and active nature of these junctions. The process of wound healing is a prime example to highlight the significance of intercellular junctions. When a tissue is wounded, cells are damaged and release their contents into the extracellular space, these signals that a wound has occurred travel quickly through intercellular junctions, called gap junctions. At gap junctions, information is exchanged between cells, including electrical impulses, signaling molecules, and

ions. Because of the specialized connections made between cells, information is transferred much more quickly than simple Brownian diffusion would allow signaling to occur. For wound healing, understanding the underlying mechanisms will allow more effective regeneration and restoration of tissues, especially significant when healing does not progress normally, such as in scarring or in patients with diabetes [2].

Due to the important and broad ranging effects of mechanical stimuli, many model systems have been developed to allow researchers to gain an improved understanding of mechanotransduction. Starting with the classical materials used for cell culture, which are glass and plastic, these materials have long been identified as providing an environment for cells that is much different from what is found at the tissue level, meaning these materials are not well suited for studying the effects of mechanotransduction. Beyond these classical materials, advanced model systems have been pursued. For the case of cellular connections to the extracellular matrix, much progress has been made with the use of polymeric substrates of adjustable stiffness. In these effective models, stiffness of the underlying polymer was manipulated, and specific cell adhesion proteins were covalently linked and presented for cell adhesion [3, 4]. Within this category, 2D and 3D models have been designed that revealed cellular response to environmental properties, such as morphology of the substrate, roughness, and elasticity [3, 5, 6].

Although sufficient progress has been made in developing model systems that lead to greater understanding of the mechanical implications at cell-extracellular matrix connections, there remains a need for the development of materials to model the adherens junction. In the current work, an advanced cell substrate material that is capable of replicating the dynamics and activity seen at adherens junctions will be shown. Building on the foundational work done to push the application of supported membranes for use as cell substrates [7-9], the current work revolves around the design, fabrication, and application of cell-surface like materials for use as a cell substrate. With the use of supported membrane materials, many critical properties of the plasma membrane are replicated in these model systems. Beginning with solid supported membranes, well suited for cells that do not generate large traction forces, such as immune cells, much has been learned about how immune cells interpret their environments using this platform [10-13]. In a distinct advancement, polymer-tethered lipid bilayers (PTLBs), developed through the 1990s and 2000s, have been shown to be a promising platform for adherent cell studies [14, 7-9].

Polymer-tethered lipid bilayers, originally developed with the main goal of lifting up the bilayer to allow improved transmembrane reconstitution [14, 15], have very interesting diffusion properties that allow these substrates to be used for the study of adherent cellular processes [16]. In PTLBs, lipid diffusion was observed to fit a model of obstructed diffusion, this is due to the presence of lipopolymers, which act as diffusion obstacles [16]. Early work done by Deverall et al. established the size dependent diffusion characteristics, where larger species diffuse more slowly laterally across the membrane [16]. Future work to establish PTLBs as an advanced cell-surface mimetic, began by plating cells on multi-bilayer stacks functionalized with cell adhesion molecules, with increased stacking cell morphology and migration were shown to modulate cell behavior [8]. Mechanical properties of the PTLB substrate were tuned by using the stacking strategy [7], but problems with correlating how the cell generated forces were transduced through this material and a limited range of elastic properties led to the further development of membrane coated materials.

Recognizing the limitations of previously developed PTLB systems, the development of tethered lipid bilayers on a hydrogel support was hypothesized to overcome these shortcomings and be a robust substrate for the analysis of cellular mechanoresponse. The development of polymer hydrogel tethered bilayers, herein referred to as PGTB, will be described in this dissertation. The research presented in the dissertation accomplishes the following objectives:

Objective One: Cell-surface like materials were designed and fabricated, specifically polymer gel-tethered bilayers.

Objective Two: Analysis of the lipid membrane coated polymer hydrogel, including: mechanical properties, protein linking, lipid membrane coverage and lipid diffusion

Objective Three: Application of the PGTB cell-like materials to study cellular adhesion and spreading

1.2 Organization

This dissertation is organized into five chapters. The first chapter describes the overall rationale, significance, and key objectives of the study and presents the organization of the

document. The second chapter describes various methods and instrumentation used to complete this research. Also presented in the second chapter are introductions to relevant topics such as polymer hydrogels, cell biology, and the previous use of artificial substrates for adherent cells. The third chapter in this document contains the materials and procedures used to produce PGTBs and analyze their properties. In chapter four the results and discussion of the development of PGTBs, describing the properties of the materials produced. In the final chapter, a summary of the key conclusions put forth by this study will be presented.

CHAPTER 2. BACKGROUND

2.1 Methodology

2.1.1 Langmuir Films

A Langmuir film is a layer of insoluble molecules organized at the surface of a subphase liquid. This layer of molecules is normally deposited in a solvent that evaporates, leaving the amphiphilic molecules covering the entire available surface area. For over one-hundred years, a trough type apparatus have been used by scientists to investigate surface phenomenon [17]. In the antecedent prototypes, which are not all that different from modern setups, used a container to hold a reservoir of liquid, a sensor and balance to measure changes in surface tension and barriers to increase and decrease surface area available to the monolayer film on the surface. One of the first scientists to develop and use a trough was Agnes Pockels and in 1891 a letter of hers was published in Nature, submitted by Lord Rayleigh, that described experiments she had completed and data collected related to surface science [17]. Building upon this work, Irving Langmuir developed the trough design and discovered surface phenomenon related to properties of adsorbed films. Langmuir received a Nobel Prize in 1932, and the name of the trough became synonymous with Langmuir [18].

2.1.2 Langmuir-Blodgett & Langmuir-Schaefer Depositions

Spreading a monolayer film of molecules on the surface of an immiscible liquid can be utilized in transfers to solid substrates forming a monolayer on the solid, assuming a positive interaction between the solid and amphiphilic molecule. In 1935, Katharine Blodgett developed a method to transfer material from a Langmuir trough to a glass coverslip [19]. With her setup a vertical transfer of calcium stearate was completed and successive transfers could be completed to form a multi-layered material of over 200 layers in her study [19]. The work of Blodgett done in conjunction with Langmuir resulted in this method of vertical dipping being named Langmuir-Blodgett.

The use of Langmuir-Blodgett (LB) transfers is particularly practical for the transfer of a monolayer of lipids to a glass substrate. Using a trough and transfer techniques, Langmuir films

can be used to form asymmetric bilayers where the inner and outer leaflet have different lipid compositions, which is stable due to the very low rate of lipid flip-flop from leaflet to leaflet [15, 20]. When lipids in solvent are placed on the surface of an aqueous subphase, the lipids align with the hydrophilic head groups toward the subphase and the hydrophobic tails at a steep angle away from the subphase liquid. During a Langmuir-Blodgett transfer the lipids maintain this orientation and are transferred to a glass substrate, constant surface pressure is maintained during the transfer by moving a barrier to decrease the area available to the lipids, depicted in Fig 1.

One method to fabricate a bilayer is to use a LB deposition followed by a Langmuir-Schaefer (LS) transfer, this leaflet-by-leaflet approach allows asymmetric lipid composition in the bilayer and produces stable, defect free lipid bilayers. Developed by Langmuir and Schaefer, the LS transfer was first reported in 1938 and has been used in various ways since introduction to transfer a monolayer of molecules from a Langmuir trough to a solid substrate [21]. Once a monolayer of lipids are transferred by LB deposition, a second monolayer can be spread on the Langmuir trough, compressed and then the LB monolayer is horizontally pressed through the lipids spread on the trough to form a bilayer, this process is shown in Fig 1.

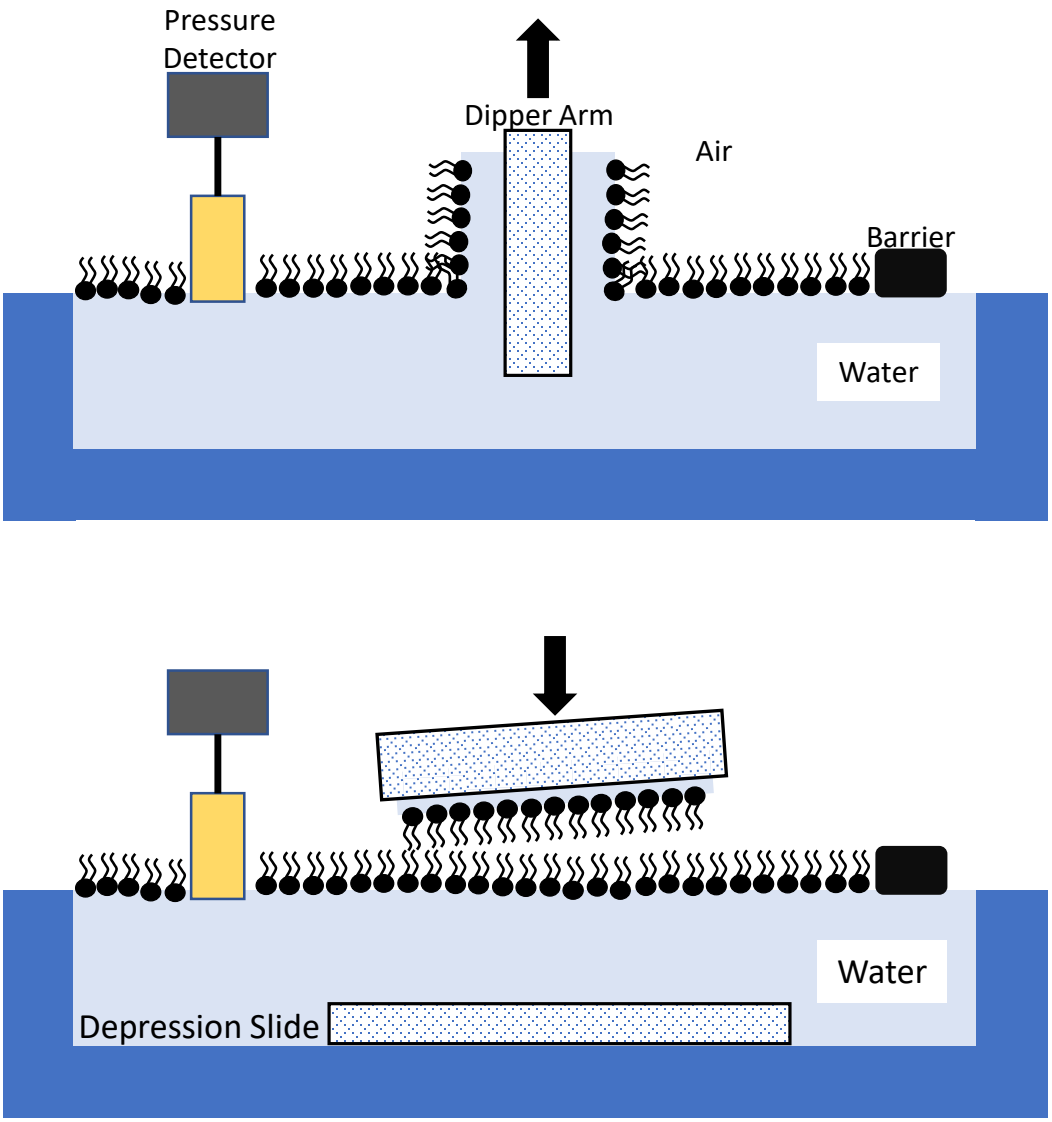

Figure 1. Langmuir-Blodgett and Langmuir-Schaeffer transfer methods done in a trough.

2.1.3 Small Unilamellar Vesicle (SUV) Formation

An alternative method for the formation of planar supported lipid bilayer is the use of lipids suspended in aqueous media that can be deposited on a solid support. When a dry lipid film is placed into aqueous solution, the lipids spontaneously form a spherical shape in a bilayer formation, this shape is also called a vesicle. This assembly of lipids is normally multi-shelled, meaning many spheres are packed into one another, like a set of Russian nesting dolls that stack one inside another. Unilamellar or single shelled vesicles are normally used to form solid supported bilayers with a

decreased amount of defects and better coverage of the solid surface versus the multi-lamellar structures. To synthesize small unilamellar vesicles (SUVs), normally in the size range of 30-50 nm in diameter, sonication is used to prepare these highly curved and high surface tension structures.

2.1.4 Epifluorescence Microscopy (EPI)

One of the most common fluorescent microscope setups utilizes a dichroic mirror that allows the excitation and emission light to pass through the same objective, with the excitation light sent to the sample and emitted light sent to a detector. A dichroic mirror is made of a material that is designed to reflect light of shorter wavelengths, below a certain threshold that is material dependent, and transmit light that is longer than the threshold wavelength. This wide-field microscopy technique, typically uses a mercury discharge lamp as the source of excitation light. Epifluorescence microscopes are commonly used for biological imaging and can be equipped with powerful cameras to record images that are output to a computer workstation. The microscope used in this research was also equipped to do Fluorescence Correlation Spectroscopy (FCS) and the side-by-side setup is shown in Fig 2.

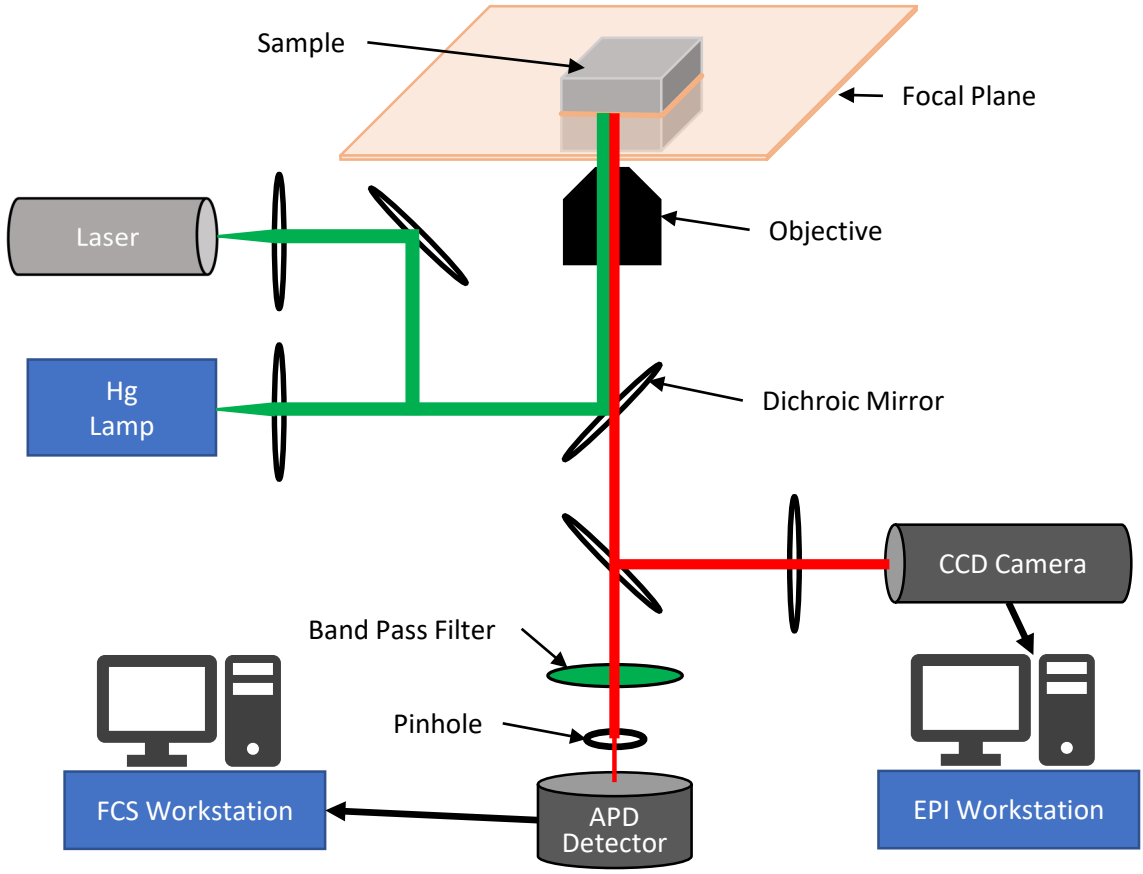

Figure 2. The combined FCS and EPI microscope setup

2.1.5 Fluorescence Correlation Spectroscopy (FCS)

FCS is a type of fluctuation analysis where light is focused into the sample and changes in fluorescent intensity are measured over time. One of the basic conditions that must be satisfied for successful measurements in FCS is the ability to limit the measurement volume to a very small size and to maintain a low concentration of fluorescent analytes [22-24]. The underlying principle is that the small detection volume, where fluorescent emission can be measured, contains either zero or very few fluorescent molecules, which produces large changes in fluorescent intensity signal. These large changes in fluorescent signal are associated with the diffusion characteristics of the analyte and when done with a statistically significant large data set the fluctuation signal can be used to calculate a diffusion coefficient. For the accurate analysis of diffusion in a sample using FCS there are several factors that should be considered: stable laser light source, high

numerical aperture objective, sensitive detectors to amplify photons measured, and computational power to perform autocorrelation and other types of analysis to the data sets.

The fluctuation data that is collected during an FCS analysis is mathematically manipulated to fit an autocorrelation analysis which reveals a characteristic diffusion time. The diffusion time, $\tau_{D,}$ represents the amount of time a fluorescent species spends in the confocal volume, if the size of the confocal volume, $\omega_{0,}$ is accurately known, then determination of the diffusion coefficient can be obtained. The following equation is used by the Zeiss Confocor2 system to determine the number of particles, N, and the characteristic diffusion time from the obtained fluctuation spectra [25]:

$$G(t) = 1 + \frac{1}{N_{avg}}\left(\frac{1}{1+{}^{\tau}/_{\tau_D}}\right)\left(\frac{1}{\sqrt{1+\left({}^{1}/_{Q^2}\right)\left({}^{\tau}/_{\tau_D}\right)}}\right) \qquad \text{Eq. 2.1}$$

Determinations of quantitative diffusion coefficients were also done with the diffusion time determined by FCS measurements. For this determination of D, an established method of high accuracy, wide-field single molecule fluorescence microscopy, was used to measure the diffusion coefficient of PTLB systems and then data was correct with what was measured at the FCS in the same systems. This method of data analysis was pursued by Hussain et al. and appears to be a highly accurate way to determine the diffusion coefficient from FCS data [15].

In the side-by-side epifluorescence imaging and FCS setup, the FCS has dedicated laser line excitation sources that lead to the body of the microscope through a specialized port. The module connected to the body of the standard microscope allows all the laser lines to be routed via glass fiber optic cable with two independent channels each with separate motorized pinholes and avalanche photodiodes. The light path and distinct features of the FCS are shown in Figure 2.

2.1.6 Confocal Laser Scanning Microscopy

The advantages of Laser Scanning Confocal Microscopy (LSCM) are reduction in background glare, a shallow XY plane of focus, and the ability to render three-dimensional images of thick samples. The operation of most modern confocal microscopes allows easy acquisition of high-quality images, normally applied to biological imaging. The light path of a confocal microscope utilizes laser excitation sources, a dichroic mirror, pinhole to reject out of focus light

and a photomultiplier tube to amplify the detected signal, details. In a standard confocal microscope, the light source is focused into a small beam that is scanned across the sample creating a raster image, whereas a widefield microscope system would shine light across the entire sample area at once. Due to using a focused beam of light, image resolution is highly improved and out-of-focus light is drastically reduced. LSCM also provides improved images from samples with multiple colors of fluorescent labels by using multiple photomultiplier tubes. An additional feature of LSCM is the ability to capture XY cross-section images that can be combined to produce three-dimensional images of thick samples.

2.1.7 Fluorescence Recovery After Photobleaching (FRAP)

FRAP is a convenient and accessible technique that allows the measurement of diffusion in a system. Like FCS, the data obtained from an experiment using FRAP can be used to determine the diffusion coefficient, D, n order to perform FRAP, the fluorescent dye molecules must be photolabile, meaning that after a certain number of cycles of fluorescence the fluorophore will permanently be unable to fluoresce caused by degradation of the dye molecule. For organic dye molecules, photobleaching is a fundamental property that all molecules will experience, but the number of cycles that can be completed is different based on each molecule's specific chemistry (e.g. fluorescein will photobleach more quickly than rhodamine). Due to the prevalence of confocal imaging systems, many researchers have the availability of FRAP, whereas other techniques, such as single-particle tracking and FCS, require specialized equipment, expertise to acquire data, and are not available to many researchers.

The data collection for FRAP occurs in three distinct phases, initial phase is to record an image containing the region where a small bleaching spot will be made, then a strong pulse of light is directed to a user specified region, after bleaching the final phase is to collect images showing the recovery and gradual increase of fluorescent intensity. Current LSCM setups allow the user to easily select a region of the sample to interrogate and a smaller region to photobleach, once these selections have been made the FRAP data collection can begin. By collecting data from before and after photobleaching FRAP can reveal the mobile component as well as the immobile components, shown by the fluorescent intensity after photobleaching not returning to the original intensity. Immobile fractions are very commonly seen in cell-based assays and provide valuable information about the composition and properties of a system [26, 27].

One of the inherent difficulties with FRAP is the ability to determine quantitative values of D. Data can be easily evaluated to determine the time needed for the intensity in the bleached region reach one-half of the steady-state intensity after photobleaching, this is defined as $\tau_{1/2}$, but this is an empirical parameter that is influenced by experimental settings making it difficult to compare data between different studies. To better evaluate FRAP data, several models have been developed to account for the radius of the bleach spot, photobleaching of fluorophores outside of bleach area, bleaching and scanning time of confocal setups. Equations derived by Axelrod [28] and Soumpasis [29] related the bleaching radius profile, time of one-half recovery, to the diffusion coefficient, below the Soumpasis equation is shown, this relates diffusion coefficient (D), to the size of the bleaching spot (w), and the time elapsed for the bleaching spot reach half of the original intensity

$$D = 0.224 \frac{w^2}{t_{1/2}} \qquad \text{Eq. 2.2}$$

Further work to optimize the evaluation of FRAP data has been done and the equation developed by Kenworthy and DiBenedetto will be used for data collected herein. The main improvements made by Kenworthy and DiBenedetto is the accounting of time elapsed during bleaching and during image acquisition [30]. This is relevant for the modern LSCM due to the slow bleaching times, on the order of seconds, and the time required to collect an image which is again on the order of seconds. Due to the long exposure and imaging times, diffusion during imaging needs to be accounted for with the model used to analyze the data. In the following equation, the user defined radius of the bleach area (r_u) and the measured radius of the resulting bleach spot (r_m) are used to determine a more accurate value for D [30].

$$D = \frac{r_u^2 + r_m^2}{8\tau_{1/2}} \qquad \text{Eq. 2.3}$$

2.1.8 Polymerization and Crosslinking of Hydrogel Supports

Polymerization of acrylamide and bis-acrylamide produce crosslinked gels that allow the specific control of mesh size, density of crosslinks, and elasticity of the resulting polymer hydrogel. Acrylamide monomers form linear chains when polymerized in the absence of bis-acrylamide

crosslinkers. In the presence of crosslinkers, a mesh type arrangement of molecules can be achieved because the crosslinkers link to four acrylamide monomers. Acrylamide and bis-acrylamide monomers are very stable in solution, to initiate polymerization a free radical approach is used. Different radical initiator molecules can be used, but the most common and highly reproducible is ammonium persulfate (APS). When APS is used in conjunction with N,N,N',N'-tetramethylethylenediamine (TEMED), which acts to stabilize free radicals, consistent polymerization reactions can occur. The radical initiation works in a chain like procession starting with the APS that decomposes and becomes a radical that coverts an acrylamide monomer to a free radical which reacts with a different acrylamide molecule to form a chain of monomers; eventually after a series of radical additions a polymer network is formed.

2.2 Background

2.2.1 Polymer Hydrogel Viscoelasticity

Soft polymer materials, such as polyacrylamide hydrogels and other biopolymers, are viscoelastic meaning they show both viscous and elastic mechanical behavior. These bulk material properties are a combination of elastic behavior, seen in solids such as metal, and viscous behavior, seen in liquids. Examples of other soft materials are colloidal suspensions or foams, interest in understanding the mechanical properties has traditionally been motivated by determining the usability in industrial applications. One of the most interesting things about measuring the properties of viscoelastic materials is the time scale dependence of elastic behavior. Purely elastic components do not have a significant time-dependent materials property, meaning that after exposure to a load, return to original shape is considered instantaneous. However, viscoelastic materials have time-dependent properties, which are affected by how quickly a load is applied and how much force is applied [31]. The measurement of viscoelasticity is traditionally performed by the use of a rheometer, and a parallel plate set up is one of the most common methods used for soft materials.

To understand some of the fundamentals of testing materials properties, the storage and loss moduli will be further described. The storage or elastic modulus, G', gives information about the amount of structure and rigidity present in a material. G' can also be described as the amount of energy that can be stored in the material, which translates to a higher G' indicates that the

material is mainly elastic. The loss or viscous modulus, G'', describes the amount of energy dissipated in the sample to heat. The sum of the elastic and loss moduli describes a materials overall property, as either more elastic (solid-like) or viscous (liquid-like) [32]. The hallmark of viscoelastic materials is the dissipation of some of the loaded force, this hysteresis effect makes viscoelastic materials, applicable for special applications where some deformation of the material is desirable.

For the measurement of elasticity with a shear rheometer apparatus, there must be a relationship established between the measured value (shear modulus) and the desired value of Young's modulus, which will allow for ease of comparing the results to other methods. Previous work in the area has shown that the Poisson distribution (ν) for polyacrylamide hydrogels reaches near incompressibility for a value near 0.5 [33]. Now utilizing the equation shown below, the shear modulus (G) can be converted easily to Young's modulus (E) by a factor of three [33].

$$G = \frac{E}{2(1+\nu)} \qquad \text{Eq. 2.4}$$

2.2.2 Polymer Chemical Structure

Likely the most well-known application of polyacrylamide hydrogels is for the separation of proteins and nucleic acid molecules in polyacrylamide gel electrophoresis, such as SDS-PAGE. Polyacrylamide hydrogels are formed from the copolymerization of acrylamide and bis-acrylamide crosslinker molecules. The most common method for polymerization is a radical addition reaction. In this method, ammonium persulfate is used as the radical generator and tetramethylethylenediame (TEMED) is used as a radical stabilizer, by using both of these molecules radicals are stabilized and produced in higher abundance and this leads to improved reaction rates. The polymerization proceeds by the production of a radical that initiates an acrylamide monomer to react with another monomer, thus activating the next monomer and forming a chain. Crosslinking occurs randomly as the polymerization reaction proceeds, meaning that crosslinks are distributed throughout the gel. There are several factors that have an effect on the polymerization of polyacrylamide hydrogels that need to be understood to establish a reproducible method for forming polyacrylamide hydrogels.

These factors include initiator and monomer concentration, reagent purity, pH, temperature, and oxygen. As the concentration of initiator and monomer increases, the rate of polymerization increases [34]. Since the polymerization reaction is carried out using a radical-initiation mechanism, any degradation of the ammonium persulfate or TEMED will result in reduced activity. To avoid inhibiting polymerization, ammonium persulfate solutions were prepared fresh daily and the TEMED was checked for oxidation products and stored at 4 °C. Reaction efficiency is optimum between pH 7 and 10 for the ammonium persulfate and TEMED system. In order to have a reproducible and reliable method of polymerization, temperature should be the same for all reactions, conveniently polymerization occurs best between 22-25 °C, meaning reactions can take place at room temperature. If reaction temperature is decreased, polymerization slows, to maintain consistent reaction parameters the stock solutions were placed at room temperature for at least 20 minutes prior to polymerization. Dissolved oxygen in the stock solutions acts as an inhibitor of the polymerization by trapping free radicals. Oxygen was removed from reaction stocks by placing under vacuum for a minimum of 10 minutes, this helps to ensure homogeneous reactions producing high quality hydrogels.

Polyacrylamides have been used in several industrial applications, such as for ground treatment for oil drilling sites, and more recently these polymer hydrogels have been developed as an injectable biomaterial [35]. Many of the desirable properties such as the water retention and hydrophilicity, which stem from the hydrophilic amine groups along the entire backbone of the polymer, have been evaluated in order to form materials with desirable physical properties. Another property that has received considerable attention is the pore size, also referred to as the mesh size, of the polymer networks.

In an AFM study of the pore size and roughness of polyacrylamide hydrogels, it was found that the surface characteristics of hydrogels can be specifically tuned by manipulating reaction conditions [36]. When the crosslinker molecule concentration is increased there is an observed change in mesh size and surface characteristics of the resulting hydrogels. The overall trend that should be noted is the decrease in mesh size with increasing concentration, or ratio, of crosslinker molecule. Interesting effects arise from manipulating the pore size, including the diffusion of nutrients through the mesh and the effects on the surface morphology.

Mesh sizes have been measured by various methods, across a wide range of functionalized and copolymer acrylamide hydrogels. Direct imaging of the microstructure of polyacrylamide

hydrogels has been pursued with Atomic Force Microscopy (AFM) and Scanning Electron Microscopy (SEM), and indirect methods such as FRAP and DNA electrophoresis. Mesh sizes have been measured to be dependent on the concentration of monomers used and environmental conditions at the time of polymerization, but the mesh size has been measured to be around 10 nm in radius in an AFM study [37]. A DNA electrophoresis study estimated the pore radii from 21 nm for a gel containing 10.5%T 5%C to 200 nm for gels made with 4.6%T to 2%C [38].

In a similar manner to mesh size, stiffness is easily manipulated in polyacrylamide networks. In a review by Tse and Engler, the results of various experimental trials that measured the resulting stiffness of polymer networks were compiled [39]. By utilizing the work that had been previously done to establish the relationship between stiffness and chemical composition, accurate predictions could be made. From data sets, %T and %C, which are shown in the following equations, can be selected with the goal of producing a hydrogel of specific stiffness.

$$\%T = \frac{m_{AA} + m_{BA}}{V_{tot}} \; x \; 100\% \qquad \text{Eq. 2.5}$$

$$\%C = \frac{m_{BA}}{m_{AA} + m_{BA}} \; x \; 100\% \qquad \text{Eq. 2.6}$$

2.2.3 Polymer-Membrane Interactions

Studies of interactions between polymers and membranes have elucidated vast conformational and mechanical effects. Studies have been performed on vesicular (spherical) and supported (planar) membranes with various polymer layers, revealing unique interactions and effects. These effects need to be appreciated in order to understand the unique mechanical and thermodynamic situation at the polymer-membrane interface in polymer gel-supported tethered bilayers.

One interesting case that has been thoroughly described in the literature is the use of hydrophilic polymers tethered to lipid vesicles [40]. Classically this technique of decorating vesicles with polymers was used in an effort to increase the blood circulation time and improve the drug delivery profile in order to deliver a therapeutic trapped inside the vesicle. To this end, vesicles have been decorated with hydrophilic polymers such as polyoxyethylene, but when this strategy is pursued there are energetic effects caused to the membrane of these systems that should

be considered. In this vesicle system, at very low polymer surface density there are interactions between the polymer and membrane, and once a high enough density is reached, repulsive interactions begin to occur between the polymers, and this leads to significant membrane perturbation.[41-43] It was observed that the bending stiffness and curvature of the membrane can be affected by the presence of hydrophilic polymers [44, 45]. Now this effect of grafting polymers to a lipid vesicle is not a direct measurement of the specific interactions occurring at a PGTB; however, the interactions are worth noting, due to the similarity of tethering a polymer moiety to a lipid membrane.

To highlight the potential for large effects of membrane destabilization, the case of stimuli-responsive polymers bound to membranes will be further detailed. Temperature or pH responsive macromolecules have been anchored to membranes of lipid vesicles and large effects of membrane destabilization have been observed. Work done by Tribet and coworkers demonstrated that amphiphilic polymers were able to induce pores into membranes [46]. To confirm this, albumin and dextran molecules were shown to be incorporated into GUVs and pass through membranes spanned across a pore, called a black lipid membrane. These results indicate that stable pores on the size order of 2-5 nm were formed due to the interaction of polymer moieties with the lipid bilayer. Polymer and lipid interactions are powerful phenomena that are still only partially understood, not enough is known to completely predict the exact interactions that will occur at the interface between the polymer hydrogel support and membrane.

2.2.4 Surface Morphology of Polyacrylamide Hydrogels

A water swollen polymer network, presents a rather heterogeneous surface in comparison to solid substrates, such as mica or glass. Particularly convincing evidence has been provided by AFM direct measurements of polyacrylamide substrates to reveal the heterogeneous nature of the surface of polyacrylamide [37]. The control of surface features in polyacrylamide hydrogels has even been demonstrated with the incorporation of surfactant molecules, with greater fraction of surfactant forming micelles in the hydrogel, an increase in surface heterogeneity was observed[47]. Beyond the minimal spacing that would occur because of the mesh pattern of the hydrogel, undulations are observed in the surface topography of swollen hydrogels. These polymer peaks and valleys present a challenge to complete a lipid membrane covering, as perturbations from planar geometry result in areas of high curvature leading to reduced membrane diffusion.

2.2.5 Mechanism of Planar Bilayer Formation from Vesicle Structure

The purpose of this section is to provide an introduction to some of the fundamental concepts that are considered when applying a planar bilayer to a substrate. The research pursued in this thesis utilized the LB/VF method, but the better understood vesicle-solid support interaction described here gives an idea about the process of planar bilayer formation on polymer hydrogel supports. As explained in Section 2.1.3 vesicles are a supramolecular assembly of lipids that form a spherical shape in a bilayer formation. Upon dissolving a dried lipid film into an aqueous buffer, the vesicles that are spontaneously formed will be many spheres thick with larger vesicles encapsulating smaller vesicles, producing what are called multi-lamellar vesicles. The mechanism of vesicle structures interacting with a solid substrate and forming a planar bilayer structure has been investigated with various techniques to reveal some of the underlying physical conditions. In addition to vesicle fusion, there are alternative methods to forming bilayers including LB/LS transfers and LB/VF described in the following section.

With quartz crystal microbalance apparatus Kasemo and coworkers showed that planar bilayer formation on a quartz support was a two-step process: first vesicles adsorbed to the solid surface and then bilayer is formed [48]. Recent work by Suman Peel and Jacob Piehler demonstrated quantitatively the rates of vesicle rupture and specifically the role of vesicle density in rupture and formation of planar bilayer [49]. The remodeling of a vesicle from a spherical structure to a planar structure has been shown to be the rate limiting step in the formation of planar bilayers, with the rate of isolated vesicle rupture being more than 3,000x slower than a cluster of three vesicles. Also confirmed from this data set is the influence of vesicle coverage or concentration; at very low vesicle coverage there can be little to no bilayer formation and by increasing concentration the likelihood of vesicle-vesicle interactions increases, thus increasing the rate of bilayer formation. The authors examined the impact of a surface coating on the glass support, using a short PEG linker of 3000 Da (about 70 PEG units) caused an order of magnitude decrease in the rate of bilayer formation compared to a glass support. This work supports the observations of scientists over the since the 1970s that planar lipid bilayers were formed when vesicle suspensions were applied to appropriately matched solid supports. With this understanding, the current work has extended the application of vesicle fusion to swollen hydrogel supports, which have proved to be very different from solid supports or nanometer thick polymer layers previously established.

In a combination of the LB and vesicle fusion methods a separate technique has emerged as a viable pathway to produce planar lipid bilayers. The LB/VF method starts with a monolayer of lipids deposited via LB and then SUVs are added to the monolayer and a planar bilayer is formed [50]. The advantage of the LB/VF to traditional SUV fusion techniques is the incorporation of a distinct inner leaflet lipid composition, which has been shown to maintain lipid asymmetry for hours [51]. For instance the LB/VF technique has been used to incorporate transmembrane proteins into a planar membrane with an inner leaflet containing lipopolymer molecules, which work to lift up the membrane from close contact to the solid substrate [52]. The utility of this method to produce high quality membranes, fabricate an asymmetric lipid composition, and incorporate transmembrane proteins to a planar membrane system shows the range of capabilities of the LB/VF method.

2.2.6 Cellular Adhesions

A fundamental building block of biology is the cell. In complex biological organisms, these self-contained units are organized into specific tissue structures that accomplish a function, which we refer to as organs. The next few sections will be dedicated to giving insights about the cellular functions that make the formation of sophisticated tissues possible. Here, attention will be given to the biology and function of cellular adhesion complexes with a focus on sensing and responding to the physical mechanics of the cell environment. Many investigations have revealed that cells are able to sense the mechanical and geometrical properties of their environments, then this information is translated into a biochemical response within the cell that causes changes in cellular fate and function. One particularly strong example of the effects of the physical environment is the capability to influence stem cell differentiation. Undifferentiated mesenchymal stem cells (MSCs), not committed to a cell type, were plated on substrates of varying stiffness; matching that of brain (E = 0.1-1.0 kPa), muscle (E = 8-17 kPa), or bone (E = 25-40 kPa) [1]. After one week, the MSCs had differentiated to the phenotype associated with the substrate stiffness, all of this was done without the use of soluble induction factors [1]. Due to insight showing that the mechanical environments around cells are highly important for proper function, much attention has been given to identifying the associated mechanisms and processes. Next, cellular adhesions will be described, and associated force sensing features will be discussed.

In order to form a complex tissue, composed of many cells, there must be stable physical connections established. For proper cellular function, attachments must be made outside the cell through the plasma membrane and to the cellular cytoskeleton. To form this transmembrane spanning architecture a protein-based assembly is used, where a transmembrane protein is commonly observed with an extracellular domain that has a receptor for an extracellular component, a conglomerate of protein-protein interactions are established that reinforce the connection from outside the cell to the cytoskeleton. Then the cytoskeleton is stressed with an active force, accomplished by the actin-myosin machinery, which leads to a stable transduction of force allowing the cell to adhere and establish the proper phenotype and biochemical responses. There are two main classes of cellular adhesions, attachments made with ECM or adjacent cells. Attachments made with the ECM are mediated by protein-based adhesion structures, and the most common class of these structures are called focal adhesions. These specific kind of adhesions are mainly composed of various forms of integrin (transmembrane heterodimeric protein) that has recognition sites for the RGD repeats found in ECM proteins, such as fibronectin and laminin [53]. Intercellular connections are similar in function and engineering, but there are many types of intercellular junctions (e.g., tight junctions [54], adherens junctions [55], and gap junctions [56]). Now the structure of cellular adhesions will be discussed in further detail to provide a fuller picture of what is occurring as cells form adhesions, whether to ECM, other cells, or an artificial substrate.

There are multiple types of ECM adhesions formed by a cell, these include, fibrilliar adhesions, podosomes, and focal adhesions [57]. These localized connections formed between cells and an underlying substrate were first described in the 1970s and 1980s as micron length elongated zones, which were associated with cytoplasmic actin cytoskeleton organization and cell function [58-61]. Since these early descriptions of cellular adhesion zones, much more has been discovered about the structure and composition of these attachment sites. The most investigated adhesion has been the focal adhesion, which is a cell-to-ECM adhesion mainly composed of integrin protein [62]. Integrin are heterodimeric, meaning they are composed of alpha and beta subunits, and are adherent to RGD sequences found outside the cell, in the ECM structures. Integrins have been found to exist in inactivated and active conformations, where the activated forms exist when exposed to proper ion conditions or ligands leading to an extended switchblade-like arrangement of the protein domains [63]. In order to form a stable attachment to the cellular cytoskeleton, associated proteins bind to the cytoplasmic region of the integrin and form a plaque

or conglomerate of proteins. When the cell is actively probing the extracellular environment, the application of cellular generated force can be a determining factor in the maturation and assembly of focal contacts, indicating the mechanosensitive nature of these adhesions [62]. One of the prime examples of the importance of force application is the role of the talin-vinculin system, cytoplasmic proteins that need to bind to integrin for proper cell adhesion [64], upon the application of force to talin a cryptic binding site for vinculin is revealed, and binding of vinculin reinforces the focal contact allowing the formation of a stronger, more stable connection to the extracellular material [65, 66].

The second class of cellular attachments, and the focus of the work in this thesis, are attachments formed directly between adjacent cells. Neighboring cells establish connections to allow the exchange of information through these protein-based adhesion zones. There are a wide variety of intercellular junctions including adherens junctions, tight junctions, gap junctions, nectin-based junctions, and desmosomes [67]. Interestingly there is evidence that different adhesion types (e.g., tight and adherens junctions) work together to confer mechanical strain on the cell to achieve proper chemical signaling responses [68]. Model systems to test new hypotheses about the interconnected and synergistic effects of multiple adhesion types have yet to be realized, however if a platform was available the information and understanding gathered would have strong implications in understanding the nature of tissue organization. Specific attention has been given to adherens junction adhesions due to their importance in cellular regulation and health. For instance, a loss of E-cadherin is relatively common in cancers of epithelial origin [69]. During normal cell function, cell growth and migration are precisely regulated through sophisticated biochemical pathways and one common feature of cancer or tumor cells is the loss of regulation of these properties. This dysregulation leads to a measured increase in rates of proliferation and migration in metastasizing cells, this process could be related to cadherin based-adherens junctions and further understanding is needed.

Now the structure, form, and biochemical pathways associated with adherens junctions will be described. The work presented herein focuses on adhesions formed between adherent cells and a biomimetic material functionalized with cadherin protein, which we hypothesize is an accurate mimetic for the adherens junction. Adherens junctions are mainly composed of the cell surface transmembrane glycoprotein family called cadherins. To form an intercellular adhesion cadherin from one cell binds to the extracellular domain of cadherin in an adjacent cell, this homophilic

bond is Ca^{2+} dependent, leading to initial binding and the formation of a nascent adhesion [70]. When an extracellular bond between cells is formed between cadherin molecules a cytoplasmic response is initiated that consists of the formation of a stable protein-based connection to the cellular cytoskeleton. The most understood biochemical pathway is the binding of catenin family proteins to the carboxy terminal of the catenin-binding domain of cadherin protein [71, 69, 72]. Now to understand the mechanosensing mechanism of adherens junctions the cytoplasmic domain will be described, specifically illustrating the modular multi-protein assembly that is tension and biochemically regulated. After initial cadherin binding in the extracellular domain, β-catenin binds to the cytoplasmic domain of cadherin, subsequently α-catenin binds to β-catenin [71, 69]. With the formation of a catenin bound cadherin domain vinculin, which will be the connecting structure to the cytoskeleton, binds and will become activated. There have been interesting studies to reveal that vinculin is a mechanosensing element in the formation of adherens junctions [66, 71]. Vinculin can be activated to provide a stronger connection between cytoplasmic cadherin protein and cellular cytoskeleton, with this activation a physical extension of the protein is observed resulting in about 30 nm of added length [71]. For the activation of vinculin to be maintained, leading to a mature, stable adhesion, there must be tension force applied from the active actomyosin machinery of the cytoskeleton and tyrosine phosphorylation of the residue at Tyr822 [71].

With the formation of an adherens junction, these intercellular adhesions can now serve as mechanical points of prestressed tension, which will allow information to be passed from cell to cell. These adhesions are not fixed in composition or position along the cell periphery, however these adhesion zones can mature into a zonula adhesion, such as what is found in epithelial sheets where these stable adhesions are found at the apical region of the cell [73, 69]. Adherens junctions, although they are dynamic, have been shown to be regulators of mechanosensitivity due to mechanisms of binding, such as that seen for vinculin and α-catenin [68, 74, 75, 72]. With the capability to differentially engage from the extracellular binding of cadherin through to the cellular cytoskeleton, mechanoresponse can be intricately structured, leading to cellular responses that include morphogenesis, the biological processes that regulate the development of an organisms shape; cell migration, invasion, tissue patterning and symmetry breaking [73, 69]. Next the three-step process of how a cell responds to the mechanical nature of its environment will be described covering the processes of (i) mechanosensing, (ii) mechanotransduction, (iii) mechanoresponse. The biochemical processes will be described, and the resulting global cell responses will be

explained. This information fits in the context of this work by providing evidence that the mechanical properties of the surrounding matrix strongly change properties of a cell and multi-cellular structures.

2.2.7 Mechanosensitivity

In this section, the example of how a cell goes from suspension to spreading on a biocompatible surface will be explained, this is done to highlight the importance of the mechanical nature of the cellular environment. The shape change and adhesion processes that allow a cell to adhere to a surface begin by transmembrane adhesion proteins binding to their appropriate receptors found in the extracellular environment, for example integrins binding to RGD sequences and cadherin homophilic binding [76]. These extracellular binding events lead to actin polymerization and Src activation, this occurs prior to the cell applying force to the bond. When a cluster of adhesion proteins come together, this forms a nascent adhesion, the cell begins to apply force from the cytoskeleton. If sufficient conditions are sensed by the cell (i.e., the matrix is sufficiently rigid for spreading) Rac-dependent actin polymerization will occur, this leads to spreading of the cell from round morphology to flatter more elongated cell shape. Nascent adhesions, small ~100 nm in diameter composed of about 50 integrin proteins, allow the cell to adhere and begin to spread with the cell front being pushed by actin flow [77]. However, if insufficient conditions are encountered by the cell, such as that seen when adherent cells spread on fluid supported lipid bilayers [78], the cell will transition to programmed cell death or apoptosis.

Early stage cell adhesion and mechanosensing happens within 30 minutes for fibroblast cells plated on fibronectin coated materials, and the cell engages in contract and relax type engagement with the extracellular materials. Here the cell engages the myosin machinery of the cytoskeleton and places tension on the nascent adhesions on the timescale of 1-2 s with a force of ~25 pN [79]. After establishing nascent adhesions, increased traction forces are generated through a stick-slip manner, where the cytoskeleton will be stressed in stretch-relaxation cycles [80]. And adhesions will enlarge by incorporating more transmembrane proteins to stabilize the attachment. During this time of maturation of cell adhesions, actin polymerization shifts to the center of the cell near the nucleus, producing a more organized cytoskeleton that can cover micron length sections of the cell. Similar mechanisms of cell adhesion have been found for cell spreading via

cadherin-based adherens junctions, as is not surprising that the mechanical nature and cell mechanics is conserved independently of the type of adhesion being formed [81].

Cells have the capability to sense and respond to sophisticated mechanical properties and these include rigidity, geometry, and curvature. [82, 83]. Geometry or the spacing and size of presented cell adhesion molecules has a impact on the global properties cell response, including the capability of regulating whether MSCs differentiate into fat or bone phenotype cells [84]. Spatial and nanoscale organization of cell adhesion area is significant because a tissue with natural ECM does not have uniformly arranged or presented adhesion sites [5]. For curvature sensing, BAR-domain (Bin, amphiphysin, Rvs domain) proteins have been proposed as a mechanism of sensing concave surfaces [85], which has been shown to cause an increase in Rac and thereby an increase in traction forces seen on nanopost coated surfaces[86, 87]. Rigidity sensing has been proposed to be regulated by the mechanical stretching of the cytoskeleton, that through the unfolding of cytoskeletal molecules biochemical signaling cascades are activated, such as the Src-family kinases which show a marked increase in phosphorylation during cell and cytoskeleton stretch [88].

2.2.8 Mechanotransduction

After mechanosensing of the extracellular environment and application of force to nascent adhesions, this information is transduced, and biochemical responses are made in the cytoplasmic region of the cell. The conversion of force into biochemical signals is the process of mechanotransduction. This conversion has been indicated to function by several mechanisms upon force exposure, including the opening of cryptic or hidden binding sites, the opening of ion-channels, and stabilizing receptor-ligand catch bonds [5]. As mentioned in 2.2.6, the stretching of vinculin at adherens junctions to allow phosphorylation and activation is an example of the opening of cryptic or hidden binding sites. At integrin-based focal adhesions in the cytoplasmic region talin binds and stabilizes the integrin protein plaque, upon force and stretching of the protein binding sites are revealed for vinculin, which leads to a stronger more stable attachment to form [66]. Mechanosensitive ion channels are a highly interesting class of transmembrane molecules that are important for processes of hearing, balance, touch and proprioception [89]. Mechanosensitive ion channels, which open in the microsecond range after force application, are sensitive to cell stretching, shear stress, and cell shape changes [90]. Inner ear has specialized

epithelial cells, with stereocilia hair extensions that are equipped with mechanosensitive ion channels called mechanoelectrical transduction channels in their tips. Positive reflection of the hair cells, activated by sound, cause the mechanoelectrical transduction channels to open and allow ions to pass through, when sound stops the hair cell relaxes thereby closing the channel [89]. Slip bonds that reinforce cell attachments and stably transfer force act against the normal behavior of noncovalent bonding. Normally, under force, noncovalent bond lifetimes are drastically shortened, this phenomenon is observed for biotin-streptavidin binding. Under normal conditions the half-life for biotin-streptavidin is over 24 hours, however when pN level force (force generated by a single motor protein) is applied the bond lifetime decreases to about 1 minute [91]. Although this is the commonly observed property, there are a few examples of a bond that becomes stronger when force is applied, specifically these are adhesion molecules like adhesin FimH and P-selectin [5]. Whether cell adhesion associated proteins exhibit this specific type of catch bond that becomes stronger with force application is yet to be investigated, nonetheless this mechanism of force application affecting bond life time could still be a mechanism for regulating the cell response to mechanical information. These noncovalent bonds under tension also requires larger numbers of adhering proteins (e.g., an increased number of cadherin proteins at each adhesion site) to be engaged due to the increased turnover rate of these complexes, this creates a scenario where a bond will break and many others are still connected, and soon thereafter another bond will be formed.

Mechanotransduction biochemical pathways utilize a large, diverse group of mechanosensing proteins, which allows for transduction to have effects on many biochemical pathways that can act in a coordinated way to accomplish proper cellular response. In some ways, these many pathways that are used to translate mechanical information into the biochemical response can be seen as a redundant backup system that allows for more precise tuning of cell response. Some of the specific mechanotransduction pathways utilized by many adherent cells are extracellular signal-related kinase (ERK), Rho superfamily of proteins are also implicated in many mechanotransduction pathways. An additional pathway is Hippo signaling, which is responsible for regulating organ and tissue size by controlling cell size, apoptosis, and stem cell self-renewal; this pathway is affected by mechanical linkage to the cytoskeleton at adherens junctions, zonula adhesions, and focal adhesions [92]. Other pathways include the Ras superfamily of proteins, specifically the Rho family of GTPases, such as: RhoA, which modulates the regulation and timing of cell division; Rac1; and Cdc42 which is implicated in the cell processes of dendritic growth,

branching, and branch stability [93]. Rho signaling at zonula adhesions has been shown to be connected to regulation of cytokinesis, which is the cytoplasmic division of a cell at the end of the cell division process [94]. Finally, receptor tyrosine kinase activity, which is regulated through mechanical biochemical transduction, phosphorylates components to activate Ras and other signaling pathways [95]. Cells, 3T3 fibroblasts, grown on fibronectin coated micropatterned substrates with various shapes including rectangle, triangle, and circular of different sizes and aspect ratios showed geometric dependent changes in gene expression [96]. Mechanotransduction pathways and the physical interaction of the cytoskeleton with the nuclear envelope can cause changes in expression of genes, and in this case actin crosslinker actinin, actin polymerization contributing gene formin [96].

2.2.9 Mechanoresponse

In this subsection three examples of cellular responses to systematic changes in artificial substrate materials properties will be highlighted to demonstrate the global effects that mechanosensing and mechanotransduction have on cellular fate and function. In the first work, Haag and coworkers fabricated hydrogel cell substrates with controlled surface roughness and stiffness [97]. Surface roughness was varied from nanoscale to microscale, whereas stiffness was varied from 3.8 to 31.3 kPa, surprisingly mechanoresponse and osteogenesis of human mesenchymal stem cells were enhanced on soft hydrogels with high surface roughness, the cell response was similar to that seen on stiff hydrogels with smooth surfaces [97]. The results from this study show an important interplay between cellular response to roughness and rigidity, that the expected results of osteogenesis seen on stiff substrates and adipogenesis observed for soft substrates can be modulated by impacting other cellular sensing and transduction pathways.

In a classic study completed by Dembo and Wang, NIH 3T3 fibroblasts were cultured on polyacrylamide sheets with regions of high rigidity and low rigidity were functionalized with ECM protein collagen [98]. Observation of these fibroblast cells revealed an interesting pattern of migration habits in direct correlation to the stiffness of the cellular environment. When a cell from the soft portion of the substrate came to the interface with the rigid material it easily crossed over and developed greater traction forces and spreading areas, however when a cell from the rigid side migrated to the boundary they either turned around or retracted from the substrate [98]. The authors

in this work coined the term, durotaxis, to describe the active preference of these cells for a stiffer substrate.

Next I will highlight a study where polyacrylamide hydrogels of varying stiffness were functionalized with the extracellular domain of E-cadherin and plated with MDCK cells [81]. Polyacrylamide hydrogels of stiffness 9, 30, and 60 kPa were used; the soft gel had minimal cell adhesion, whereas the 30 and 60 kPa hydrogels showed small punctate type adhesions [81]. However, from this study there were interesting results from the mechanotransduction assays, for instance Cdc42 activity was required for cell adhesion on the 30 kPa PA gel, but not the 60 kPa gel and Rac1 inhibition had little effect on cells adhered to these substrates [81]. There are limitations for this kind of system to accurately represent the architecture of a cadherin-based adherens junction, these include the ligand density presented to the adhering cells, fixed presentation of the cadherin molecules, and the range of stiffnesses assessed. When using a polyacrylamide hydrogel directly functionalized with cell adhesion molecules the adhering cell is unable to rearrange the presented molecules, this presents a different situation than found in a biological system where the cells allow adhesion molecules to accumulate in a specific region of the cell membrane area. With this type of fixed system there are limitations to how the results can be directly interpreted to biological systems and the properties of intercellular adhesions.

2.2.10 Polymer Gel with Covalent Linkers for Cell Assays

This content in Section 2.2.11 through 2.2.15 was previously published, Shilts, K. and C. A. Naumann (2018). "Tunable cell-surface mimetics as engineered cell substrates." Biochimica et Biophysica Acta (BBA) - Biomembranes **1860** (10): 2076-2093, 10.1016/j.bbamem.2018.06.009.

Previous advancements in the understanding of cellular mechanosensitivity have been closely linked to the development of engineered cell substrates of adjustable viscoelasticity, which allow a direct correlation between substrate stiffness and cell response. So far, this strategy has been mainly demonstrated on functionalized polymeric gels, whose substrate elasticity can be controlled through polymer crosslinking density. Such polymeric substrates have been instrumental in confirming that substrate stiffness significantly impacts cellular properties

including morphology, cytoskeletal organization, and motility [3, 98-102]. Most prominently, the significance of cellular mechanosensitivity was demonstrated by the observation that stem cell differentiation can be regulated by substrate stiffness [1]. Initial progress was made using artificial polymers, such as polyacrylamide [3], whereas later cellular mechanosensing experiments also included natural polymers of adjustable viscoelastic properties [103, 104]. Meanwhile, polymeric materials were also employed, which allow adjustment of substrate viscosity [105, 106]. In another ECM mimetic approach, cell adsorption was investigated on a cell substrate of amphiphilic peptides with RGD linkers [107].

While linker-functionalized polymeric gels can be considered as attractive ECM mimetics, they are usually limited in their ability to replicate the rich dynamics at cell-cell junctions, which include remarkable long-range movements, such as the observed basal-to-apical flow and treadmilling movements of AJs between polarized cells [108, 109]. Instead, alternative design strategies were needed in order to develop a more realistic cell surface-mimicking substrate for the analysis of cell adhesion and cell migration across cell-cell interfaces. As Fig 3 illustrates, such a substrate should fulfill several important requirements. First, to enable cell adhesion and spreading on a cell surface mimetic, substrate-bound ligands for cell adhesion receptors should be able to dynamically assemble into clusters to allow the formation and maturation of stable cell-substrate linkages. Next, engineered cell surface mimetics for the analysis of cell migration should enable the transmission of cytoskeleton-generated cellular traction forces to the underlying solid substrate across cell-substrate attachments. Finally, such artificial cell substrates should permit the adjustment of substrate mechanical properties to make them suitable for the characterization of cellular mechanosensitivity.

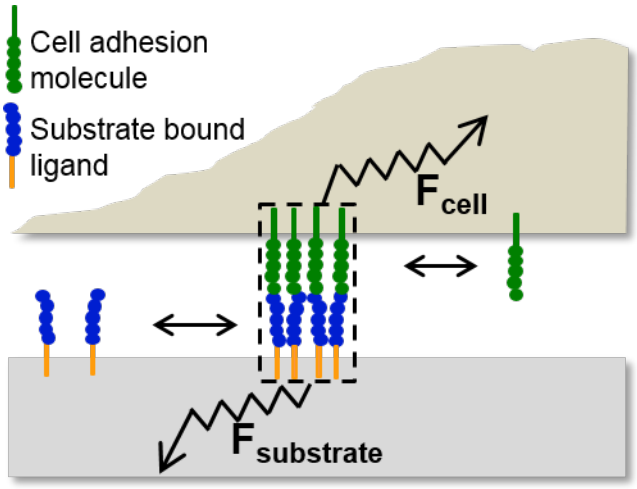

Figure 3. Schematic illustrating the functionality of an advanced cell surface-mimicking cell substrate, which allows: (i) dynamic assembly of linkers into linker clusters at cell-substrate contacts, shown in dashed line; (ii) transduction of cytoskeletal forces through cell-substrate contacts to enable cell spreading and migration, shown with force vector; and (iii) dissipative long-range movements of cell-substrate contacts.

2.2.11 Cell Free Assays on Solid-Supported Membranes

Since introduction by McConnell and coworkers more than three decades ago, SLBs have developed into a widely employed model membrane platform for biophysical and biotechnological applications [110-112]. Formation of a planar lipid bilayer by roll out and fusion of unilamellar vesicles represents the most widely established SLB fabrication method [113]. Alternatively, a SLB can be built through monolayer transfer from the air-water interface [110] or via spreading from a lipid reservoir [114]. Importantly, physical interactions lead to an energy minimum that position the SLB ~10 Å above a hydrophilic solid substrate, separated by a thin water layer [115, 116]. Due to the resulting lubrication effect of the thin water layer, lipids in both leaflets and lipid-anchored proteins in the top leaflet of the SLB display lateral mobility, resembling an important property of plasma membranes [110]. In contrast, transmembrane proteins with a cytosolic domain are typically immobilized in such model membranes [117]. Like other lipid bilayer systems, SLBs have highly anisotropic mechanical properties. They show a liquid-like in-plane shear viscosity and a rather elastic response with respect to out-of-plane deformations [118, 119]. Fluid SLBs have also emerged as a useful, but limited experimental platform for the analysis of adhesion processes of functionalized vesicles and plated cells.

In part, motivated by the classical model of Bell, Dembo, and Bongard that cell adhesion depends on the competition between specific and generic interactions [120], in a series of papers Sackmann and coworkers explored the biophysical aspects of cell adhesion by investigating the interaction between functionalized giant vesicles and SLBs. In this cell-free assay, giant vesicles are doped with glycocalyx-mimicking lipopolymers, acting as repellers, and ligand molecules, which enable specific binding to reconstituted receptors in the SLB that may also contain lipopolymers (Fig 4 panel on the left). A hallmark of such an assay is the ability of laterally mobile ligands, receptors, and repellers to dynamically rearrange during the adhesion process. This model system is attractive because both the ligand and receptor concentrations in the SLB and giant vesicles can be adjusted quite accurately. This feature enables the design of experiments, which provide insight into the role of receptor and ligand concentrations on the vesicle adhesion process. For example, the RICM data in Fig 4 upper right show that systematic variation of contact site A (csA) ligand on the vesicle alters the contact zone between adhering vesicle and SLB [121]. Interestingly, at lower csA concentrations, domains of tight adhesion and weak adhesion can be observed underneath the adhering vesicle. Similarly, the fluorescence data in Fig 4 bottom right demonstrate the ability to investigate the impact of a controlled receptor shortage on the vesicle adhesion process to a SLB [122]. They show that such a receptor shortage results in an adhesion zone of coexisting regions of tighter and weaker adhesion.

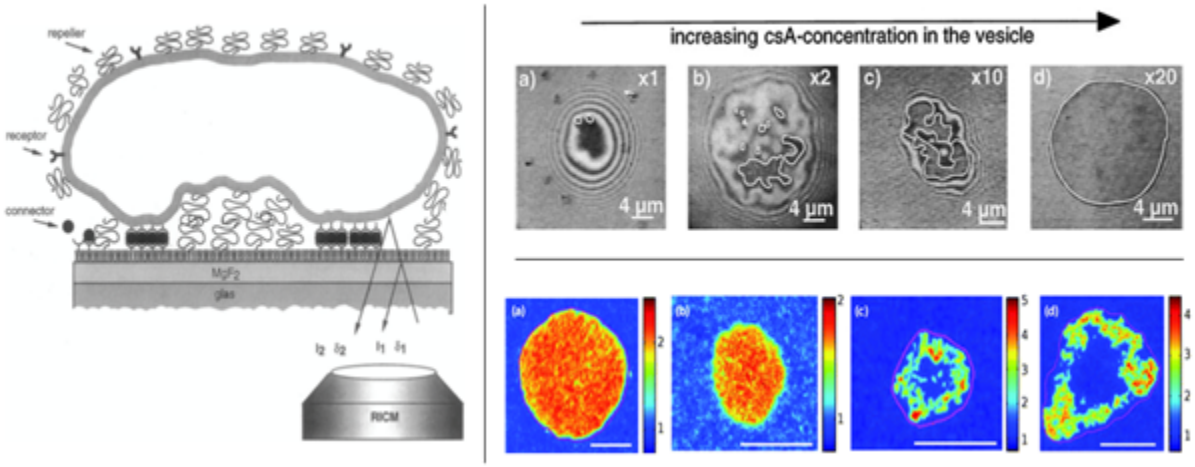

Figure 4. Left panel: Schematic of a cell-free assay for the study of cell adhesion processes. Here, a giant vesicle is doped with glycocalix-mimicking lipopolymers, acting as repellers, and ligand molecules, which enable specific binding to reconstituted receptors in the SLB. The adsorption process can be monitored using microscopic techniques, such as reflection interference contrast microscopy (RICM). Top right: RICM data illustrate the impact of csA ligand concentration in the vesicle on the vesicle adsorption to a csA-functionalized SLB. Fluorescence microscopy methods (bottom right) may provide important insight into the subtle interplay between ligand-receptor pairs if ligands and/or receptors are fluorescently labeled. Left panel [123], top right [121], and bottom right [122].

Previously, adhesion experiments with this cell-free assay were conducted using different ligand-receptor pairs, including heterophilic biotin-streptavidin [123] and RGD-αIIβ3 integrin [124], as well as homophilically binding contact site A (csA) receptors [121]. These experiments showed that low receptor concentrations can trigger the adhesion process between giant vesicle and SLB by forming tightly binding adhesion domains of ligand-receptor pair clusters, thereby displaying remarkable parallels to the assembly of adhesion proteins at cellular contacts [125]. The observed ligand-receptor segregation was described by a double minimum free energy of adhesion and was interpreted in terms of a competition between short-range attractive forces and long-range repulsive forces. By combining the described cell-free assay with a magnetic tweezer setup, Sackmann and coworkers also demonstrated force-induced adhesion strengthening in such a model system [126]. Smith and coworkers, using a cell-free adhesion assay with cadherin receptors, also reported that membrane fluctuations may have a significant impact on adhesion processes between functionalized giant vesicles and SLBs [127]. Taken together, the described experiments not only established the significance of specific key-lock binding processes during giant vesicle adhesion

to the SLB, but also illustrated the importance of physical interactions in the adhesion process. Interestingly, Parthasarathy and Groves also reported that adhesion of ligand-free vesicles without specific ligands may cause segregation of SLB-bound proteins into micron-size clusters [128].

2.2.12 Solid-Supported Lipid Bilayers (SLBs)

In addition to cell-free adhesion assays, SLBs of well-defined ligand composition have also been utilized as an in vitro experimental platform for investigating adhesion processes of plated cells. Most prominently, this experimental strategy was successfully applied in combination with immune cells to study artificial immunological synapse formation [10, 12]. McConnell and coworkers first reported the activation of CD8 positive T-cells on supported lipid membranes with incorporated major histocompatibility complex class I proteins [113]. By building on these pioneering experiments, the SLB platform was next applied to investigate the adhesion of lymphocytes to a supported lipid bilayer via heterophilic CD2/CD58 interaction [10]. These experiments not only identified the formation of ligand-receptor pairs, but also established the accumulation of laterally mobile CD58 at contact areas between Jurkat T lymphoblasts and SLB. Analysis of cellular adhesion processes was not limited to a CD58-containing SLB, but also included other ligands, such as ICAM-1 [129, 130]. Notably, in such experiments, CD58 and ICAM-1 in the planar bilayer were found to dynamically redistribute into segregated CD2-CD58 and LFA-1-ICAM-1 adhesions between SLB and adhering cell. This finding was significant because it illustrated that ligand-containing SLBs allow the dynamic rearrangement of adhesion proteins into distinct synaptic patterns underneath plated cells. As illustrated in Fig 5, quantitative analysis of fluorescence data of fluorescently labeled ligands in such an in vitro assay demonstrated that immunological synapse formation goes through distinct stages, including junction formation (stage 1), MHC- peptide transport (stage 2), and synapse stabilization (stage 3) [131]. These findings were intriguing in light of the detected synaptic pattern formation between antigen-presenting cells and T-cells during T-cell activation [132]. They illustrate that SLB of well-defined ligand composition have become a valuable tool of immune cell adhesion/activation research [11, 132]. SLBs were also employed to explore molecular processes associated with artificial neuronal synapse formation [133] and to investigate the mechanobiology of nascent integrin and cadherin adhesions [134, 135, 77]. Furthermore, comparing experiments on ligand-functionalized SLB versus control substrates with corresponding immobilized ligands allowed

valuable insight into the role of ligand mobility during cell adhesion and activation. For example, cell adhesion experiments on SLBs revealed that ligand mobility may modulate artificial immunological synapse formation and activation of plated T-cells [136]. In this case a more rapid formation of the central supramolecular activation cluster as well as enhanced tyrosine phosphorylation and Ca^{2+} levels were seen as indicators of cell stimulation on SLBs with laterally mobile ligands. Similarly, the lateral mobility of E-cadherin in a SLB was reported to influence E-cadherin-mediated intracellular signaling in epithelial cells [137]. In the latter case, laterally mobile E-cadherin in the SLB was observed to enhance recruitment of the Rho GTPase family member Rac1 (relative to immobilized E-cadherin) that plays important roles in downstream E-cadherin signaling and as an upstream effector of cytoskeletal dynamics influencing E-cadherin behavior [137]. Another noteworthy development has been the introduction of molecular tension sensors to probe cellular tensions during cellular adhesion to a SLB [138-140]. Specifically, molecular tension fluorescence microscopy (MTFM) sensors have been applied to measure cellular tensions on a SLB [138, 139]. These experiments demonstrated that the presence of the planar model membrane leads to reduced cellular tensions relative to substrates with corresponding immobilized tension sensors. For example, T-cells showed a cellular tension of 4.7 pN on a SLB [138], but were able to open immobilized 12 pN tension gauge tethers [141]. Similar results were obtained using B-cells, which showed unzipping of 7 pN sensors but no unzipping of 9 pN and 14 pN probes on SLB [139], whereas a 56 pN tension probe was opened on a glass substrate [142].

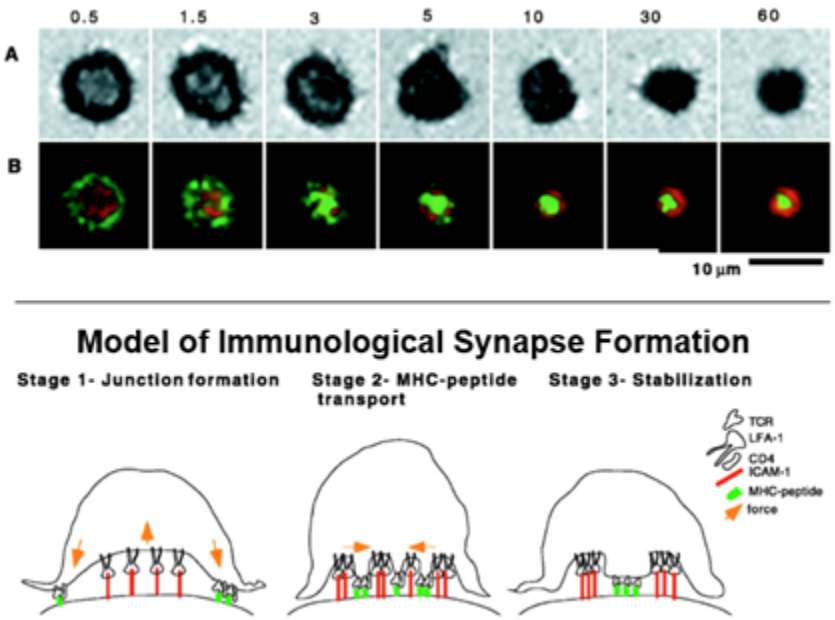

Figure 5. Formation of immunological synapse, between 2B4 cells and SLB containing MHC-peptide and the adhesion ligand ICAM-1. Information about synapse formation can be obtained by acquiring images of contact formation (A) and distribution of fluorescently tagged MHC-peptide (green) and ICAM-1 (red) shown in (B). Model of immunological synapse formation, as derived from quantitative analysis of fluorescence data, shown in bottom panel. According to this model, immunological synapse formation goes through three stages: junction formation (stage 1), MHC- peptide transport (stage 2), and synapse stabilization (stage 3). Reprinted from [131].

Despite their suitability in deciphering processes of immunological synapse formation and nascent cellular adhesion formation, SLBs have been limited in their applicability as an artificial cell substrate because adhering cells are typically unable to develop cellular tractions on a fluid SLB of negligible shear viscosity. Consequently, such a fluid bilayer system may allow the formation of nascent adhesion structures, but suppresses the development of matured cellular adhesions required in a process, such as cell migration [135]. To overcome this limitation, SLBs have been previously compartmentalized using lithographically patterned grids [143]. For example, MCF-7 cells were unable to spread on a planar fluid lipid bilayer with laterally mobile hEGF-linkers, but showed good spreading behavior on corresponding substrates with incorporated micropatterns of immobilized anchors [144]. SLBs with engineered micropatterns have also been employed to impose constraints on immunological synapse formation, resulting in altered TCR signaling [145]. A corresponding experimental strategy was applied to demonstrate that physical

restriction of laterally mobile ephrin-A1 ligands in a patterned SLB impacts the organization and physical force sensing of EphA2 receptors in adhering breast cancer cells [146]. Another interesting example represents a SLB where neuronal adhesion protein was conjugated to an Fc-domain of IgG, thus enabling neuronal adhesion and growth [147]. An alternative patterning strategy has been the incorporation of surface-functionalized nanoparticles and nanodot arrays into SLBs, enabling the design of cell substrates with well-defined regions of immobilized and laterally mobile ligands [148, 149]. Such patterning strategies are also noteworthy because they provide some tunability in terms of substrate mechanical properties. Interestingly, Biswas et al. previously demonstrated the formation of stable AJ and cell spreading on a SLB without micropatterns [78]. In this case, the SLB contained lipids with a bulky dye moiety, resulting in a bilayer of higher viscosity. Their study was also notable because, unlike in the case of FAs, the presence of diffusion barriers in a fluid SLB was insufficient to result in the formation of AJs, indicating the significance of long-range movements of cadherins during AJ formation [150]. Taken together, the described applications illustrate the significance and versatility of SLBs as an artificial cell substrate [133]. Moreover, it should be emphasized that key aspects of vesicle/cell adhesion on ligand-functionalized SLBs are also applicable to other cell surface mimetics with laterally mobile ligands, such as PTLBs discussed in the next subsection.

2.2.13 Polymer-Tethered Lipid Bilayers (PTLBs)

Polymer-supported lipid bilayers have been introduced to overcome the limitations of SLBs for the study of transmembrane proteins [14]. Their hallmark is the presence of a soft polymer layer underneath the lipid bilayer, causing the lift up of the bilayer from the underlying solid substrate. Depending on the type of fabrication method and polymer system used, the addition of the polymer layer can result in bilayer substrate distances of 5–100 nm, making these model membranes suitable as experimental platforms for the analysis of transmembrane proteins. However, the assembly of polymer-supported membranes is usually more complex than the previously described fabrication of SLBs. In fact, great care should be taken in the selection of the polymer, lipid bilayer composition, and surface chemical properties of the solid substrate to build a thermodynamically stable polymer-supported lipid bilayer. One key requirement of a successful fabrication method is the ability of the selected polymeric material to form a continuous, defect free thin film on the solid substrate proteins [14, 151]. Moreover, the surface properties of the

polymer film should allow the reliable attachment of a lipid bilayer, resulting in a stable polymer-supported lipid bilayer system. In addition to these stability requirements, the chosen polymeric material should also fulfill other important functional roles. Most obviously, the polymer should be hydrophilic to maintain an aqueous reservoir between bilayer and solid substrate. Finally, it is beneficial to employ a polymer with chemically inert bulk properties to minimize unwanted perturbations on the functionality of reconstituted membrane proteins.

One limitation of artificial phospholipid bilayers, as found in liposomes and SLBs, is that they are substantially softer than cellular membranes, making them rather poor biomembrane mimetics in terms of their elastic properties [152, 153]. This limitation can be partially overcome in polymer-supported membrane systems, whose mechanical properties are more similar to those of cellular membranes. Valuable information about mechanical properties of polymer-supported membranes was obtained using the surface forces apparatus (SFA) [154]. These experiments revealed that the presence of the polymer cushion in the membrane system leads to the presence of long-range interaction forces. Moreover, the SFA data showed that the cushion elasticity can be modeled using a simple spring model [154].

Another important aspect represents the tunability of mechanical properties in polymer-supported membranes. For example, lipopolymers in a PTLB not only provide membrane stabilization and enable adjustment of obstructed lipid/protein diffusion, but also allow controlled modification of membrane elasticity. Mean-field calculations previously showed that bilayer bending modulus and compressibility in such membrane systems can be regulated by both the density of polymer-tethered lipids and the molecular weight of tethered polymer chains [155, 42]. Exemplarily, the bending modulus of a red blood cell of 50 kBT was found to be comparable to that of a polymer-tethered lipid bilayer containing 5 mol% of the poly(ethylene oxide) lipopolymer DSPE-PEG5000, whereas a corresponding membrane system with 20 mol% DSPE-PEG5000 resulted in a bending modulus of 400 kBT, comparable to that of *Dictyostelium discoideum* (wild type) [156, 157]. The ability to modify membrane elastic properties in liposomes by incorporation of lipopolymers was confirmed experimentally using the micropipette technique [158].

Interestingly, it was also demonstrated that elevated concentrations of lipopolymers lead to membrane buckling, a stress relaxation phenomenon, in physisorbed polymer-tethered monolayer and bilayer systems without exhibiting phospholipid-lipopolymer phase separation (Fig 6) [159]. Formation of a homogeneous bilayer was reported on top of a buckled polymer-tethered

lipid monolayer containing poly(2-methyl-2-oxazoline) lipopolymers. However, bilayer formation on top of buckled monolayer regions was precluded in the presence of the less hydrophilic poly(2-ethyl-2-oxazoline) and poly(ethylene oxide) lipopolymers, leading to the compartmentalization of the polymer-tethered membrane into 1–2 μm compartments at higher lipopolymer concentrations. FRAP using dye-labeled lipids and long-term tracking experiments using quantum dot-conjugated lipids confirmed that buckling-induced compartment boundaries act as diffusion barriers, causing length scale-dependent diffusion properties, with remarkable parallels to those found in plasma membranes. Buckling amplitude and width were previously analyzed as a function of lipopolymer concentration using EPI and atomic force microscopy (AFM). These data could be used to combine mean-field theory of a polymer-tethered membrane with buckling theory of an Euler column to derive a metric between experimentally determined buckling parameters and mechanical membrane properties (Fig 6c(i–k)) [160].

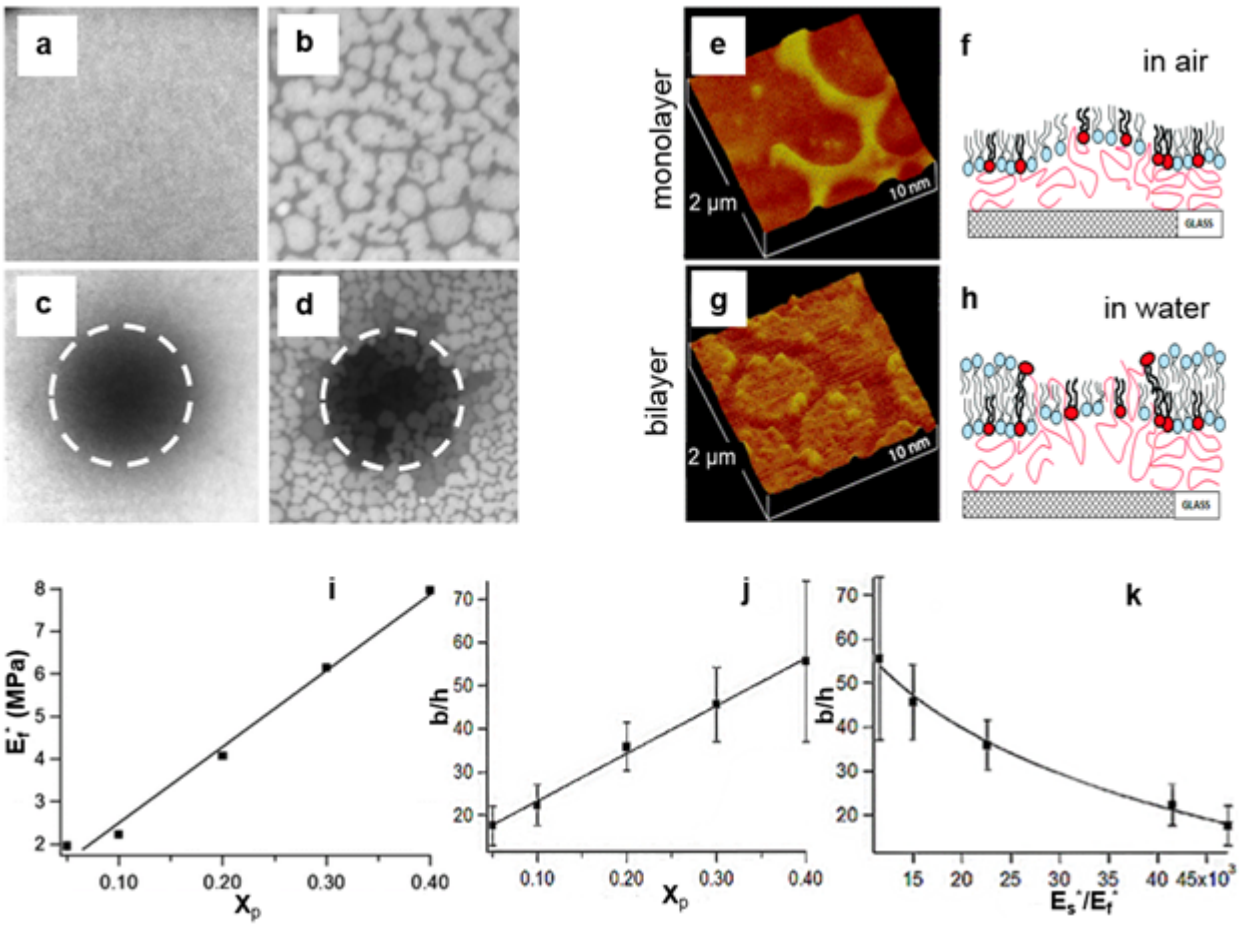

Figure 6. Lateral stress imposed by elevated concentrations of lipopolymers causes membrane buckling in physisorbed polymer-tethered monolayer and bilayer systems. (**a-b**) Impact of increasing lipopolymer concentrations on fluorescence micrographs of dye-labeled lipids in physisorbed PTLBs. Corresponding spot bleaching experiments reveal that dark areas act as lipid diffusion barriers (**c-d**). Atomic force microscopy data confirm formation of buckling structures in polymer-tethered lipid monolayer (**e**) and compartmentalization of polymer- tethered lipid bilayer (**g**). Model of lipopolymer-induced monolayer buckling (**f**) and compartmentalization of physisorbed polymer-tethered lipid bilayer (**h**), as derived from fluorescence and atomic force microscopy analyses. (**i-k**) Buckling structure information in combination with results from mean-field theory of polymer-tethered membranes and buckling theory of straight-sided blisters illustrate that variations in lipopolymer concentration lead to changes of elastic properties in a physisorbed polymer-tethered lipid bilayer. (**a-h**) were reprinted from [159] with permission from publisher. (**i-k**) were reprinted from [160] with permission from publisher.

The size-dependent diffusion properties in lipopolymer-containing PTLBs, suggest the potential suitability of these model membranes as artificial cell surface-mimicking substrates for

the analysis of cell spreading and migration. In this case, the PTLB contains a well-defined amount of reactive lipids, which serve as anchor sites for ligands. Adjustment of ligand density can be accomplished by controlling the molar concentration of reactive lipids in the bilayer of the cell surface mimetic. Previously it was reported that 3T3 fibroblasts, which are known for their ability to develop substantial pulling forces, readily adhere and spread on a physisorbed PTLB that is surface-functionalized with laminin ligands (attached to thiol lipids in the bilayer using a maleimide-NHS ester crosslinker molecule) [7, 8]. Minner et al. conducted several complementary experiments, which confirmed the integrity of the PTLB substrate in the presence of plated cells [8]. In one set of experiments, confocal spot bleaching of dye-labeled lipids in a laminin-coated PTLB underneath FA regions of plated 3T3 fibroblasts confirmed good fluorescence recovery, which was comparable to corresponding fluorescence recovery results obtained from cell-free PTLB regions (Fig 7 a–d). In another set of experiments, the cellular phenotype of 3T3 fibroblasts was compared 20 and 40 h after plating. These experiments determined a small, unchanged population of stress fiber-laden polygonic cells of<4%, a substantial reduction of crescent cell shapes from 44% (20 h) to 14% (40 h), and an increase of spindle-like cells from 18% (20 h) to 38 at (40 h), as well as an increase of dendritic phenotypes from 5% (20 h) to 18% (40 h). More importantly, no increase of stress fiber-forming cells was observed over time, confirming the inability of plated cells to directly bind to the glass substrate by penetrating through potential bilayer defects.

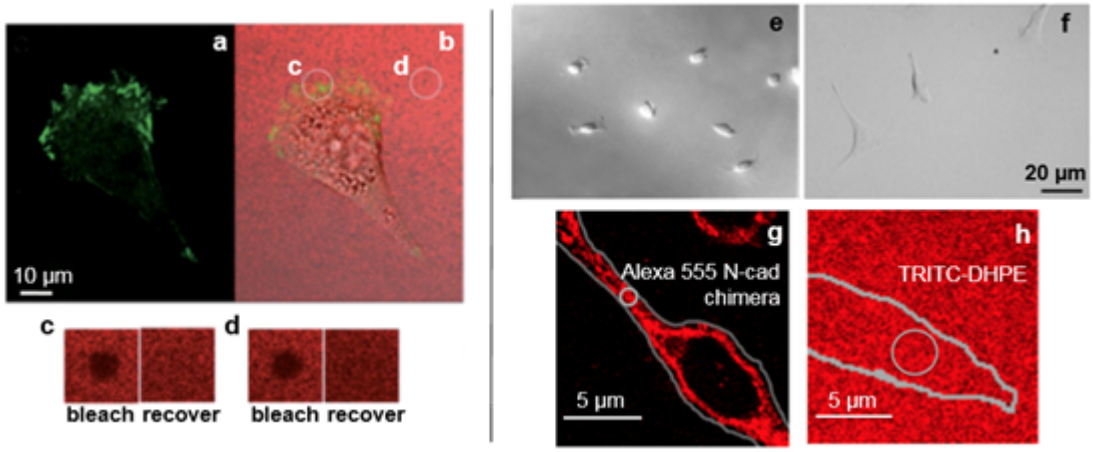

Figure 7. In this confocal experiment, FA regions were visualized using GFP-FAK (**a**), a marker of cellular FAs, and the integrity of the PTLB system was monitored using the dye-labeled lipid TR-DHPE, (**b**). Individual FRAP experiments were conducted underneath FA regions in (**c**) and outside cells in (**d**)**;** each area shows fluorescent lipid recovery after bleaching. C2C12 myoblasts are unable to spread on a linker-free PTLB (**e**), but display good spreading on a PTLB with N-cadherin linkers (**f**). Plated C2C12 myoblasts cause the accumulation of N-cadherin linkers in a PTLB (**g**), but have no influence on the homogeneous distribution of dye-labeled lipids (**h**) in such a planar membrane. Images in (**a-d**) were reprinted from [8], (**e-h**) were reprinted from [9].

While the above described experiments with 3T3 fibroblasts on laminin-coated PTLB systems confirmed the general suitability of PTLBs as engineered cell substrates, the ultimate potential of PTLBs as advanced cell surface mimetics was demonstrated more recently using C2C12 myoblasts on PTLB surfaces with embedded N-cadherin chimera [9]. In this sample architecture, individual His-tagged N-cadherin ectodomain constructs are directly conjugated to lipids with a Ni-chelator group in the PTLB. Unlike laminin ligands, which are able to crosslink [161], lipid-anchored N-cadherin chimera are free to diffuse in the PTLB, as verified by FCS autocorrelation analysis and PCH method. In contrast, clusters of lipid-anchored N-cadherin chimera, induced by binding of N-cadherin-functionalized fluorescent beads (size: 500 nm), were immobilized in the same membrane system, illustrating the size-dependent diffusion properties of PTLBs. Importantly, analysis of plated cells established that C2C12 myoblasts are able to adhere and spread on a PTLB with N-cadherin ligands, whereas cell spreading was efficiently suppressed on a corresponding ligand-free substrate (Fig 7 e) [9]. Confocal experiments demonstrated furthermore that dye-labeled N-cadherin chimera accumulate into larger cluster assembly's underneath C2C12 cells (Fig 7 g). These clusters are heterogeneously distributed, thereby

exhibiting enrichment at the periphery and extensions of adhering cells. Accompanying FRAP experiments determined a partial fluorescence recovery of N-cadherin chimera within such clusters of about 40%, in good agreement with similar results of cadherin diffusion in cellular adherens junctions [9]. While accumulation of mobile ligands into clusters at adhesion sites is a common feature during cell/vesicle adhesion on SLBs and PTLBs, which are both characterized by comparable lipid lateral mobility, the latter membrane system is distinct in its ability to enable accumulation of linkers into linker clusters without impairing cell spreading and migration. This peculiar behavior can be attributed to the size-dependent diffusion properties in PTLBs, enabling lateral diffusion of single lipids and other lipid-anchored molecules, but suppressing the mobility of corresponding molecular clusters.

Another potentially attractive feature of PTLBs as a cell surface-mimicking cell substrate was previously demonstrated by conducting a spatiotemporal analysis of dye-labeled N-cadherin chimera in the presence of plated C2C12 cells. These experiments revealed the long-range movement of N-cadherin clusters underneath migrating cells (Fig 8 a–e), thereby displaying remarkable parallels to corresponding movements of cellular contacts between polarized cells [108, 109, 9]. Because lipid-anchored N-cadherin clusters are unable to freely diffuse in a PTLB, their long-range movement underneath adhering cells should be attributed to cytoskeleton-induced cellular pulling forces. Consistent with this interpretation, formation and long-range movement of N-cadherin clusters was largely suppressed after addition of Blebbistatin, a myosin II inhibitor, illustrating the importance of the cytoskeleton of adhering cells in the observed cluster movement of N-cadherin chimera on the PTLB surface in Fig 8 f, g. Here cluster-tracking analysis revealed the Blebbistatin-induced slowdown and eventual dissolution of Alexa 555 labeled N-cadherin chimera clusters on the PTLB surface. Taken together, the described experiments of C2C12 myoblasts on N-cadherin-functionalized PTLBs demonstrate that this artificial cell substrate fulfills several important requirements for a cell surface mimetic, which include: (i) the free assembly of ligands into ligand clusters underneath cellular contacts and (ii) the ability of adhering cells to develop cellular tractions, enabling cell spreading and migration. Moreover, these substrates better replicate the long-range movements of adhesion clusters at cell-cell contacts than traditional polymeric films with chemically conjugated linkers. It should be mentioned that the application of PTLBs has not been limited to the characterization of 3T3 fibroblasts and C2C12

myoblasts. In another study, a similar membrane architecture was successfully employed to monitor different stages of neuronal network formation using a PTLB system [162].

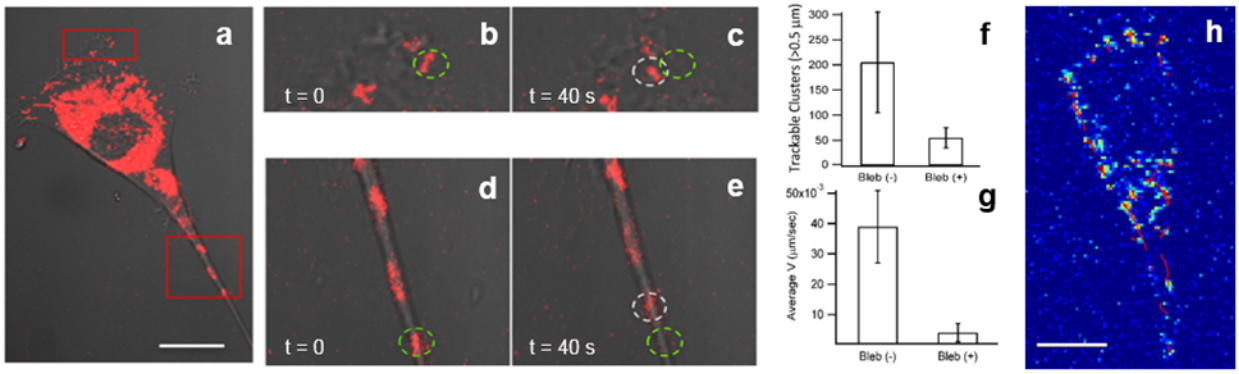

Figure 8. Spatiotemporal analysis of a PTLB functionalized with Alexa 555-labeled N-cadherin chimera illustrates accumulation of N-cadherin linkers into linker clusters (**a**). Cluster analysis reveals long-range movements of clusters underneath migrating cell (**b-e**). Blebbistatin treatment shows reduction of cluster size (**f**) and mobility (**g**). Cell depicted in (**h**), shows the tracking program used to analyze confocal imaging data, revealing cluster size, speed, and number from time lapse imaging. Figure was reprinted from [9]

Incorporation of polymer spacers, with a known concentration, has been shown to allow adjustment of frictional coupling between membrane proteins and the underlying solid substrate [163]. Another key signature of PTLBs is the presence of polymer-tethered lipids or polymer-tethered proteins in the bilayer. They not only play an important role in the stabilization of the PTLB, but also have a profound influence on the lipid diffusion properties of the bilayer. While there is a relatively weak size dependence of protein lateral diffusion in a free lipid bilayer [164], embedded polymer-tethered membrane constituents in the PTLB cause a substantially enhanced size dependence of lipid/protein diffusion properties. This effect can be best demonstrated in PTLBs comprised of phospholipids and lipopolymers, which allow a precise adjustment of polymer-tethered lipid (lipopolymer) concentration. Due to this ability, physisorbed polymer-tethered lipid bilayers comprised of phospholipids and lipopolymers have previously been introduced as an attractive model membrane platform for the quantitative characterization of obstacle-induced obstructed diffusion, a process challenging to characterize in cellular membranes (Fig 9 a). To study diffusion of membrane constituents, wide-field single molecule fluorescence microscopy experiments were conducted on dye-labeled lipids (TRITC-DHPE) and

bacteriorhodopsin (monomeric mutant W80i) in physisorbed PTLBs of varying lipopolymer concentration (Fig 9 b) [16].

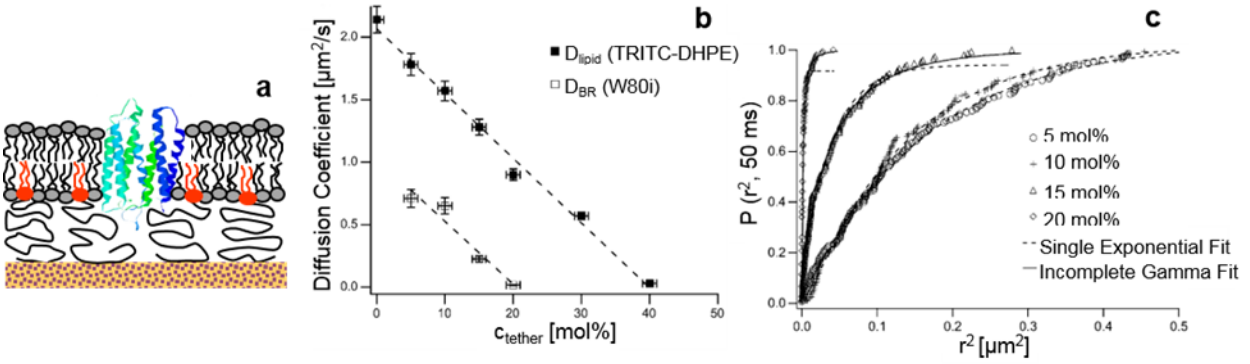

Figure 9. Schematic of a physisorbed PTLB (**a**), which contains a well-defined concentration of lipopolymers in its inner leaflet. This model membrane architecture allows the incorporation of transmembrane proteins, such as bacteriorhodopsin. (**b**) Impact of lipopolymer molar concentrations, described by tether concentration, c_{tether}, on the lateral diffusion of phospholipids (TRITC- DHPE) and the monomeric bacteriorhodopsin mutant (W80i). (**c**) Cumulative distribution function analysis of single molecule tracking data shows Brownian lipid diffusion at lower lipopolymer concentration, but anomalous lipid diffusion at elevated tethering densities. Reprinted from [16]

These single molecule-tracking experiments confirmed that, due to the presence of lipopolymers, the lateral diffusion of both TRITC-DHPE, located in the bottom (lipopolymer-containing) leaflet of the bilayer, and the bilayer-spanning W80i mutant are well described by that in a percolating system with distinct percolation thresholds. Moreover, lipid diffusion data were determined to be in good agreement with a free area model of obstructed diffusion, suggesting repulsive interactions between lipid tracers and tethered lipids. Comparison of lipid tracking data with Monte Carlo simulations also showed that lipopolymers in the bottom leaflet of the bilayer behave like immobile obstacles. Furthermore, cumulative distribution function (CDF) analysis indicated Brownian lipid diffusion at low to medium lipopolymer concentration, but anomalous lipid diffusion at elevated tethering densities. (Fig. 9 c) These CDF data suggest the random distribution of lipopolymers in the PTLB at lower tethering and the assembly into small lipopolymer aggregates at higher tethering concentration. It should be noted that reported diffusion data may depend on multiple factors, including the chemical nature of the polymer, the viscosity and thickness of the polymer layer, and the type of linkage between polymer chains and solid

substrate. For example, there have been reports where no notable obstruction of lipid diffusion over a limited concentration of lipopolymers with reactive groups was observed [165].

Leaflet-specific tracking experiments of TRITC-DHPE revealed that lipopolymers in the bottom leaflet of a physisorbed PTLB also cause obstructed lipid diffusion in the opposite (lipopolymer-free) leaflet of the bilayer, indicating a strong interleaflet coupling of obstructed diffusion [166]. Here TRITC-DHPE tracking experiments in the top leaflet of the bilayer mirrored those obtained in corresponding inner leaflet studies, displaying again Brownian diffusion behavior at low to medium lipopolymer concentrations and anomalous diffusion at elevated lipopolymer content (Fig 10 a). Strong interleaflet coupling of obstructed TRITC-DHPE diffusion was observed regardless of variations in polymer moiety [poly(ethylene glycol), poly(2-methyl-2-oxazoline), and poly(2-ethyl-2-oxazoline)] of lipopolymers. Systematic analysis of lipid tracking data in terms of the parameter λ, which simply describes the ratio of mean-square-displacement values of TRITC-DHPE from tracking experiments in the inner vs outer monolayers, provided valuable insight into the strength of coupling of obstructed lipid diffusion (Fig 10 b). This analysis demonstrated that the coupling of obstructed lipid diffusion depends on the molecular weight of the polymer moiety of lipopolymers, but remains largely unchanged by a variation of lipopolymer concentration, c_{tether}, at least, within a range of $0 \leq c_{tether} \leq 20$ mol%.For example, a strong interleaflet coupling of obstructed lipid diffusion was observed for the longer chain poly(2-ethyl-2oxazoline) [DODA-E_n (n=85)] and poly(2-methyl-2-oxazoline) [diC18-M_n (n=50)] lipopolymers. In contrast, reduced coupling of obstructed diffusion, comparable to that found in a SLB, was observed with shorter chain versions of both types of lipopolymers [DODA-E_n (n=35) and diC18-M_n (n=15)]. In light of existing theoretical work on the problem of bent membranes around pinning sites [167-171], the observed interleaflet coupling of obstructed lipid diffusion was attributed to polymer-induced bilayer deformations around membrane pinning sites (Fig 9 c). Indeed, such a scenario is supported through results from control tracking experiments on physisorbed polymer-tethered lipid bilayers containing phospholipids and cholesterol, which demonstrated that increased bilayer bending stiffness, through addition of cholesterol, leads to reduced interleaflet coupling of obstructed TRITCDHPE diffusion [16]. Distinct bilayer morphologies presumably also explain the observed differences in obstructed diffusion and coupling of obstructed diffusion of lipids between physisorbed and chemisorbed polymer-tethered lipid bilayers [165, 16, 166].

Interestingly, strong interleaflet coupling of obstructed lipid diffusion was also determined after polymer adsorption to the top leaflet of a SLB [172]. In this case, the diffusion data were explained using a model of slaved diffusion, where a membrane bound polymer moiety, lipids underneath this moiety and the lipids in the bottom leaflet show the same diffusion [173].

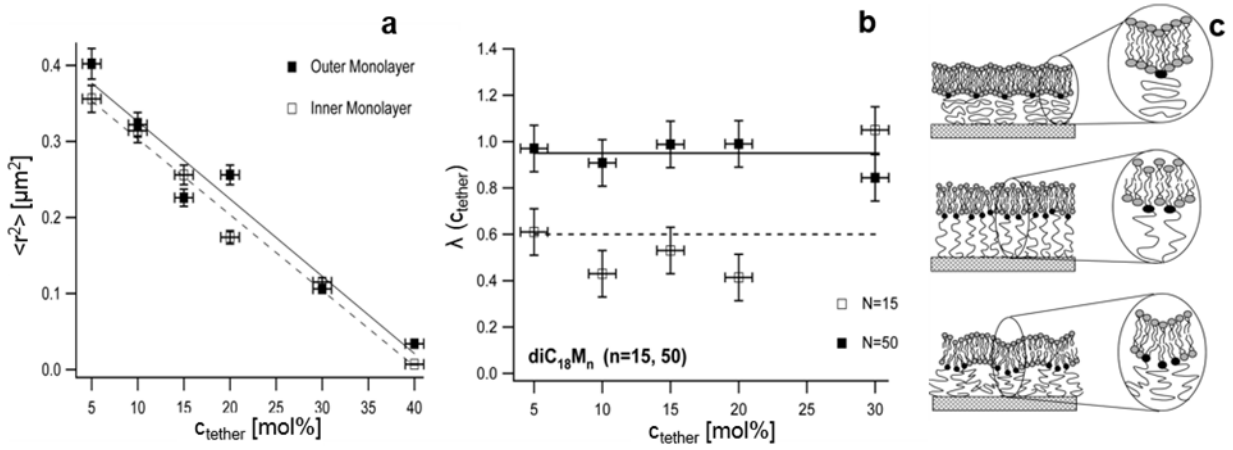

Figure 10. Leaflet-specific tracking experiments of dye-labeled lipids, shown in (**a**), reveal a strong coupling of obstructed lipid diffusion in a physisorbed PTLB. Lipid tracking data are presented as mean- square displacement ($<r^2>$) vs tethering concentration (c_{tether}). (**b**) Comparison of inner and outer leaflet lipid tracking data (through coupling parameter λ) demonstrates strong inter-leaflet coupling for longer polymer chain lipopolymers ($diC_{18}M_{50}$) and reduced coupling for shorter polymer chain lipopolymers ($diC_{18}M_{15}$). (**c**) Strong inter-leaflet coupling of obstructed lipid diffusion has been attributed to polymer-induced deformations of the bilayer around tethering points. Reprinted from [174].

2.2.14 Adjusting Substrate Mechanical Properties in PTLBs

It is well known that anchorage-dependent cells have a preference for a specific set of mechanical properties in the microenvironment. To explore properties of cellular mechanosensitivity, one attractive experimental strategy has been the development of cell motility assays using polymeric substrates with an elasticity gradient [98]. For example, various fabrication methods for the design of polymer thin films with gradients [175] and sharp boundaries in particular polymer properties [176, 177] have been reported. In contrast to polymeric films, traditional SLBs cannot be built with static elasticity gradients. An interesting exception represents a planar lipid bilayer, which contains heterogeneously distributed polymerizable lipids, resulting in a SLB with region-specific lipid diffusivity [178]. Another promising technology that can be

applied to create patterned PTLBs represents the incorporation of nanopatterns of biomolecules using nanoparticle arrays [149].

Previously, patterning strategies have also been reported for PTLBs [179]. In one case, PTLBs have been built, which are characterized by a sharp boundary between regions of low (no buckling structures) and high (with buckling structures) lipopolymer concentrations (Fig 11 a). Such a patterned PTLBs can be accomplished by regulating the phospholipid-lipopolymer mixing ratio at the air-water interface and by conducting partial LB transfers at altered lipopolymer concentrations. In another patterning strategy, a lateral tethering (elasticity) gradient was achieved by regulating the phospholipid-lipopolymer mixing ratio at the air-water interface prior to LB transfer and by subsequent transfer of the polymer-tethered membrane to the solid (glass) substrate (Fig 11 b).

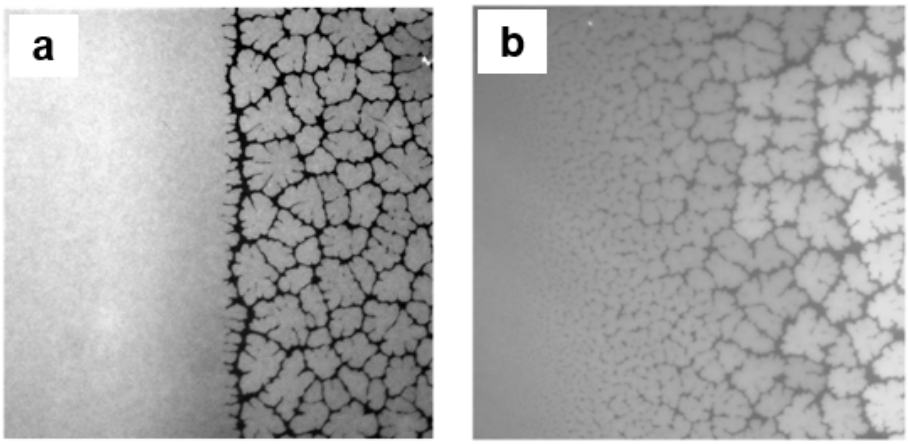

Figure 11. Controlled adjustment of the lateral distribution of lipopolymers enables fabrication of patterned PTLB systems. Such adjustments may lead to the formation of a sharp boundary between regions of low (no buckling structures) and high (with buckling structures) lipopolymer concentrations (**a**). Alternatively, PTLBs with a lateral gradient in tethering concentration can be achieved (**b**). Results reprinted from [179].

As shown in Fig 11, membrane patterns can be visualized on the basis of membrane buckling structures at elevated lipopolymer concentrations. An attractive feature of such patterned substrates is that, due to the physisorption of lipopolymers at the glass surface, resulting patterns and gradients of lipopolymers remain static. This allows the design of PTLBs with exciting properties, including gradual changes in length scale dependent lipid diffusivity and membrane elasticity. An important benefit of patterned PTLBs is the ability to modify a single parameter in

a multivariate environment and to study the system's response to changes of this single parameter. Another interesting patterning strategy represents the controlled formation of stripe phases in polymer-tethered lipid bilayers comprised of lipids and lipopolymers, in which stripe formation was controlled through changing LB transfer conditions [180].

In addition to the above described patterning methods, patterning strategies, developed for SLB, should also be applicable to PTLB. In particular to *bottom-up* fabrication method of PTLB should it make feasible to build compartmentalized PTLB on substrates with engineered patterned grids using photoresist, aluminum oxide, or gold on oxidized silicon substrates [143, 181, 182] This capability was previously demonstrated by Waichman et al. who showed that the technique of creating patterned membranes can be extended to polymer-supported systems. [183]. They employed their patterned substrate to create membrane corrals, in which diffusion properties of individual transmembrane receptors could be studied [183].

Previous advancements in the understanding of cellular mechanosensitivity have been closely linked to the development of engineered cell substrates which allow the controlled adjustment of substrate stiffness. Similarly, substrate mechanical properties in a single PTLB can be altered by changing the concentration of polymer-tethered lipids in the bilayer. Tunable material properties illustrate the potential of PTLBs to serve as cell surface-mimicking materials for the analysis of cellular mechanosensitivity. The impact of such lipopolymer adjustments on properties of plated cell is shown in Fig 11. Specifically, the micrograph in the upper left of Fig 12 illustrates the spreading of GFP-actin transfected 3T3 fibroblasts on a single, laminin-coated PTLB substrate, which is characterized by a sharp boundary (yellow dashed line) between regions of high (left side) and low lipopolymer concentrations (right side). It demonstrates that elevated lipopolymer concentrations lead to: (i) increased cell spreading areas and (ii) more pronounced actin stress fibers. As depicted in the histogram in the bottom left of Fig 12, increased cell spreading can also be observed on homogeneous PTLBs of gradually increasing lipopolymer concentrations. The observed cell behavior in Fig 12 correlates well with the known impact of lipopolymer concentration on film elasticity in a single PTLB [179]. The micrograph in the upper left of Fig 12 also illustrates the ability to combine single PTLBs with membrane patterning strategies [179].

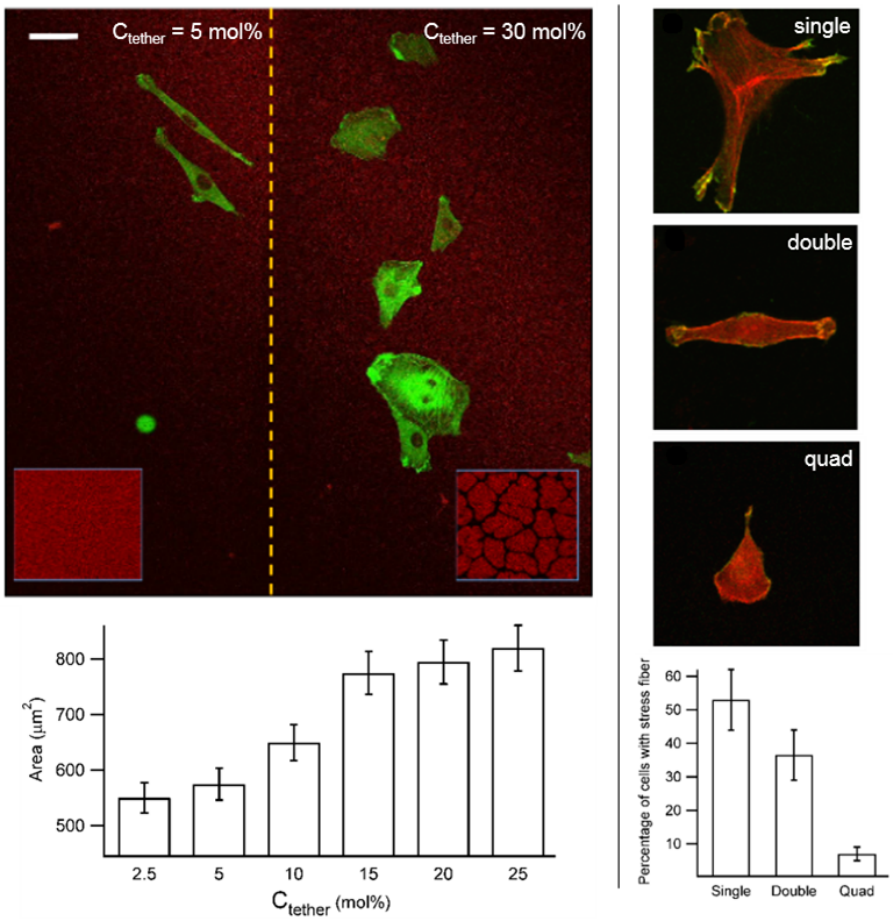

Figure 12. Cell spreading area depends on concentration of lipopolymers in a single PTLB, as illustrated on a patterned PTLB with sharp boundary (micrograph in upper left), illustrated by the yellow dashed line, between regions of high (right side) and low (left side) tethering concentrations (insets illustrate differences in membrane buckling). Gradual increase of lipopolymer concentration (c_{tether}) causes an increase in cell spreading area in single PTLB, histogram shown in bottom left. Immunofluorescence micrographs show substantial differences in cell spreading, actin organization (red channel), and β-catenin (green channel) distribution on N-cadherin-functionalized PTLB systems with one to four bilayers in a stack. These changes in bilayer stacking have a profound impact on the population of stress fiber-forming cells (histogram shown in bottom right). Data shown on the right were reprinted from [9].

In addition to single PTLBs, polymer-tethered lipid multi-bilayers have emerged as an alternative planar model membrane platform. Multi-bilayer stacking provides a viable pathway for the fabrication of planar model membranes, which are less influenced by the underlying solid substrate than SLBs. Previously, several different approaches of supported lipid double bilayer formation have been reported. Kaizuka and Groves described the formation of double bilayers by fusing GUVs containing negatively charged glycolipids or anionic lipids, respectively, to a SLB

containing cationic lipids [184]. Alternatively, double bilayer formation was accomplished by linking two lipid bilayers, which are partly comprised of cationic lipids and DNA duplexes, respectively [185], as well as through DNA hybridization [186]. However, in these cases, there were either uncertainties about the DNA orientation and associated inter-bilayer distance or the double bilayer system showed limited stability. In contrast, formation of a stable double bilayer system was achieved by using biotin-streptavidin or NHS/EDC coupling strategies [187, 188].

Our group previously reported an alternative approach of multibilayer fabrication [189]. In this case, a single PTLB containing phospholipids and lipopolymers was first assembled using the LB/LS method and additional bilayers were attached by addition of GUVs containing a portion of membrane constituents with either thiol or maleimide functional groups. This strategy allows the formation of stable interbilayer linkages in the polymer-tethered lipid multi-bilayer stack. Notably, the described multi-bilayer assembly method was not limited to the fabrication of a double bilayer system, but also included the assembly of stable stacks containing three and four bilayers. Here the layer-by-layer assembly can be considered conceptually similar to the assembly of polymer multilayers using oppositely charged polyelectrolytes [190]. Fluorescence microscopy demonstrated that bilayers within the stack are free of optically visible defects and show good stability [189]. They were found to be durable over a time period of at least 48 h. Complementary AFM experiments showed furthermore that the stacking of multiple bilayers also changes bilayer morphology, leading to less planar bilayers with increasing bilayer-substrate distance [7]. Changes of morphology with bilayer number were also reported elsewhere [191]. AFM analysis also revealed the occasional formation of small, sub-optical resolution size bilayer defects, which presumably were caused by membrane-penetrating polymeric chains [192].

Like single PTLBs, polymer-tethered lipid multi-bilayers also allow the controlled adjustment bilayer fluidity. However, the GUV assembly of the latter membrane system, which limits the range of accessible lipopolymer molar concentrations [155], makes modification of bilayer fluidity by variation of lipopolymer concentration impractical. Instead, the lipid lateral diffusion in a polymer-tethered lipid multi-bilayer system of ~50–200 A thickness can be adjusted by the number of bilayers in the stack. Indeed, systematic lipid tracking experiments in a single polymer-tethered lipid bilayer and the top bilayer of corresponding double, triple, and quadruple bilayer stacks using wide-field single molecule fluorescence microscopy (SMFM) demonstrated a gradual increase of lipid diffusion with increasing degree of bilayer stacking [7]. Because the

concentration of 5 mol% tethered lipids in these multi-bilayer stacks was previously shown to have no significant influence on obstruction of lipid diffusion [16, 166], the observed diffusion changes could largely be attributed to changes in substrate-bilayer distance, characterized by distinct degrees of frictional coupling between bilayer and underlying solid [193].

Due to the presence of polymer-tethered lipids, polymer-tethered lipid multi-bilayers are also characterized by size-dependent diffusion properties. This feature was previously demonstrated on a polymer-tethered multi-bilayer system, which contained lipid-anchored N-cadherin constructs in its top bilayer [9]. In this case, confocal fluorescence correlation spectroscopy (FCS) experiments showed good lateral mobility of individual N-cadherin constructs in the top bilayer of polymer-tethered multi-bilayer stacks. In contrast, clusters of N-cadherin constructs, induced through adsorption of N-cadherin-functionalized fluorescent beads of 500 nm size, were found to be completely immobilized in the same membrane system. In contrast, similar changes in probe size have substantially less influence on probe diffusivity in a viscous SLB without polymer-tethered lipids [194]. Consistent with the observation of immobilized N-cadherin-coated beads on a polymer-tethered lipid bilayer system with N-cadherin linkers, a predominantly elastic materials response was previously reported in magnetic tweezer microrheometer experiments of laminin-coated superparamagnetic beads, which are bound to the surface of polymer-tethered single and multi-bilayer systems via laminin-laminin linkages [7]. One important outcome from these magnetic tweezer experiments was that elastic compliance does change with an increasing degree of stacking, illustrating the potential suitability of such membrane systems for the analysis of cellular mechanosensitivity. Interestingly, these experiments also showed that the crosslinked laminin coating on the multi-bilayer surface partly contributes to the overall bead response. The latter finding suggests that cellular tractions on laminin-coated polymer-tethered multi-bilayer systems should, at least in part, be attributed to the presence of the crosslinked laminin layer on the surface of the cell surface mimetic.

Polymer-tethered multi-bilayers can also be applied as cell substrates for cellular mechanosensing studies. It has been shown that diffusion and mechanical properties in such multi-bilayer systems can be modified by altering the number of bilayers in the polymer-tethered multi-bilayer stack [7]. While diffusion experiments confirmed increases in lipid diffusivity with increasing stacking [8], corresponding bead rheology measurements established that such adjustments of bilayer number reduce the stiffness of the multi-bilayer substrate [7]. The observed

tunable properties have been attributed to the intricate coupling phenomena in polymer-tethered multi-bilayer systems, which include strong interleaflet coupling of immobilized membrane constituents, coupling of obstructed diffusion, and coupling by lipopolymer-mediated inter-bilayer connections [192, 173, 166].

To test the suitability of polymer-tethered lipid multi-bilayers for the analysis of cellular mechanosensitivity, properties of 3T3 fibroblasts were previously analyzed on such membrane systems containing laminin ligands [7]. In these experiments, cell spreading area was found to show a statistically significant ($p < 0.05$) inverse correlation with the elastic compliance of the substrate, meaning that cell area decreases with increasing number of bilayer stacks. Interestingly, changes in bilayer stacking between single and quadruple bilayer systems had a similar impact on cell spreading area, as variations in substrate stiffness between 4% and 6.1% PAA gels.

Several groups have previously reported phenotype transitions in 3T3 fibroblasts in response to substrate elasticity and in all cases, cells have displayed rounder shapes, and at times an increased tendency to form cellular extensions when plated on softer hydrogel substrates [195, 99, 101]. Similarly, experiments on laminin-functionalized polymer-tethered single and multi-bilayer systems have demonstrated that 3T3 cells alter their phenotype as a function of bilayer stacking [8]. These experiments also determined that changes in bilayer stacking affected cytoskeleton organization as well. On laminin-coated glass, EPI micrographs of 3T3 fibroblasts predominantly showed polygonic and crescent shapes, a typical cellular response to a rigid substrate. On single bilayer substrates, the overall number of cells with static stress fibers was greatly reduced and cortical actin structures emerge; however, the overall cellular phenotype distribution is similar to the phenotypes on glass. On double bilayer substrates, these stress fiber-laden shapes are almost completely replaced with polarized phenotypes exhibiting lamellipodium-like regions at one end and stretched processes at the opposite end. Here, cells take on more spindle-like shapes and show an enhanced ability to form dendritic-like extensions, and typically display a meshwork of cortical actin structures evenly distributed throughout the cell with short, radially-oriented actin bundles at the leading edge. On quadruple bilayers, spindle-like shapes become most prevalent and their stretched processes span distances of up to 50 μm. The fraction of cells showing these processes increases with bilayer stacking: on single bilayers only 22% of the cells show extensions of >5 μm but this value increases to approximately 39% and 57% on double and quadruple bilayer systems, respectively [8]. Moreover, comparison of these results

with microrheology data of cell-bound superparamagnetic beads show that the stiffness of cells plated on polymer-tethered lipid multi-bilayers decreases with increasing number of bilayers in the multi-bilayer stack [7]. These results demonstrate a direct correlation between substrate stiffness and the extent of cellular stress fiber formation [7].

More recently, the functionality of polymer-tethered multi-bilayers for the characterization of cellular mechanosensitivity has also been tested on C2C12 myoblasts, which are bound to the biomembrane-mimicking substrate via N-cadherin linkages [9]. In good agreement with results obtained on laminin-coated PTLB systems, changes in bilayer stacking have a notable impact on both cell morphology and cytoskeletal organization (Fig 12). Myoblasts on single bilayer architectures frequently display polygonic morphologies with well-developed ventral stress fibers spanning the entire cell, whereas those on multi-bilayer substrates lack visible actin stress fibers and show less pronounced AJ formation. Furthermore, analysis of β-catenin, an AJ marker, demonstrates that changes in bilayer stacking influence AJ formation. Consistent with these findings, the population of stress fiber-forming cells decreases with increasing numbers of bilayer in the stack.

CHAPTER 3. MATERIALS AND EXPERIMENTAL PROCEDURES

3.1 Materials

3.1.1 Phospholipid Membrane Materials

Lipids including 1-palmitoyl-2-oleoyl-sn-glycero-3-phosphocholine (POPC), 1,2-dioleoyl-sn-glycero-3-phosphocholine (DOPC), 1,2-dioleoyl-sn-glycero-3-[(N-(5-amino-1-carboxypentyl)iminodiacetic acid)succinyl] Ni^{2+} salt (DGS-NTA), 1,2-dipalmitoyl-sn-glycero-3-phosphothioethanol Na^{+} salt (DPTE), 1,2-dioleoyl-sn-glycero-3-phosphoethanolamine-N-biotinyl Na^{+} salt (Biotin-PE) were purchased from Avanti Polar Lipids (Alabaster, AL) stored at -20 °C and used without further modification or purification. (N-(6-tetramethylrhodaminethiocarbamoyl)-1,2-dihexadecanoyl-sn-glycero-3-phosphoethanolamine, triethylamonium salt (TRITC-DHPE) fluorescently labeled lipid was purchased from Invitrogen (Eugene, OR). Fluorescently labeled lipids (N-(7-nitrobenz-2-oxa-1,3-diazol-4-yl)-1,2-dihexadecanoyl-sn-glycero-3-phosphoethanolamine, triethylammonium salt (NBD-PE) were purchased from Avanti Polar Lipids (Alabaster, AL). Glass coverslips size 24 x 40 mm, No. 1.5 were purchased from Fisher Scientific (Pittsburgh, PA) and 24 x 40 mm, No. 1 from VWR Scientific (Radnor, PA). Cleaning solutions for the preparation of glass coverslips included sodium dodecyl sulfate (SDS) (Sigma-Aldrich; St. Louis, MO), sodium hydroxide, methanol (HPLC grade), and hydrochloric acid were purchased from Fisher Scientific (Pittsburgh, PA). Ultrapure water filtered to a resistivity of 18.2 MΩ·cm was used for all work with phospholipids and was obtained from a Barnstead E-Pure purification system (Thermo Scientific; Marietta, OH).

3.1.2 Polymer Gel Support Materials

Glass coverslips were silanized with a solution of allyltrichlorosilane (ATCS) (Acros Organics; Geel, Belgium) and triethylamine (Sigma-Aldrich; St. Louis, MO) in HPLC grade chloroform (Fisher Scientific; Fair Lawn, NJ). Acrylamide monomers and crosslinkers were mixed in the desired proportions from 40% acrylamide solution and 2% bis-acrylamide (Fisher Scientific; Fair Lawn, NJ). For the polymerization of acrylamide, chemical initiators were purchased from Sigma-Aldrich (St. Louis, MO) and included ammonium persulfate and N,N,N',N'-

tetramethylethylenediamine (TEMED). Polystyrene carboxylated micron sized spheres (Polysciences, Inc.; Warrington, PA) were used as spacers to control the thickness of the hydrogel layer according to a previously established protocol [196]. To synthesize a biotinylated polyacrylamide hydrogel, sulfosuccinimidyl-6-[biotin-amido]hexanoate (sulfo-NHS-LC-biotin) (Pierce Biotechnology; Rockford, IL) and allylamine (Acros Organics; Geel, Belgium) were used. Crosslinker molecules obtained from Pierce Scientific (Rockford, IL) included sulfosuccinimidyl-6-[4'-azido-2'-nitrophenylamino]hexanoate (sulfo-SANPAH) and N-(γ-maleimidobutyryloxy)sulfosuccinimide ester (sulfo-GMBS). Proteins used included fibronectin (EMD Millipore Corp.; Temecula, CA), streptavidin and neutravidin DyLight 488 conjugated (Invitrogen; Rockford, IL), and streptavidin FITC conjugated (BioLegend; San Diego, CA). For membranes directly crosslinked to the supporting polyacrylamide hydrogel, a heterobifunctional pegylated crosslinker from Nanocs (New York, NY) with maleimide and amine functionalities was used.

3.1.3 Cell Culture Materials

C2C12 myoblasts were obtained from American Type Culture Collection (ATCC) and cultured according to normal protocol published by ATCC. Dulbecco's Modification of Eagle's Media (DMEM) powder cell growth media with 4.5 g/L glucose, L-glutamine, sodium pyruvate (GIBCO; Grand Island, NY), and sodium bicarbonate (Fisher Scientific; Fair Lawn, NJ) was used for subculturing. Trypsin (1x) was purchased from Grand Island Biological Company (Grand Island, NY) and used without any modification or dilution. Phosphate buffer solution (PBS) for cell washing was diluted from a 10x stock purchased from Fisher Scientific (Fair Lawn, NJ). All disposable plastic materials for cell culture, including culture flasks, serological pipets, centrifuge tubes, and pipet tips, were obtained from Fisher Scientific (Fair Lawn, NJ). For the plating of cells to polymer gel-supported bilayers, N-cadherin chimera with a histidine-tag from R&D Systems (Minneapolis, MN) was labeled with a protein labeling kit from Invitrogen (Eugene, OR).

3.2 Experimental Procedures

3.2.1 Langmuir Film Preparation: LB and LS Transfers

Following established procedures to prepare solid supported lipid bilayers, a method utilizing a Langmuir trough was used to transfer lipids to glass support and polyacrylamide hydrogel substrates. To prepare solid supports, glass coverslips were placed in an oven at 515 °C for a minimum of 30 minutes, this process efficiently produces glass with a highly hydrophilic surface. Next, slides were cleaned with solutions of 1% (w/w) sodium dodecyl sulfate (SDS) in milli-Q water, saturated sodium hydroxide in methanol, and 0.1% hydrochloric acid in milli-Q water. For each of the cleaning solutions, slides were immersed and placed in a bath sonicator for 30 minutes followed by several rinses with milli-Q water. After all cleaning steps were completed, slides were stored in milli-Q and used within one week.

To form a monolayer of lipids on a glass support or polyacrylamide hydgrogel, a Langmuir trough equipped with a mechanical dipper arm was used to complete a Langmuir-Blodgett (LB) transfer. A trough system (KSV-Nima) with a Teflon coated surface was cleaned according to manufacturer's suggested procedure by adding chloroform to trough and manually cleaning all surfaces of the trough, followed by several washes with milli-Q water. For lipid transfers, milli-Q water was used to fill the trough and the known surface tension of the water (72 mN/m at 25 °C) was used to calibrate the surface tension sensing element. After calibrating the surface tension, a solution of lipids dissolved in chloroform was carefully added to the top surface of the water, after a few minutes to allow chloroform solvent to evaporate away, the lipids were compressed to a smaller surface area until the desired surface tension was reached, in these experiments a pressure of 30 mN/m was used. After compressing for several minutes, the dipper arm was activated to bring the glass coverslip vertically through the water, during this process a single layer of lipids was transferred to the glass coverslip. These monolayers on glass are stable in air and can be used as a base for subsequent transfers to complete a water stable lipid bilayer. One method of completing a lipid bilayer is the Langmuir-Schaefer (LS) transfer, which utilizes a horizontal transfer. The Langmuir-Schaefer method is completed as follows, a monolayer of lipids is spread on the Langmuir trough and compressed to the desired surface tension of 30 mN/m, then the substrate with the LB layer is pressed through the monolayer of lipids on the trough forming a lipid bilayer. Benefits of the LB/LS method of forming bilayers is the ability to control the exact

lipid composition of the bilayer, even control over leaflet specific lipid composition, and the ability to incorporate lipopolymer molecules to high concentrations.

3.2.2 Vesicle Preparation

Lipid vesicles were used to form bilayers on top of hydrogel supports and vesicle solutions were prepared following a common protocol. A lipid mixture of POPC and 5 mol% functional lipids, selected based on the linking chemistry being used, were placed under a flow of nitrogen gas for 20 minutes to remove the bulk of the solvent. The dried lipid film was then placed in a vacuum chamber overnight to remove any residual solvent. Lipid film was then resuspended into aqueous solution of 150 mM sodium chloride (NaCl) to a concentration of 3-5 mg/mL and sonicated with a rod sonicator for 50 minutes at 31% amplitude with a pulse setting of 15 seconds on and 3 seconds off. After sonication, centrifugation was used to separate small vesicles from large vesicles and multi-lamellar vesicles. First, the vesicle solution was centrifuged at 14,000 rpm for 15 minutes, supernatant removed and subsequently centrifuged at 40,000 rpm for 50 minutes with the temperature held at 4 °C. Once again, the supernatant was removed and stored at 4 °C for less than 2 days prior to use.

3.2.3 Hydrogel Support Fabrication

Polymer gel-tethered lipid bilayers (PGTBs) were fabricated by the formation of a stable polyacrylamide hydrogel of adjustable stiffness and then the functionalization of the hydrogel to allow the formation of a covalently tethered lipid bilayer. To begin, glass coverslips were placed in an oven at 515 °C for a minimum of 30 minutes, followed by immersion in a solution of 0.1% (v/v) allyltrichlorosilane and 0.1% (v/v) triethylamine in chloroform solvent for 15 minutes. After the silanization reaction, the glass coverslips were hydrophobic due to the nature of the surface chemical groups from the allyltrichlorosilane leaving an exposed alkene group. These silanized coverslips were then used as the support for the formation of a polyacrylamide hydrogel.

Polymerization of acrylamide was completed with a protocol routinely used to form hydrogel slabs for separating proteins in polyacrylamide gel electrophoresis. The stiffness of the polyacrylamide hydrogels can be controlled by manipulating the total concentration of acrylamide and bis-acrylamide molecules, with a greater combined concentration increasing stiffness and an

increase in bis-acrylamide ratio will also increase the stiffness of the resulting hydrogel. In the following experiments, a range of stiffnesses were achieved by using the formulations presented in Table 1. To prepare hydrogels, 40% acrylamide and 2% bis-acrylamide stock were mixed and diluted to the proper concentrations for each of the different gel stiffnesses, these monomer mixtures were stored at 4 °C for up to three months.

	Soft	Med	Reg	Hard
%T	4.03	7.5	7.61	8.15
%C	0.74	0.05	1.4	1.84

Table 1. Formulation of acrylamide and bis-acrylamide used. %T is the total concentration of acrylamide and bis-acrylamide and %C is the concentration of bis-acrylamide crosslinker molecule.

After the acrylamide and bis-acrylamide monomer mixtures were prepared, a 500 µL aliquot of monomer mixture was obtained and degassed in a vacuum chamber for a minimum of 10 minutes. For the polymerization of acrylamide, a radical initiation reaction was used with ammonium persulfate (APS) and N,N,N',N'-tetramethylethylenediamine (TEMED). APS was prepared to a concentration of 0.1 mg/mL and used on the day the solution was prepared, TEMED was used as the neat amine compound directly with no modification. To the degassed monomer mixture, 2.5 µL of APS and 1.0 µL of TEMED were used to initiate the polymerization reaction. Polystyrene (PS) beads, were used in an effort to control the thickness of the resulting hydrogel supports, PS beads were diluted 100x in milli-Q water and added to the monomer solution at a concentration to maintain 100 µm spacing between beads. To prepare biotinylated polyacrylamide hydrogels, a crosslinker molecule with a free biotin group was also added to the monomer solution. Heterobifunctional crosslinker, sulfo-NHS-LC-biotin, was dissolved to a concentration of 2 mg/mL in PBS and 2-3 drops of allylamine, excess allylamine will evaporate from the reaction vessel, were allowed to react for one hour. The resulting crosslinker molecule was stored at 4 °C and used within one month, for each aliquot of monomer solution 3.2 µL of sulfo-allyl-LC-biotin was added.

To achieve the formation of a flat, thin, and homogeneous hydrogel a sandwich technique was used. One coverslip was allyltrichlorosilane functionalized and the opposing coverslip was untreated, 8 µL of the monomer solution was sandwiched between the slides and small weight of

around 50 g was placed on top. The polymerization reaction was allowed to proceed for 30 minutes, after which coverslips were separated, the gel stayed on the allyltrichlorosilane functionalized coverslip, and hydrogels were soaked in milli-Q overnight to remove any unreacted monomers and allow the hydrogels to reach equilibrium swelling.

3.2.4 Rheology of Hydrogels

Shear rheology was performed in the laboratory of Dr. Chien-Chi Lin, using a Bohlin CVO 100 digital rheometer. To prepare polyacrylamide hydrogels for rheology, flat disc shaped hydrogels were formed between glass coverslips with a 1 mm spacer, a range of stiffnesses were prepared according to Table 1. After the polymerization reaction, hydrogels were placed in petri dishes with milli-Q water overnight to allow expansion and swelling of the polymer. A circular biopsy punch with a diameter of 8 mm was used to remove a uniform sample to be placed on the rheometer and measurements were completed on 3 hydrogel punches from each stiffness. The measured shear modulus was then converted to Young's Modulus for comparison to previously published results.

3.2.5 Surface Functionalization of PGTB

With the prepared polyacrylamide hydrogels, further modifications of the surface chemistry were completed to form a tethered membrane on top of the hydrogel support. For fibronectin linked membranes, sulfo-SANPAH was diluted to a concentration of 0.5 mg/mL in PBS and 0.125 mg were placed onto each hydrogel sample and exposed to UV light. After 15 minutes of reaction time, samples were placed on a shaker table with PBS buffer to remove excess sulfo-SANPAH. Now the hydrogel surface has free N-hydroxysuccinimide (NHS) ester molecules available to react with amine groups, fibronectin can be added and covalently linked to the hydrogel. Fibronectin was added in PBS and allowed to link to the hydrogel for 4 hours prior to washing away excess. To covalently link the fibronectin layer to the lipid layer, sulfo-GMBS, which is a water-soluble heterobifunctional crosslinker molecule with maleimide and NHS ester functionality, was added in excess to the FN linked hydrogel and allowed to react for 30 minutes prior to rinsing. Next, the addition of lipids containing thiol head groups will be able to covalently bind to free maleimide groups from the hydrogel support to form covalent linkages.

Another crosslinking strategy pursued used a biotinylated hydrogel to bind and immobilize streptavidin and neutravidin, which are biotin binding proteins. With a biotinylated hydrogel, 0.25 μg of streptavidin or Neutravidin were incubated on for 15 minutes, followed by rinsing with PBS to remove any unbound protein. Lipids with biotin conjugated head groups were next used to bind to the streptavidin or Neutravidin coated hydrogel and form a tethered bilayer structure.

The final crosslinking strategy pursued did not utilize a protein crosslinking method, but used a direct chemical linkage from the polyacrylamide hydrogel to the lipid bilayer. For this method, two crosslinkers were first reacted together to form a heterobifunctional crosslinker with UV-activated and maleimide termini. Molar equivalents of sulfo-SANPAH and amine-PEG_{10}-maleimide were mixed into PBS and allowed to react for at least 1 hour. Without further modification, the reaction mixture was added to polyacrylamide hydrogels and exposed to UV light, following the same protocol as the sulfo-SANPAH reaction described above. To remove excess reactants, the hydrogels were placed on a shaker table for 30 minutes and rinsed three times with PBS. After this reaction, the polyacrylamide hydrogel is now surface functionalized with maleimide groups available to react with thiol containing lipids and form a polymer gel-tethered lipid bilayer.

3.2.6 Confocal Laser Scanning Microscopy

To obtain confocal micrographs an Olympus FV1000 confocal laser scanning microscope equipped with live cell incubator was used. A 60x water immersion objective was used for live cell imaging as well as PGTB sample analysis. For the analysis of live cells on PGTBs, an onstage incubator was used to maintain temperature and CO_2 conditions. Temperature was maintained at 37 °C with a Tokai on stage incubator and CO_2 at 5% by flowing a blend of carbon dioxide and air to provide the correct environment for the live cells. An additional feature of the Olympus FV1000 was the use of Differential Interference Contrast (DIC) microscopy to image cell shape and outlines to collect data for cell size and shape interpretation. For DIC images, the 488 nm laser line was utilized to allow the visualization of transparent and unlabeled cellular features.

3.2.7 Fluorescence Recovery After Photobleaching (FRAP)

The Olympus FV1000 microscope was also used to capture quantitative FRAP data. The tornado, or circular bleach pattern, was used to quickly bleach a specified region of the sample so the most accurate bleaching analysis could be achieved. With a series of images showing the recovery of fluorescent lipids, a diffusion coefficient can be obtained as an estimate of the average lipid diffusion in the sample. An advantage of FRAP is the acquisition of information regarding both the mobile and immobile species in a sample. For quantitative FRAP, steps were taken to remove background artifacts and photobleaching of the fluorophores by analyzing the brightness of a region outside the bleached area. This was done by determining an average over the series of the images, and then applying a correcting factor to the brightness averages in the bleach area. Also, to make data interpretation more accurate from sample to sample, the brightness of the bleached area measured immediately after photobleaching was set as an intensity of zero, and all other brightness values were corrected by subtracting the bleached area brightness.

Figure 13. A simulated FRAP experiment showing the recovery of fluorescent signal over time and an indication that there is likely background bleaching that should be corrected.

3.2.8 Thickness Measurement of the Hydrogel Support

The polyacrylamide hydrogel fabricated as the support for the PGTB system was analyzed via confocal microscopy to measure the thickness of this layer. In this assay, fluorescein, a fluorescent dye, was added to a swollen polyacrylamide hydrogel. Once excess dye was rinsed away, the thickness of the hydrogel was measured by obtaining confocal XY images in a series from below, through, and above the stained sample. The thickness was determined by analyzing changes in the average fluorescent intensity, specifically the average fluorescent intensity for each image in a series was determined using ImageJ analysis and the averages were displayed on a

graph and a parabolic fitting was applied. The x-value for the second derivative was used as the determination of the bottom and top interface of the hydrogel sample with the total thickness simply being the distance between these two points.

3.2.9 EPI Widefield Microscopy

EPI fluorescent microscopy was used to analyze the homogeneity and lateral mobility of fluorescently labeled species in polymer gel-tethered bilayers. A Zeiss Axiovert 200M inverted microscope equipped with an AxioCam MRm camera was used to capture widefield images through Axiovision software. Fluorescent lipid concentration in the monolayer or bilayer samples was 0.2 mol% of either TRITC-DHPE or NBD-PE, depending on other fluorescent species in the sample. Spot photobleaching could also be done with this system by closing the field stop shutter to the smallest size possible and allowing the Hg bulb (AttoArc, 100 watt) to bleach the sample until a dark region was observed in the bleached area. After photobleaching, the sample was imaged to analyze the recovery of fluorescently labeled species in the sample.

3.2.10 Fluorescence Correlation Spectroscopy (FCS)

An additional function of the Zeiss 200M microscope is the availability of the Confocor2 fluorescence correlation spectrometer. The light source for FCS measurements was a 1.8 mW HeNe laser with emission at 543 nm. The method setup for acquiring time fluctuation data included bandpass filters and a pinhole to reject out of focus light. From the raw fluorescent intensity fluctuation data, autocorrelation analysis was completed to determine the characteristic diffusion time and observe any populations within the sample. FCS experiments were pursued using TRITC-DHPE fluorescent lipids at a concentration of 0.002 mol%. Measurements were made after adjusting the pinhole on the instrument with a 70 nM solution of Rhodamine6G, also running a 7 nM solution of Rhodamine6G to verify the instrument was functioning properly. The average diffusion time of Rhodamine6G in this method setup was 45 μs.

CHAPTER 4. RESULTS AND DISCUSSION

4.1 Assembly of Hydrogel Supports

4.1.1 Functionalized Glass for Covalent Assembly to Polymer Hydrogel

Plain microscopy glass coverslips were placed into the oven and then silanized with allyltrichlorosilane, leaving a hydrophobic surface characteristic. The reaction scheme is demonstrated in the figure below, showing the change in functional groups on the glass coverslip surface.

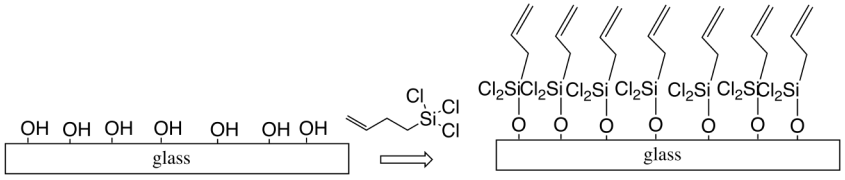

Figure 14. Schematic shows the treatment of glass coverslips with allyltrichlorosaline to provide a covalent connection to polyacrylamide hydrogels.

Prior to silanization, the coverslips are highly hydrophilic as demonstrated by the very small surface contact angle shown in Fig 15; however, after silanization of the same glass surface the surface contact angle is greatly increased. This increased contact angle indicates a hydrophobic surface, which is expected since the silane used has a terminal alkene group. This transition from hydrophilic to hydrophobic was analyzed using a goniometer and contact angles were measured using ImageJ.

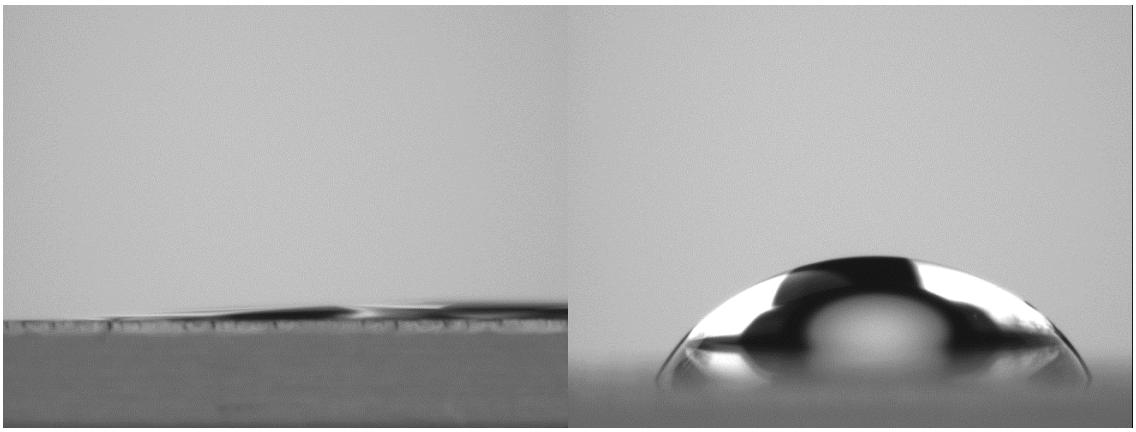

Figure 15. Images taken with a goniometer, after the addition of a 10 μL drop of water, show the stark changes in contact angle. The left panel shows glass after treatment in the oven and the right panel shows glass treated with allyltrichlorosilane.

4.1.2 Tunable Elasticity of Polymer Gel-Tethered Bilayers

Rheology measurements were obtained that demonstrated the capability of the polyacrylamide system to produce hydrogel materials that cover a wide range of stiffnesses, these stiffnesses cover the physiologically relevant range for the materials properties of many tissues. Rheology was done using a shear rheometer (Bholin CV100) on samples cast to a thickness of 1 mm and swollen in buffer for a minimum of 24 hours. To change the resulting stiffness of the polyacrylamide hydrogel, the ratio of acrylamide and bisacrylamide in the initial monomer solution must be manipulated. Acrylamide:bisacrylamide formulations were chosen that produce homogeneous network structures [197]. The table below shows that the polyacrylamide is a tunable material, and advantageous for the use in the assays to test mechanosensitivity and mechanisms of mechanotransduction.

%T %C	T4 C0.7	T7.5 C0.05	T7.6 C1.4	T8.2 C1.8
E (kPa)	0.5 ± 0.1	8.4 ± 0.2	11.0 ± 0.5	38 ± 3

Table 2. Polyacrylamide formulations were selected to produce hydrogels with a wide-range of stiffnesses. Rheology was performed with a shear rheometer to measure elastic modulus.

4.1.3 Control of Hydrogel Thickness as Measured by Confocal Microscopy

Thickness of the resulting polyacrylamide hydrogel can be controlled through two pathways, one is to use spacer beads and the other is to simply modify the amount of monomer solution for each sample, with a greater amount of material leading to thicker hydrogels [196]. For the work in this study, the bead spacing approach was utilized. This was the chosen path because of the desire to be able to complete assays such as traction force microscopy, which require beads to be embedded in the hydrogel, and to establish a method that produces thin gels. After polymerizing hydrogels using various size bead spacers the hydrogel thickness was measured. To complete the thickness measurement by confocal microscopy, the hydrogels were stained with fluorescein, a green fluorescent dye. Images were acquired with the Olympus FV1000 in z-scanning mode using a sufficiently small step size to reveal detail about the thickness of the stained hydrogel. After obtaining images, the fluorescent intensity was measured using ImageJ, an average of fluorescent intensity at each step along the z-scan was done, intensity versus Z-position of the objective was plotted to reveal a peak profile like that seen in the Fig 16.

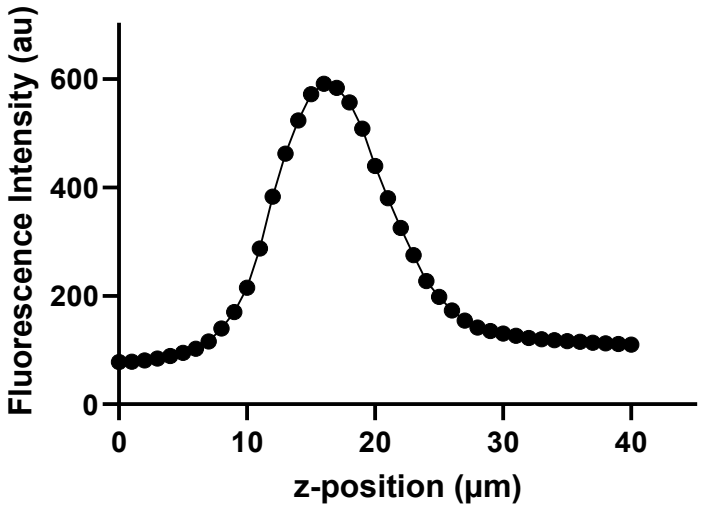

Figure 16. Confocal microscopy scans along the z-axis were used to measure the thickness of polyacrylamide hydrogels stained with fluorescein.

Resulting hydrogel thicknesses from the bead spacing assay are shown in Table 3. These results indicate that the thickness of the gel can be controlled by the use of specific sized beads to

achieve a desired hydrogel thickness, with control on the micron scale. With the polymerization parameters understood we were able to fabricate hydrogels of desired thickness, depending on the specific application, which also allows us to utilize assays such as traction force microscopy in the future.

Bead spacer	50 nm	500 nm	6 μm
Thickness ± SE (μm)	7.0 ± 0.2	10.0 ± 0.5	17 ± 0.5

Table 3. Hydrogel thickness was measured using confocal z-scan analysis, different size polystyrene bead spacers were used to allow the adjustment of hydrogel thickness.

4.2 Characterization of Biotin:Avidin Linked Polymer Gel-Tethered Bilayers

4.2.1 Synthesis of Biotin Functionalized Hydrogels Coated with Streptavidin and Neutravidin

Hydrogels functionalized with biotin molecules were fabricated, so a subsequent addition of biotin binding protein would result in a stable connection to the polymer hydrogel. Biotin to streptavidin binding is considered the strongest non-covalent bond in nature and has been shown to have very long half-life of binding, on the scale of weeks [198]. After washing a polymerized hydrogel to remove unreacted monomers, buffer was exchanged for PBS and streptavidin or neutravidin was added without further modification. Streptavidin and avidin are similar proteins, both are tetramer proteins capable of binding four biotin molecules per protein; however, streptavidin lacks carbohydrate groups that contribute to avidin having a higher non-specific adsorption profile. Neutravidin is a deglycosylated version of avidin, which reduces the charge on the protein, resulting in a pI near neutral pH. To analyze the resulting protein coated system, fluorescently labeled streptavidin and neutravidin were used. Figure 17 shows streptavidin and neutravidin coated systems, it is observed that the protein forms a flat, homogenous layer on top of the biotin-functionalized hydrogels. This result demonstrates that the hydrogel surface is flat and without observable cracks or creases and the surface is capable of binding streptavidin or neutravidin. Although there were no observable differences between the addition of streptavidin or neutravidin, neutravidin was chosen as the linking protein due to the lower amount of charge on the protein at neutral pH. Reducing the amount of ionic or charge based interactions between

the lipid membrane and supporting layer is hypothesized to produce membranes with improved lateral diffusion properties. After observing that the polymer hydrogel and protein layer are flat, stable, and reproducible; the next step of adding a membrane to this system was pursued.

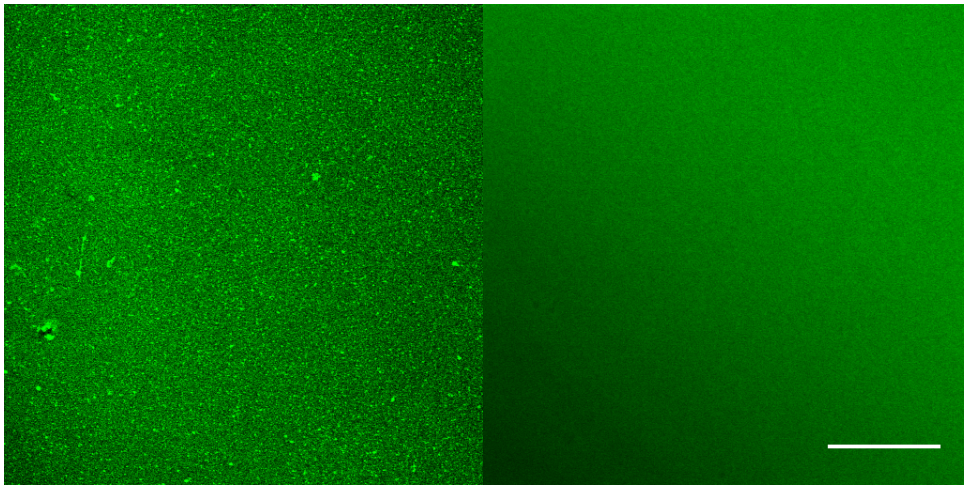

Figure 17. Confocal microscopy was used to visualize streptavidin (left panel) and neutravidin (right panel) coated hydrogels.

4.2.2 Lipid LB Monolayer Homogeneity and Diffusion Characteristics

An LB deposition is routinely used as a way to add a single layer of molecules to a supporting substrate and has been established as the first step in a route to form lipid bilayers on solid supports. Previous work in the Naumann lab has utilized the LB addition of lipids to a hydrophilic glass substrate followed by a horizontal dipping, LS, to produce highly mobile and consistent membranes. To perform a LB deposition with a neutravidin functionalized hydrogel, normal procedures for a LB dipping were followed with the modification of the aqueous solution added to the trough, opting for 150 mM NaCl solution. After submerging the coverslip with the hydrogel into the LB subphase, lipids in chloroform solvent (POPC, 5 mol% Biotin-PE, 0.2 mol% TRITC-DHPE) were spread at the surface of the water and compressed to 30 mN/m. Dipping was completed with the mechanical dipping arm and active surface tension mechanism to maintain consistent area/lipid and surface tension. Polymer gel-tethered neutravidin was found to be an excellent supporting substrate for the addition of LB monolayers.

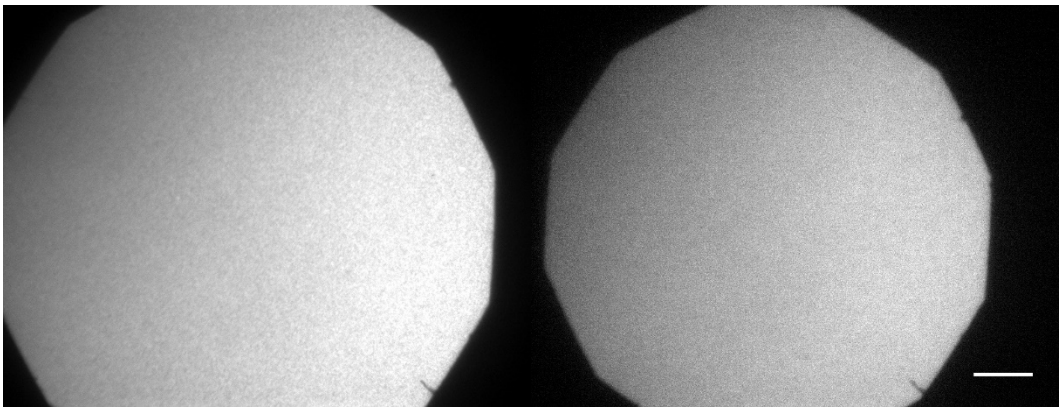

Figure 18. Lipid monolayers, containing TRITC-DHPE lipids, were transferred to streptavidin (left panel) and neutravidin (right panel) functionalized hydrogels, and imaged with Epifluorescent microscopy. Scale bar = 50 μm for both images in the frame.

Surprisingly to us, after the transfer of a monolayer, it was found that the lipid layer presented diffusion characteristics, which is distinct from solid supported monolayers that are known to have no lateral lipid diffusion. Later when consulting the literature, it was found that similar experiments were completed by Kuhner and Sackmann, in their work a monolayer of lipids was transferred to an unfunctionalized polyacrylamide substrate and diffusion was also seen in the monolayer [199]. Specific evidence showing the formation of polymer gel-tethered monolayers and their diffusion properties is presented in the next subsections, discussion will be presented to compare previous work to the current data presented.

4.2.3 Polymer Gel-Tethered Monolayer FRAP Analysis

In order to investigate the properties of polymer gel-tethered monolayers EPI microscopy and spot photobleaching were used to observe lipid monolayers containing a small mol fraction of fluorescent lipids. Shown in Fig 19 are EPI micrographs that demonstrate the consistent monolayer coating on the neutravidin coated polymer gel. The formation of a monolayer demonstrates the complementary interaction between the lipid and protein layers, and the presence of attractive forces, on this complex support material. Diffusion properties of the monolayer are qualitatively shown with the spot photobleaching performed, where the field stop of the microscope was closed to allow the 100 W Hg bulb to irradiate only a small portion of the sample for enough time to produce an observable bleach spot. The photobleaching assay indicates that the lipids in this sample are laterally mobile. Here, after bleaching the dark bleach spot becomes smaller and

brighter, due to the lateral diffusion of unbleached fluorescent molecules into the bleached zone. In the next section, a more quantitative investigation of the monolayer diffusion properties was pursued with FCS autocorrelation analysis after the qualitative FRAP assay revealed this interesting property.

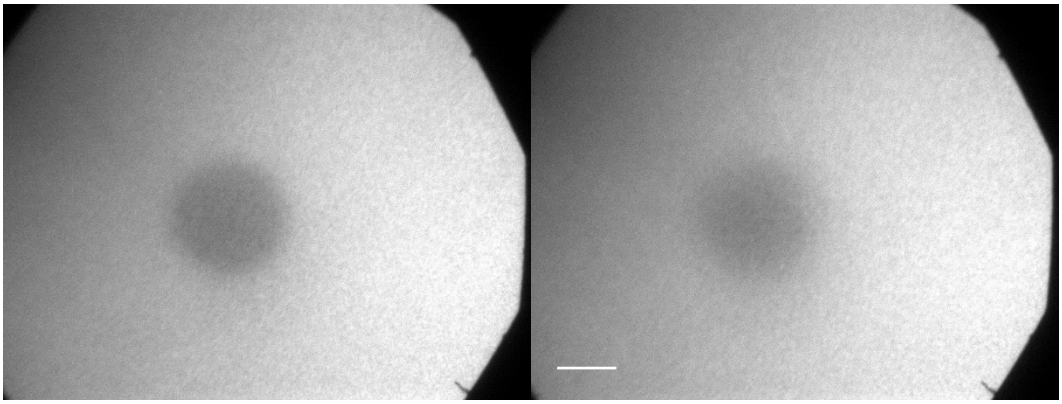

Figure 19. A lipid monolayer transferred to a neutravidin linked hydrogel was spot photobleached (left panel) and allowed to recover for two minutes (right panel), images were acquired with EPI fluorescent microscope. Scale bar = 50 μm

4.2.4 Polymer Gel-Tethered Monolayer FCS Autocorrelation Analysis

A second complementary assay was performed to better determine the diffusion coefficient of the polymer gel-tethered neutravidin linked monolayer system. By using the FCS, a diffusion time across the confocal volume can be ascertained and related to a quantitative diffusion coefficient. To perform this assay, a very small amount of fluorescent lipids is used, in this case 0.002 mol% TRITC-DHPE. The small amount of fluorescent lipids decreases the background and allows for improved detection of fluorescent molecules passing through the confocal volume. To complete the data set eight samples were analyzed with five runs of 50 s per sample, and FCS autocorrelation analysis of the raw data showed excellent fits, Fig 20. Diffusion times and diffusion coefficients were calculated as explained in Section 2.1.5 and shown in Table 4.

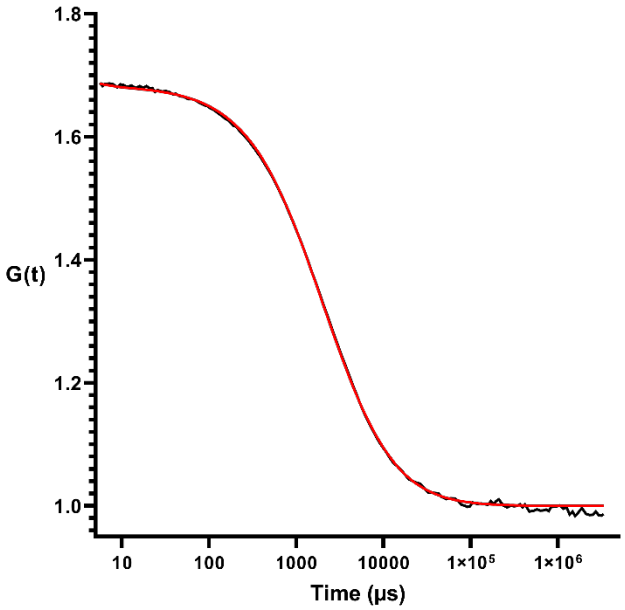

Figure 20. Autocorrelation analysis of FCS data from polymer gel supported monolayer.

In order to accurately compare the data from the previous study by Kuhner and Sackmann the difference in the methods should be discussed. Kuhner and Sackmann prepared polyacrylamide hydrogels and transferred lipids directly, meaning there are no specific tethering points between the lipids and hydrogel support; however, in the neutravidin linked polymer gel-tethered monolayer there is a supporting protein layer and specific connections between the lipid and protein layers. The method of measuring lipid diffusion was also different, Kuhner and Sackmann used quantitative FRAP and we used FCS [199]. Also worthy of noting is the use of different acrylamide:bisacrylamide monomer compositions. Although there are differences between the studies, the results are consistent. As seen in Table 4, lipid diffusion on a Langmuir trough, understood as the 'speed limit' of lipid diffusion in a planar setting, and as expected, is greater than what is observed on the polymer supports. Diffusion coefficients from both studies fall into the same range, which is similar to the diffusion coefficient measured for solid supported membranes, such as polymer-tethered lipid bilayers.

	Diffusion time (μs)	D (μm^2/s)
	2210	2.41
TRITC-DHPE, Neutravidin linked monolayer		
NBD-DMPE, T20C0, T20C1		1 - 3
NBD-DMPE, T20C5		3.5 - 5
NBD-DMPE, * air-water interface on film balance		13

Table 4. Diffusion data from various experiments to compare with measured diffusion times and coefficients [199].

4.2.5 Lipid Membrane Homogeneity Observed by Confocal Microscopy

Much care was taken to develop a method to add a lipid bilayer to the polymer gel-tethered system. Attempts were made to add a bilayer on these substrates via several different strategies, including: Langmuir-Blodgett/Langmuir-Schaeffer, direct addition of Giant Unilamellar Vesicles (GUVs), direct addition of SUVs, and LB/vesicle fusion (LB/VF). In the end, the best method for producing high quality reproducible films was the use of LB/VF with very small SUVs isolated by ultracentrifugation. In Fig. 21, lipid bilayers are shown to be flat and homogeneous, with some bright or dark structures that are likely bound vesicles or lipid structures. Overall the quality of films produced on this complex substrate was improved by the use of ultracentrifuged vesicles, which have a high curvature and high membrane tension that causes them to be less stable in the vesicle structure and more likely to rearrange to a planar structure when they contact a surface.

This result is similar to work performed by Espinosa-Marzal and coworkers at the University of Illinois Urbana-Champaign [200]. In this complementary work, a polymer hydrogel was coated with a polyelectrolyte multilayer film and then coated with a lipid bilayer.

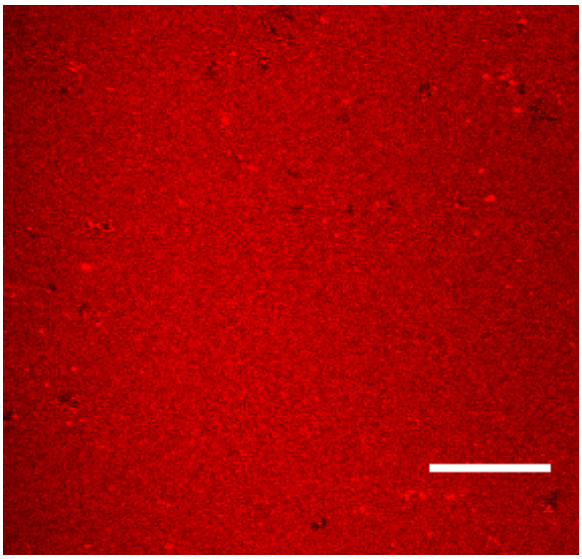

Figure 21. A neutravidin linked PGTB with TRITC-DHPE lipids to enable imaging, confocal microscopy was used to capture micrograph. Scale bar = 25 μm

Of particular note, is the use of the polyelectrolyte multilayer film, which seemed to act as a lubricating layer underneath the lipid bilayer, would likely inhibit the transduction of cell-generated forces, preventing the use of this platform for adherent cell assays [200]. Beyond the differences in the study, the data sets demonstrate that the formation of bilayer structures on soft, swollen hydrogel supports is possible and that maintaining lipid diffusion in these membranes can be accomplished. Properties of biotin:neutravidin linked polymer gel-tethered bilayers on is presented in the next section.

4.2.6 Confocal FRAP Analysis of Biotin:Neutravidin Linked PGTBs

In order to quantify lipid diffusion in PGTB with biotin:neutravidin linkages, two complementary methods were employed: FRAP and FCS. First analysis with quantitative confocal FRAP measurements. Advantages of FRAP analysis are the determination of the immobile fraction of lipids and that slower diffusing systems can still be analyzed. For this analysis, the tornado bleaching function on the Olympus FV1000 confocal scanning microscope was used to quickly and accurately bleach circular regions of the membrane. The workflow for measuring a diffusion coefficient from FRAP data was followed as described in Section 2.1.7, according to the model proposed by Kenworthy and coworkers [30]. Fig. 22 shows the bleaching of a biotin:neutravidin linked PGTB containing fluorescently labeled lipids (panels A and B) and labeled neutravidin

(panels C and D). Bleaching spot is indicated with the yellow circle in A, where the intensity of fluorescence does return in the lipid membrane images; however, the protein channel does not display any recovery of the fluorescent signal. These results indicate that a stable connection has been established between the biotinylated hydrogel and the neutravidin protein layer, indicating that this is a suitable platform for use as a cell substrate.

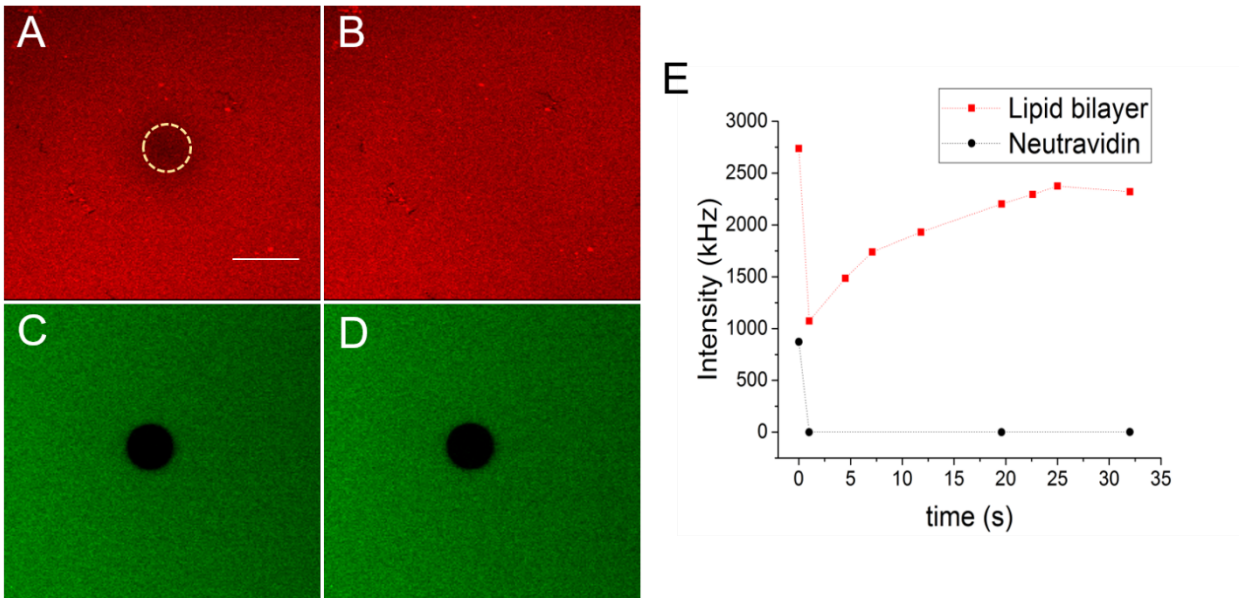

Figure 22. Confocal microscopy was used to measure the lipid diffusion of neutravidin linked PGTBs. Micrographs in A-B show the TRITC-DHPE lipid diffusion, C-D show the bound neutravidin is unable to recover. Data shown in E were used to determine the diffusion coefficient of neutravidin linked PGTB, where the fluorescence intensity was measured over time after a bleaching spot was made. Scale bar = 20 μm

Quantitative measurement of the diffusion coefficient is supported by data previously published for similar systems. Of particular note is the diffusion coefficient established using wide-field single molecule microscopy, here polymer-tethered lipid bilayers on solid supports were found to have diffusion properties that are strongly influenced by the presence of tethered lipids, also called lipopolymers [16]. Specifically, the use of a solid support, which is a very common method, has been shown to decrease diffusion when compared to lipid diffusion in a vesicle [201] or on a Langmuir trough [202]. The combination of coupling between the solid support and lipids with the use of tethered lipids demonstrated there are multiple mechanisms that can impede lipid diffusion [14].

Diffusion coefficients, shown in Table 5, determined from FRAP analysis are greater than D measured for PTLB systems, which could be accounted for by the different interactions occurring at the underlying substrates in each system. Comparison with data presented by Kuhner and Sackmann, they produced bilayers by LB followed by LS transfers; however, membranes produced in this manner showed a heterogenous and inconsistent fluorescence signal, suggesting lower quality membranes were formed and increased the difficulty of evaluating FRAP data. Kuhner and Sackmann reported bilayer diffusion coefficients ranging from 2 to 10 $\mu m^2/s$, dependent upon degree of crosslinking and fluorescent labeling [199]. The data reported here for neutravidin linked PTLB fall within the range of previously reported values, supporting the formation of a bilayer structure and validity of the methods used.

4.2.7 Diffusion Properties in Biotin:Neutravidin Linked PGTBs: FCS Autocorrelation Analysis

FCS was used in a complementary manner to determine the diffusion properties of lipid bilayers coated on these neutravidin linked supports. Diffusion coefficients were calculated from diffusion times in the same manner as the monolayer diffusion analysis, shown in Section 4.2.4. In Fig 23, the autocorrelation curve shows an accurate fit of the data, and determination of the characteristic diffusion time.

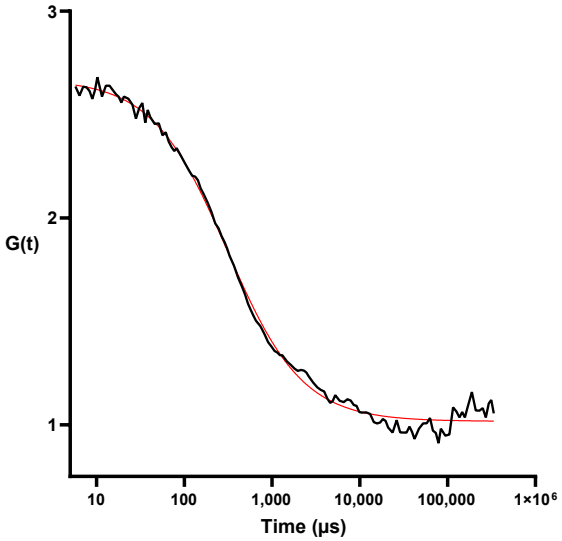

Figure 23. FCS autocorrelation analysis was performed on biotin:neutravidin linked PGTBs, data showed a strong correlation that was used to determine the diffusion coefficient.

Diffusion times reported in Table 5 for neutravidin linked PGTB line up very closely to data presented in a previous study from Hussain, et al. [15]. Here the diffusion times reported from FCS for a PTLB at 5 mol% tethered lipids is very similar to the measured value for PGTB. Although the D value, determined by FRAP and FCS are slightly inconsistent, differences in measuring methods should be noted. Due to the fact that FCS is only capable of measuring the mobile fraction of lipid species (FRAP data can determine both the mobile and immobile components) and the difference in the dimensions of the sample that was analyzed. For FRAP analysis a ~10 µm micron diameter bleach area was made, whereas FCS analysis captures the fluorescence fluctuation signal from a diffraction limited spot, around 250 nm in diameter. Overall, both sets of data support that a bilayer was formed on this substrate, which maintained lipid diffusivity, and that the membranes appear to be suitable for further functionalization and plating of adherent cells.

	Diffusion time (ms)	D ($\mu m^2/s$)
PGTB, TRITC-DHPE	3.4 ± 1.2	1.54
PTLB, 5 mol% Lipopolymer	3.16 ± 0.34	1.68
T20C0, T20C1, FRAP data	-	2-4 6-10
PGTB, FRAP	-	3.3 ± 1.4

Table 5. Diffusion data from similar experiments is compared to measured diffusion in neutravidin linked PGTBs.

4.2.8 Homogeneity and Lateral Diffusion Properties of N-Cadherin Chimera Functionalized Biotin:Neutravidin Linked PGTBs

In order to plate cells, specific cell adhesion linkers must be added to the substrate. Here this was done by incorporating a small mol fraction of chelating lipids (DGS-NTA), which will bind to a histidine-tag, into the membrane of PTLB. For the mimicking of cell-to-cell adhesions, neuronal-cadherin (N-cadherin) protein was chosen as the cell adhesion molecule, N-cadherin are a major component of adherens junctions formed between cells. The N-cadherin molecule used in this study is a histidine-tagged chimera, meaning that only the extracellular domain of the protein is present, additionally this protein was fluorescently labeled with a commercially available labeling kit. Figure 24 shows a PGTB after the addition of N-cadherin and the coverage of the system, the amount of N-cadherin was decreased when samples were to be used for cell plating.

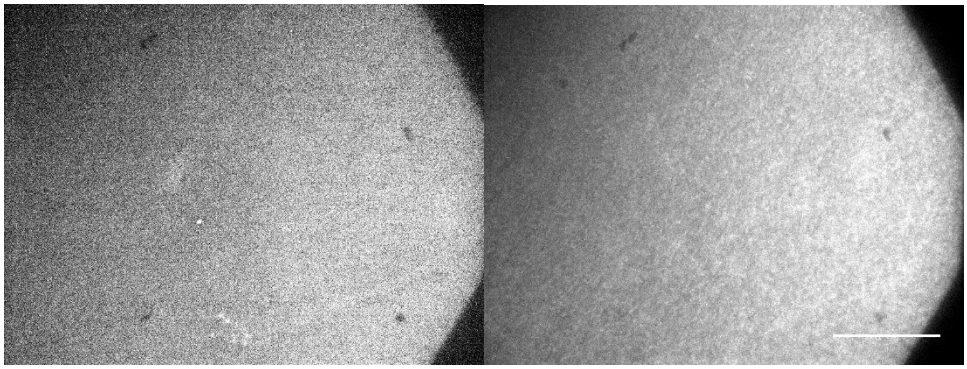

Figure 24. A PGTB containing NBD-PE lipids (left panel) functionalized with Alexa555 labeled N-cadherin (right) was imaged with EPI microscopy. Scale bar = 100 μm

4.2.9 Cellular Interaction with Biotin:Neutravidin Linked PGTBs

After preparing samples for plating with C2C12 myoblasts by the addition of N-cadherin cell adhesion proteins, these samples were analyzed to view cell spreading and the formation of cellular adhesion zones. It was observed that cells were able to spread on these neutravidin linked PTLB, indicating that traction forces generated by the cell were transduced to the substrate. However, cells were also able to uptake some of the neutravidin, as shown as bright spots in the right panel of Fig 25. This means that by some mechanism the non-covalent bond between the biotinylated hydrogel and neutravidin protein was being broken. Although the biotin:neutravidin is known to be a connection with a high energy of binding and a long half-life, when under force the bond half-life is drastically reduced as shown in recent work by paper about the streptavidin half-life under load [203]. This result indicated that the neutravidin linked system may not well suited for cell substrate assays and has led us to develop covalently tethered systems, hypothesized to be better suited to withstand cellular generated forces. Now, even though this system may not be well suited for adherent cell assays, this type of platform could be very well suited for the incorporation of membrane proteins, as a platform to study effects on lipid diffusion, and studies using cells which do not generate large traction forces, such as immune cells.

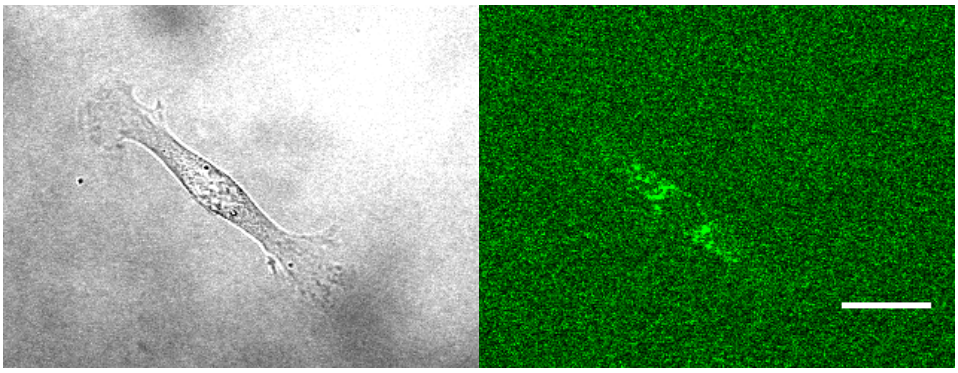

Figure 25. Confocal microscopy reveals cell spreading on a neutravidin linked PGTB. DIC imaging showing the cell outline (left panel). In the fluorescent image on the right, accumulation of DyLight488 labeled neutravidin is shown. Scale bar is 25 μm.

4.3 Characterization of Fibronectin Linked Polymer Gel-Tethered Bilayers

4.3.1 Surface Functionalization of Polyacrylamide Hydrogels and Covalent Crosslinking of Fibronectin Protein

To achieve covalent crosslinking from the membrane to polymer hydrogel support, the following strategy was pursued. After polymerizing the hydrogel, functionalization began with the UV light-initiated reaction of sulfo-SANPAH, a heterobifunctional crosslinker, to the acrylamide polymer, leaving activated NHS esters available for the next step of the reaction. Fibronectin was added and the crosslinking reaction proceeded between the free amine groups on the protein and the sulfo-SANPAH molecule. The image in Fig 26, shows that FN was able to bind to the polymer substrate and formed a type of meshwork organization that is commonly observed when FN is used to coat planar substrates. After this another heterobifunctional crosslinker molecule, sulfo-GMBS, was used to covalent couple with lipids containing a thiol head group.

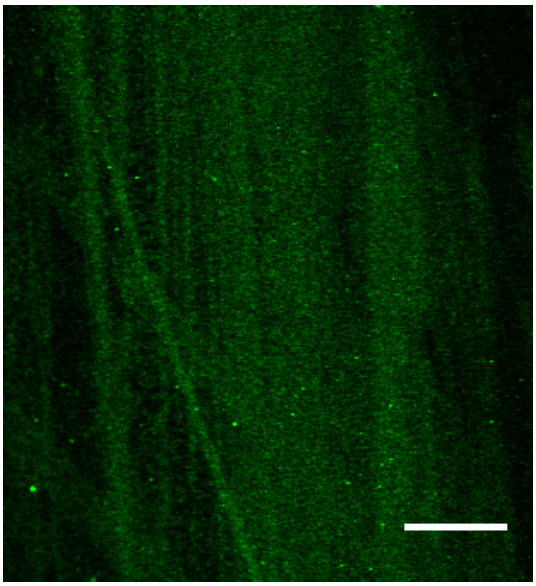

Figure 26. A polyacrylamide hydrogel functionalized with fibronectin protein. Scale bar is 50 μm.

4.3.2 Lipid Monolayer Homogeneity on Polyacrylamide Support

Once again, the lipid monolayer was deposited to a polyacrylamide hydrogel functionalized with a protein, currently FN, and was efficiently completed. After the polymer hydrogel was functionalized with FN and sulfo-GMBS added, a Langmuir trough was used to accurately add a monolayer of lipids with functional DPTE lipids, containing a thiol head group, to the substrate. The composition of lipids was prepared with 5 mol% of DPTE to covalently crosslink to the polymer hydrogel, 0.2 mol% TRITC-DHPE for fluorescent microscopy imaging, and POPC for the remaining fraction of lipids. Upon performing an LB deposition, the following image, shown in Fig 27, was acquired. The consistent fluorescent signal across the image demonstrates a flat and homogeneous lipid layer. Addition of the monolayer to the FN functionalized polymer gel will allow for the efficient addition of a bilayer via vesicle addition. Also accomplished in this LB deposition is tethering of the sulfo-GMBS functionalized FN and the fraction of thiol containing lipids in the LB layer. Tethering of some lipids in the membrane is critical to preparing a substrate that will allow the transduction of cellular generated forces [204].

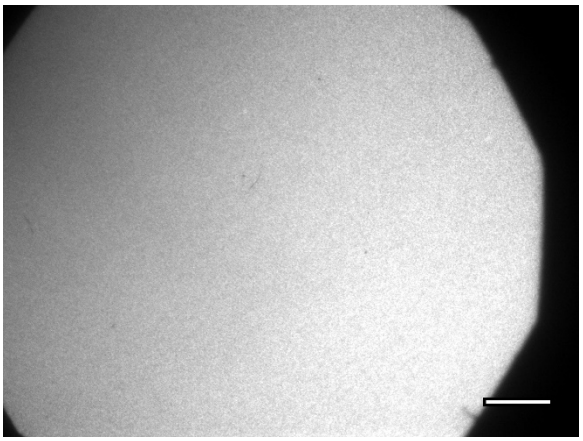

Figure 27. LB lipid transfer to a fibronectin functionalized hydrogel support. Scale bar is 50 μm.

4.3.3 Lipid Membrane Homogeneity and Lateral Diffusion Properties in the Membrane of Fibronectin Linked PGTBs

Lipid bilayers were formed on the substrate by LB/VF as established with the biotin:neutravidin linked system. SUVs formed by sonication, followed by centrifugation to remove large lipid aggregates were synthesized and prepared for the bilayer formation step. The vesicle suspension was composed of POPC, 5 mol% DPTE, and 0.2 mol% TRITC-DHPE. After incubation of the vesicle suspension on the fibronectin-linked polymer gel-tethered monolayer, excess vesicles were washed away, and EPI microscopy was used to examine the bilayer. Lipid bilayers were shown to be largely defect free, homogenous across the sample area, and lipid diffusion was observed. Also shown in Fig 28 is a qualitative spot photobleaching, this was done by closing the field stop of the EPI microscope and exposing a small area to the 100-watt Hg bulb to produce a bleached spot of reduced fluorescence intensity. The bleached spot in the image on the left side of Fig 28 shows a radially increasing fluorescence intensity. It is important to note that while the bleaching of a small area occurs, lipid diffusion is simultaneously happening, this means that the bleached region will have a nonuniform fluorescent intensity when the sample is laterally mobile. Observing that the bleached area immediately after exposure has a radially disperse intensity profile means that lipids show lateral diffusion in the membrane. The image on the right in Fig 28 was taken after 30 seconds of time, and the fluorescence intensity increased inside the bleached area. Lipid diffusion is a critical property needed for the replication of cell-like properties, due to critical functions of the plasma membrane requiring lateral diffusion and reorganization of

lipids and proteins. With the formation of a bilayer demonstrated, further work was done to functionalize the substrate with N-cadherin and plate with cells.

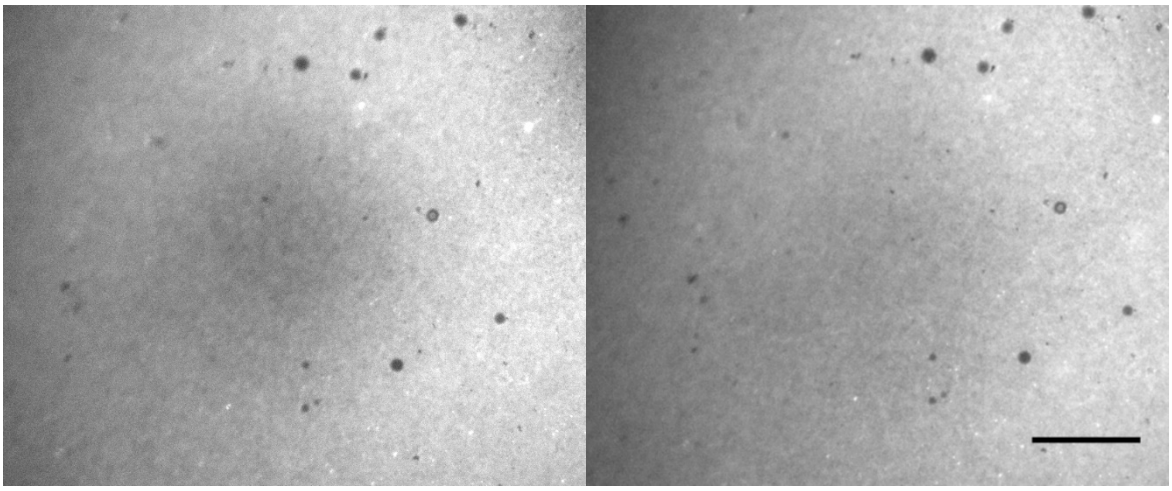

Figure 28. Spot photobleaching assay was performed on a FN linked PGTB containing TRITC-DHPE lipids. Scale bar is 50 μm.

4.3.4 Homogeneity and Lateral Diffusion Properties of N-Cadherin Chimera Functionalized Fibronectin Linked PGTBs

With the FN linked PGTB formed, N-cadherin was added to the membrane, which contained chelating lipids. For EPI microscopy analysis, the amount of DGS-NTA and N-cadherin was increased beyond what was needed for cell plating. As seen in Fig 29, the N-cadherin, shown in grayscale, are spread across the sample and do appear to be distributed evenly. Further confirmation of the linking of N-cadherin to the lipid membrane was done with FCS measurements. In this assay, FCS was used to measure the diffusion of labeled N-cadherin that were membrane bound. The FCS has the advantage of being able to separate lipid bound species and any unbound species. If there was an unbound fraction of N-cadherin present, possibly diffusing in solution near the membrane, a faster diffusing species would be seen in the autocorrelation curve, and the autocorrelation curve would likely be best fit by a two-component model. As seen in Fig 29, the autocorrelation curve is fit by a one component model and a diffusion time consistent with lipid diffusion, whereas if unbound N-cadherin was detected the diffusion time would indicate a faster moving species. From the FCS data, it is shown that the N-cadherin is bound to the lipids in the membrane and that these molecules are diffusing as expected. Additionally, a cell free assay was

completed to analyze the change in diffusion characteristics when N-cadherin chimera clusters were formed.

The hallmark property of PTLBs, formed on solid substrates, is the change in diffusion properties between individual cell adhesion molecules, which show slow lateral diffusion, and clustered adhesion molecules, which show decreased diffusion. This phenomenon is observed in PTLB, which allows adherent cells to transduce traction forces through the lipid based materials due to the size specific diffusion properties. In a cell free assay, this size diffusion property was tested in PGTBs by using polystyrene microspheres functionalized with N-cadherin chimera protein. Due to the large size of the sphere, many cadheriN-cadherin interactions between the bead bound cadherin and the substrate bound cadherin are expected to occur. When binding of the PGTB bound N-cadherin occurs, diffusion of the N-cadherin through the sample is expected to be shut down as a large cluster of proteins are formed. This size dependent diffusion property was observed in this assay with PGTB, shown in Fig 29 on the right panel is the autocorrelation of normal diffusion PGTB bound N-cadherin is shown in red, after addition of the cadherin functionalized microspheres autocorrelation fit is no longer present. This decrease in measured diffusion is attributed to the size-dependent diffusion property that is shown to be present in PGTBs.

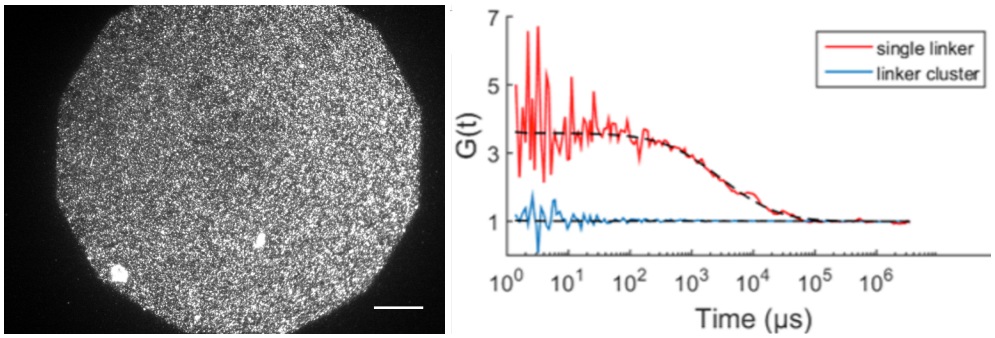

Figure 29. EPI micrograph shows the distribution of Alexa555 labeled N-cadherin on a FN linked PGTB containing DGC-NTA chelating lipids. FCS autocorrelation analysis was performed before and after the addition of N-cadherin functionalized microspheres to induce clustering of N-cadherin. Scale bar is 50 μm.

4.3.5 C2C12 Myoblast Adhesion and Spreading on Fibronectin Linked PGTBs of Tunable Elasticity

Once FN linked PGTBs are functionalized with N-cadherin molecules, these substrates are ready for the plating of adherent cells. In this assay, C2C12 myoblasts were plated and analyzed after allowing the cells to adhere and spread for 48 hours. First to evaluate the stability of the substrate, FN was labeled with a commercially available Alexa633 labeling kit and evaluated with confocal microscopy, shown in Fig 30 As seen here, there is no accumulation of labeled FN indicating that the covalent linking strategy produced a more robust system that is capable of withstanding cellular generated forces. Further analysis was completed to analyze the cellular response to changing mechanical properties of the substrate and cell adhesion formation.

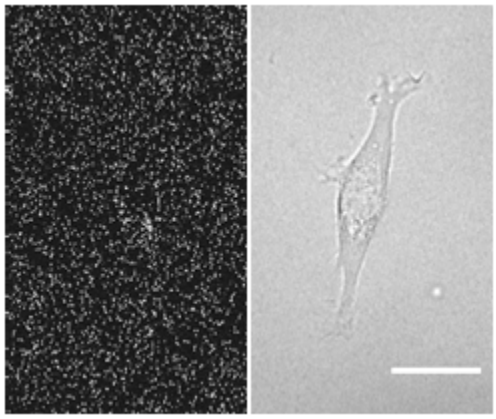

Figure 30. Shows an adhered C2C12 myoblast on a fibronectin linked PGTB, fluorescent signal from fibronectin (left panel) and DIC cell shape images were captured with confocal microscopy. Scale bar = 25 μm

Exhibited in Fig 31 is the role of the cell adhesion molecules. When a cell is plated on a FN linked PGTB that does not have a N-cadherin coating on the surface, cells are unable to spread. Figure 31 shows a cell on a soft substrate, where the cell is round and has difficulty spreading, and a cell on a harder gel, in which this cell has spread. In the inset of the Fig 31, a cell is adhered on a PGTB with a stiffness of 38 kPa, but it is unable to spread, due to the lack of cell adhesion molecules. This is an important result because cell adhesion can be attributed to attachments made to specific molecules, in this case N-cadherin, and not attributed to non-specific interactions between the cell and substrate.

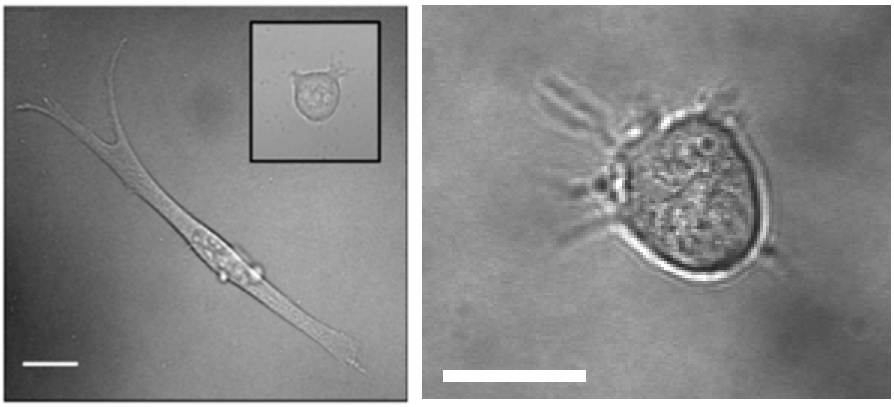

Figure 31. Cells shown in the image on the left are plated on a 11 kPa stiff gel, inset shows a cell plated on a PGTB without N-cadherin, and the image on the right shows a cell plated on a 500 Pa gel. Scale bars are all 25 μm

4.3.6 Cell Spreading Area Changes in Response to Substrate Mechanical Properties

The analysis of how cells respond to changes in stiffness is a classic experiment in mechanobiology and was pursued with the FN linked PGTB system. For this assay, polyacrylamide hydrogels were cast at four differing stiffnesses, as reported in 4.1.2, and the same procedure was done to produce FN linked PGTBs functionalized with N-cadherin to prepare for cell plating. These hydrogels were prepared to cover the physiological range of stiffnesses, to serve as a demonstration of the capability of the PGTB substrates.

In Fig 32, cell spreading area is shown on the four substrate stiffnesses tested. This data demonstrates that there is a statistically significant difference between cell spreading area on several of the stiffnesses. As expected, there is an increase in cell spreading area on stiffer substrates, this has been demonstrated many times in previous studies. Worth specific mention is the use of multi-bilayer substrates done by Minner et al. [8]. In this study, multi-bilayer stacks of lipid membranes were prepared by the roll-out of GUVs, the outer layer of these substrates were coated with laminin and then plated with 3T3 fibroblasts. Laminin was used a model for the extracellular matrix, and focal adhesions formed in the cell were analyzed, overall cellular behavior showed that cells formed smaller spindle and dendritic shapes. As shown in the current work and the study by Minner et al. cells show a differentiated response in global properties when plated on substrates of differing stiffness.

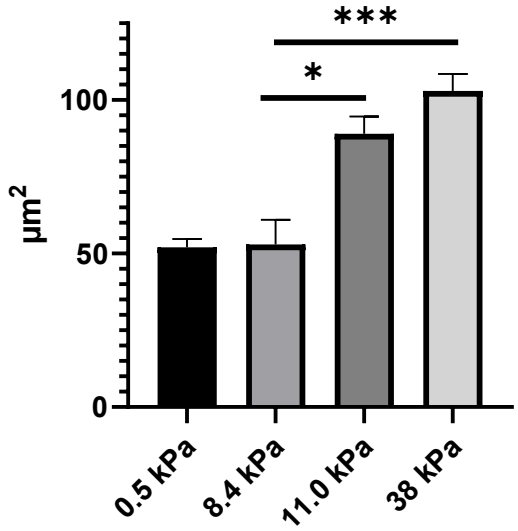

Figure 32. Spreading area of C2C12 myoblasts on PGTB, where the underlying hydrogel support was changed across a range of stiffness values. The y-axis reports the spreading area, in square microns, and the error bars show the standard error. Statistical significance in spreading error is shown with p-values indicated with asterisk, * for $p < 0.05$ and *** for $p < 0.001$.

4.3.7 Myoblast Cell Adhesion Clustering

One of the most important characteristics of adherens junctions, which requires advanced materials development, is the formation of cell adhesion clusters that show long range motion. Unlike a cellular connection made with ECM, which are stable and static, adherens junctions are dynamic in motion across the entire cell [109]. This means that to replicate and model an adherens junction, cells in contact with the fabricated material need to be able to move these formed cell adhesion clusters in a dynamic fashion. To investigate the capability of PGTBs to allow cells to behave in this manner, single cells were analyzed in a time dependent manner. Again, fluorescently labeled N-cadherin was used, note there is no fluorescent labeling done to the cells, all accumulation of N-cadherin cell adhesion proteins are molecules connected to the PGTB. Figure 33 shows a cell that is able to form specific connections to the PGTB at the N-cadherin molecules and time exposures reveal movement of these clusters.

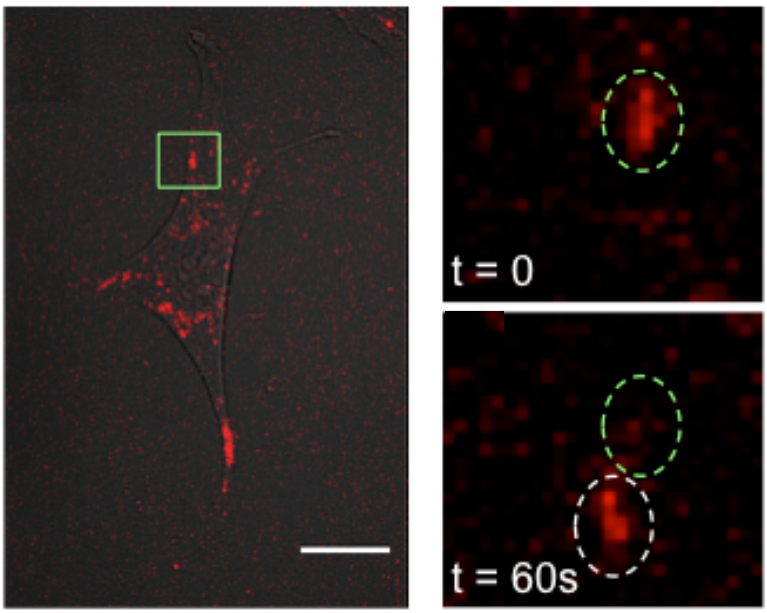

Figure 33. Fluorescent signal is showing the presence of Alexa555 labeled N-cadherin chimera, which have been collected and organized by the adhered cell. Zoomed in panels on the right are from the area indicated with the green box in the left panel, showing cluster movement directed by cell generated forces. Scale bar is 20 μm

Observing the first panel in Fig 33, the spread cell has bright red spots that appear directly underneath the cell. These red localized signals are the accumulation of many labeled N-cadherin molecules, all of this organization is accomplished by the cell. Taking repeat images of the cell show that the clusters are moving, this indicates that as the cell generates traction forces the substrate bound N-cadherin are being reorganized in an active fashion. Shown in Fig 34 is the requirement of the cellular cytoskeleton for maintaining cell shape and connections to the underlying substrate. After addition of Latrunculin B, which is a known cytoskeleton disruptor, the spread cell shrinks in overall area and the bright accumulations of labeled N-cadherin are no longer visible. This means that the addition of Latrunculin B, which does not affect cadherin homotypic binding, prevents the cytoskeleton from maintaining connection to the cell adhesion clusters, thus being unable to develop traction forces. This result agrees with previous studies carried out by Ge et al. where N-cadherin chimera functionalized polymer-tethered lipid bilayers (on a solid substrate) were analyzed after cell plating [9]. Here in this study, accumulations of N-cadherin were observed under spread cells and these motions were further analyzed to reveal very interesting dynamics. These dynamics are biologically relevant and need to be replicated in order

to produce an accurate mimetic of the cell-to-cell adhesion processes. Here the FN linked PGTB architecture is shown to be a stable platform to allow adherent cells to transduce traction forces, even quantitative analysis of cell response to changing mechanical properties has been demonstrated. After observing that an increased stability was gained with a covalently linked architecture, future design strategies were pursued to increase the stability of the system further. One potential shortcoming of the FN linked PGTB is the complexity that is added by the FN protein layer, which is known to crosslink spontaneously, which could contribute to the materials properties of the PGTB architecture. To overcome this challenge a direct linkage from polymer hydrogel to lipid bilayer was hypothesized to be an advanced system, this was pursued in Section 4.4.

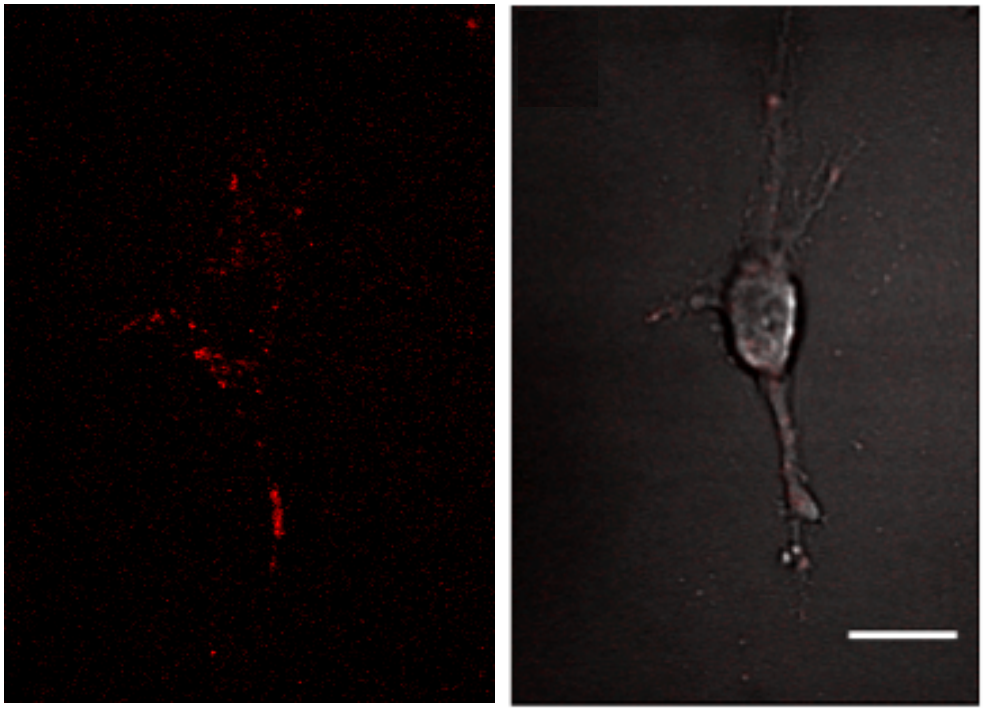

Figure 34. Shows the same cell in Figure 33, here an additional assay is completed to demonstrate the importance of cytoskeleton generated forces in maintaining the organization of the substrate bound N-cadherin chimera. The micrograph on the right shows the cell shape and Alexa555 labeled N-cadherin chimera signal, but the N-cadherin signal has drastically decreased after treatment with Latrunculin B (10 μM). Scale bar is 25 μm.

4.4 Characterization of Direct Covalently Linked PGTBs

4.4.1 Surface Functionalization of Polyacrylamide Hydrogels with UV-Activated Crosslinker Molecules

Using the idea of covalent bonding to produce robust substrates capable of withstanding cell generated traction forces, a strategy was implemented to link the lipid membrane directly to the underlying polymer hydrogel. To covalently link from the membrane to the polyacrylamide hydrogel a suitable crosslinker molecule was needed. Beginning with a polyacrylamide hydrogel, the UV-activated crosslinker sulfo-SANPAH was used to react with the backbone of the polymer via a radical insertion mechanism. To achieve covalent linking to thiol containing DPTE lipids in the membrane a free maleimide group was needed. After the sulfo-SANPAH reaction was carried out, a short heterobifunctional PEG molecule (10 units long) with terminal amine and maleimide moieties was added. Now the substrate was prepared for covalent reaction to functional lipids.

4.4.2 Lipid Monolayer Homogeneity on Direct Linked PGTBs

After thoroughly rinsing the functionalized polymer hydrogel, to remove any unbound small molecules from the crosslinking molecules, a monolayer of lipids was added via LB deposition. When using fluorescently labeled lipids in the transfer, EPI imaging was done, and the resulting micrograph shows that the transfer was complete and efficient. There is an effective transfer of lipids because of the attractive interface presented by the polyacrylamide, this is worth noting since previous LB transfers were completed on protein functionalized hydrogels. Observed from the micrograph is the complete, homogeneous coverage of lipids across the sample, indicating that the support material is suitable for the formation of planar lipid bilayers. This is in agreement with previous data reported by Kuhner and Sackmann,

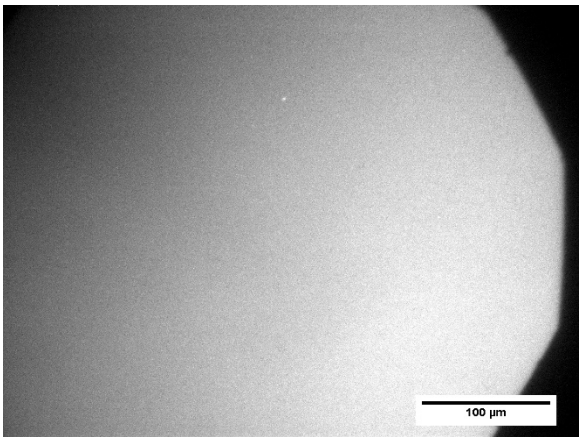

Figure 35. Shows a directly linked monolayer of lipids (POPC, 5 mol% DPTE, 0.2 mol% TRITC-DHPE) transferred by LB dipping and imaged with EPI fluorescent microscope.

where they transferred a lipid monolayer to polyacrylamide hydrogels with various crosslinking densities [199]. In both the Kuhner and Sackmann work and this work lipid monolayers were transferred under normal dipping conditions of surface tension and subphase conditions; however, in the current work there is a PEG supporting layer and covalent connections established between the lipid layer and polymer support. With a lipid monolayer transferred, once again the LB/VF strategy for forming a lipid bilayer was pursued.

4.4.3 Lipid Bilayer Homogeneity on Directly Linked PGTBs

With the addition of SUVs; lipid composition was POPC, 5 mol% DPTE, and 0.2 mol% TRITC-DHPE; a bilayer was formed on the direct linked PGTB system. When the excess vesicles were removed by washing with milli-Q water, the resulting membrane was imaged with EPI microscopy. Figure 36 shows a membrane that is complete and homogenous, there are no dark areas that are not covered by the lipid membrane. In this micrograph there are some bright spots in the image, these bright defects are thought to be excess lipid vesicle material that is bound to the membrane and unable to be rinsed away. Achieving complete coverage of the membrane indicates that the directly linked PGTB system will likely be suitable for the plating of cells.

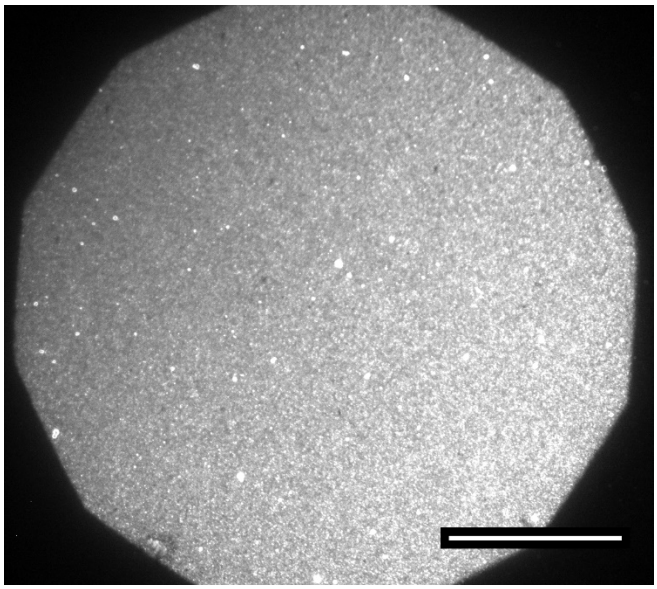

Figure 36. Formation on a planar lipid bilayer on the polyacrylamide hydrogel was imaged with EPI microscopy. Scale bar = 100 μm.

4.4.4 Spot Photobleaching Analysis on Directly Linked PGTBs

Further analysis was completed with EPI microscopy, spot photobleaching was again used as a qualitative indication of the diffusion properties of the lipid bilayer, shown in Fig 37. After bleaching a small area of the sample, the fluorescence in the bleached area is replenished, although there is a sizable immobile fraction in this sample. The main objective of fabrication and synthesis of a lipid bilayer is the presence of lateral lipid diffusion, this is a critical property of the plasma membrane that will be integral to reproducing realistic cell-to-cell like interactions. The presence of an immobile fraction does not mean that the membrane system will be unsuitable for the plating of adherent cells, and on the contrary increasing the viscosity of the membrane has been used as a means to accomplish cell spreading on solid supported membranes, which are usually not suitable for this type of analysis [78]. The main findings from this analysis is the capability to form a membrane on a polyacrylamide hydrogel support using a short heterobifunctional linker architecture and that this system maintains some lipid diffusion.

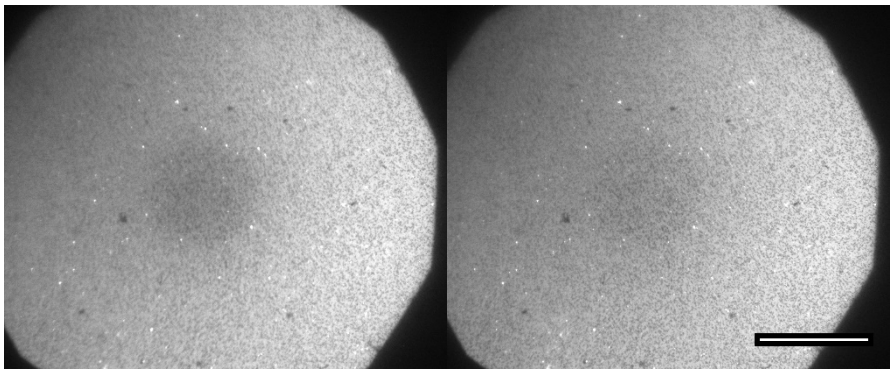

Figure 37. Spot photobleaching assay showing recovery of fluorescent lipid signal of directly linked PGTB. Scale bar = 100 μm.

4.4.5 FCS Autocorrelation Analysis on Directly Linked PGTBs

In addition to spot photobleaching, FCS autocorrelation analysis was pursued in the directly linked bilayer system. Figure 38 contains intensity versus time data collected as fluorescent lipids pass through the confocal volume and emit light. The presence of peaks in the raw data indicate that fluorescent molecules enter and exit the confocal volume and the fitting of the autocorrelation analysis both support that there is lateral mobility in the directly linked PGTB. Here the difference in length scale of analysis between FCS and spot photobleaching are easily observed. From the spot photobleaching data in Fig 37, there was a considerable immobile fraction of lipids and the presence of mobile lipid fraction was observed. These two fractions are observed due to the imaging of a large area, and the bleaching of a square micron sized area. However, in FCS, observation of the sample only occurs at a small, optically limited confocal volume that is on the nm^2 area. As seen in Fig 38, there are intensity peaks in the left panel, these are the raw data peaks that indicate the passing of a fluorescent molecule into and out of the observation area. In Fig 38 only laterally mobile lipids are observed diffusing through the membrane, there is no capability of the system to observe lipid species that do not diffuse. The autocorrelation fit of the raw data, shown in the right panel of Fig 38, indicate that the laterally mobile lipids in the directly linked PGTB have a characteristic diffusion time in the range expected for lipids in a supported membrane.

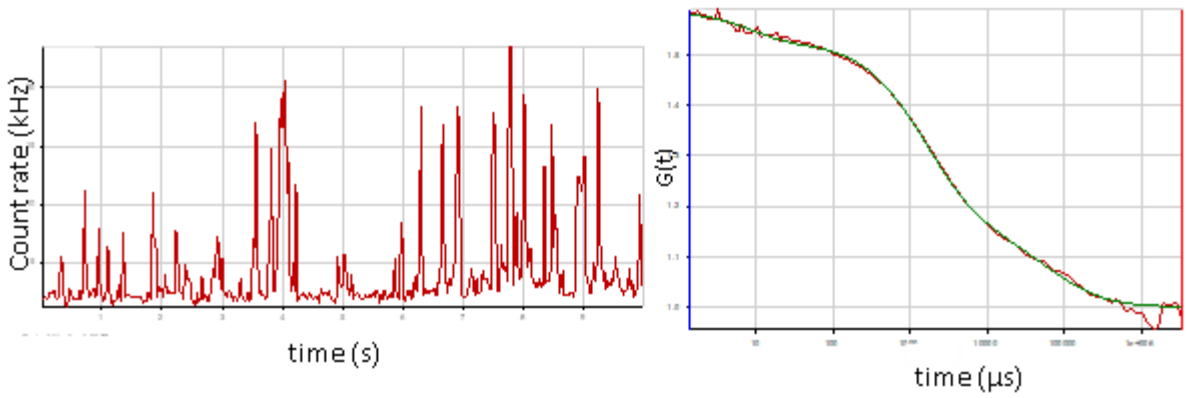

Figure 38. FCS microscopy was used to analyze the diffusion properties of directly linked PGTB membranes, TRITC-DHPE fluorescent lipids were used to label the bilayer. The panel on the right shows the raw data, the peaks are intensity spikes that are measured as fluorescent species pass through the confocal volume. On the left, the resulting autocorrelation analysis is shown.

4.4.6 N-Cadherin Chimera Functionalized Directly Linked PGTBs

After confirming the formation of a lipid bilayer on the directly linked PGTB architecture, further steps were taken to prepare the substrate for plating of adherent myoblast cells. Functionalization of the directly linked PGTB containing DGS-NTA lipids was accomplished with the addition of histidine-tagged N-cadherin chimera. After the addition of N-cadherin, the confocal micrograph in Fig 39 was captured. This micrograph shows an evenly distributed fluorescent signal of N-cadherin that was bound to the membrane. Prior to imaging, excess N-cadherin molecules that were not bound to the DGS-NTA chelating lipids were rinsed away with excess PBS buffer, this was done to ensure that no non-specifically adsorbed protein remained on the surface of the lipid bilayer.

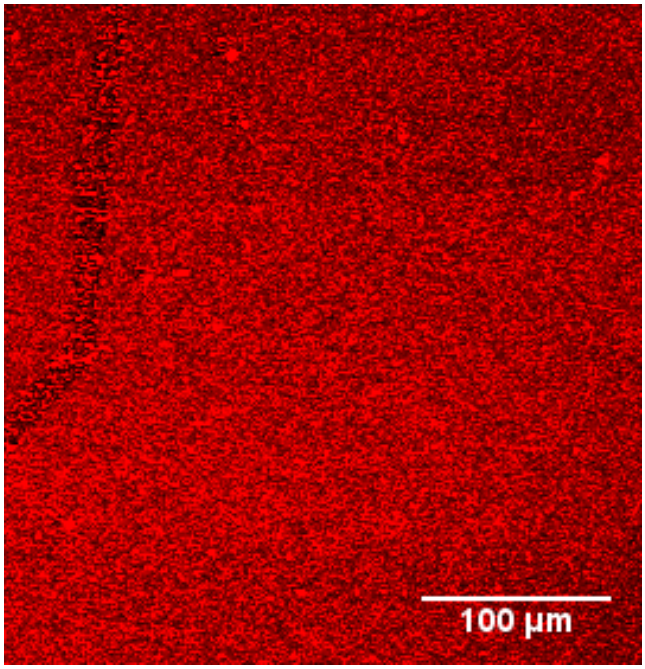

Figure 39. Confocal microscopy was used to analyze the distribution of N-cadherin added to PGTBs that contained DGS-NTA chelating lipid.

4.4.7 Cell Spreading on Direct Covalently Linked PGTBs

After functionalization of the directly linked PGTB with N-cadherin was confirmed, samples were prepared for the plating of adherent cells to test the suitability of this architecture for studies of cellular interaction. Upon plating C2C12 myoblasts to the directly linked PGTB, cells were able to adhere and spread; however, there was no accumulation of N-cadherin observed under plated cells. Figure 40 shows two channels, the DIC revealing cell shape and the Alexa555 channel for the N-cadherin. Here in the directly linked PGTB cell spreading is observed, but there is a lack of accumulated N-cadherin molecules, as has been previously shown to be a characteristic of PTLB [9] and PGTB systems, for the mimicking of cell-to-cell adhesions. These preliminary results indicate that further optimization of directly linked PGTB is needed, but this appears to be a promising platform for the study of cellular mechanoresponse. The current hypothesis is that the directly linked PGTB architecture will be an even more robust and stable system for interaction with adherent cells. Advances beyond the FN linked PGTB system include the simplification of the covalent linking from polymer hydrogel to the lipid bilayer and the removal of a protein layer. This protein layer may reduce the mechanical stability of the architecture if not all molecules are

covalently bound to the polymer hydrogel, which may occur in a system where non-covalent interactions between FN proteins spontaneously form networks. This would be overcome with a PGTB architecture, similar to that presented in Section 4.4.

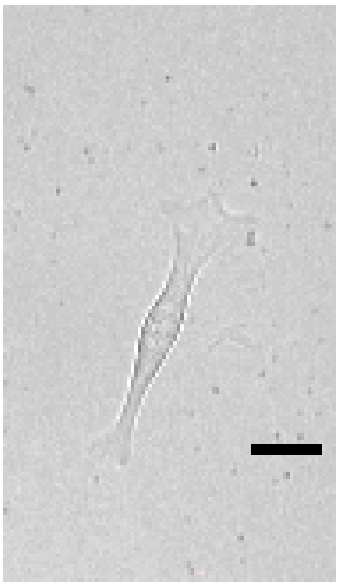

Figure 40. The confocal micrograph shows a cell spread on a directly linked PGTB functionalized with N-cadherin, the image was taken 24 hours after cell plating, and the image is a composite of DIC channel showing the cell outline and Alexa555 labeled N-cadherin. Scale bar = 25 μm

CHAPTER 5. CONCLUSIONS AND OUTLOOK

5.1 Conclusions

Because of the remarkable dynamics and plasticity seen at intercellular junctions, such as adherens junctions, fabricating model systems proved to be challenging and out of reach of technical capabilities. To replicate the properties of an intercellular junction in a model system there needs to be a viable route to allow the dynamic reorganization of the material, while maintaining stability to allow cellular generated traction forces to be transduced. Another requirement for a viable model system is the ability to fabricate systems that are elastically tunable, physiological relevant range would be the most desirable. Previous advancements utilizing lipid bilayer materials have showed promise to be model systems that allow the reproduction of intercellular adhesion properties [7-9].

Within this dissertation, a platform was presented for the fabrication and utilization of polymer and lipid-based materials for the study of mechanotransduction at intercellular junctions. The selection of each material used in the fabrication strategy was done with care to produce a material that mimicked the plasma membrane surface. Starting with the polyacrylamide, which is a hydrophilic, inert, water filled polymer, that provided a hydrogel network that could be accurately tuned across a wide range of physiologically relevant stiffnesses. Building on this stable polymer hydrogel, further functionalization was pursued to stably link proteins to the polymer via specific chemistry routes. Also demonstrated was the applicability of the polyacrylamide and protein linked systems to act as a support material for the addition of a lipid bilayer. When care was taken to produce high quality vesicles, following a LB deposition, lipid bilayers were efficiently produced, and membranes maintained important diffusion properties.

Three distinct substrate designs were pursued: neutravidin linked, fibronectin linked, and direct covalent. Each of these substrates were designed, fabricated, and analyzed within this dissertation work. Each system pursued has many similarities, but distinct properties allow for specific strengths for use with future applications. For the neutravidin linked system, high quality membranes were formed, possibly because of the stability provided by the tetrameric binding protein to connect the membrane and hydrogel components. On the neutravidin linked PGTB system, stable monolayers were formed, FRAP and FCS evaluation demonstrated that lipids were

laterally mobile. This result is in contrast to solid supported monolayers, which are known to be immobile, frozen to the solid support until the bilayer structure is formed and the membrane is hydrated. However, on PGTBs monolayers maintain diffusion while the system is hydrated and interesting properties of the obstructed diffusion and coupling of the membrane to the underlying substrate can be evaluated. Furthermore, on neutravidin linked PGTBs, lipid diffusion was investigated and lipids were found to be laterally mobile and showed consistent diffusion characteristics similar to PTLB systems previously reported.

The FN linked system was shown to be a powerful platform for the analysis of cell adhesion and future studies of mechanotransduction. Once again seen on the FN linked PGTB system, was the formation of monolayers and bilayers that were homogeneous, and minimal adsorbed vesicles were observed. When the FN linked PTLB was labeled with TRITC-DHPE, FCS and FRAP data showed lateral diffusion properties, which are important for the replication of intercellular junction properties. In this PGTB model system, it was shown that the covalent linking strategy produced membranes capable of withstanding cell generated forces from C2C12 myoblasts. When the polyacrylamide hydrogel stiffness was changed from 500 Pa up to 38 kPa, statistically significant changes in cell spreading area were observed. Like that seen in cell clusters, attachments between cells and the PGTB material were dynamic, while allowing for the transduction of cellular generated traction forces. C2C12 myoblast cells were also shown to be able to rearrange N-cadherin molecules bound to the membrane surface. This rearrangement and organization at cellular adhesion sites, is a very interesting property seen in cell clusters [109] and in previous work with PTLB systems [9]. Another relevant characteristic of the strategy pursued in this study is the method used for the visualization of cellular adhesions. In this work, no fluorescent staining or transfection methods were used, which eliminates potential artefacts produced by the incorporation of plasmid DNA. Without the requirement for labeling cell components, it is also more efficient to utilize different cell lines in these assays, as only traditional cell culture according to established protocols is needed. Evaluating cell data set from the FN linked PGTB, the capability of the PGTB platform as a viable material for use in studies to investigate the effects of stiffness on cellular properties was demonstrated.

Finally, the direct covalent linked system provides an interesting pathway to produce a more simplified system, here the advantage may lie in the ability to more fully understand the transfer of cell generated forces to the substrate. Synthesizing a novel crosslinker molecule allowed

the functionalization of the polyacrylamide and covalent attachment to thiol functional lipids in the membrane. Once again stable bilayers were formed in this direct link system, with qualitative spot photobleaching and FCS autocorrelation analyses demonstrating the lateral mobility of the lipids. Cells were shown to be able to spread, and further work can be done to verify the capability of the directly linked system to serve as a cell substrate.

In summary for use as a platform to study interactions with adherent cells, PGTBs were shown to be robust and stable systems on which cells can spread, which indicates that enough traction forces could be transduced through the PGTB substrate. The active accumulation of cell adhesion molecules into clusters mimics cellular junctions and demonstrates the significance of obstructed diffusion in allowing cells to spread, where a size-dependent diffusion pattern is observed. The individual N-cadherin adhesion molecules diffuse randomly in the PGTB; however, when a cell organizes a cluster of substrate-bound N-cadherin there is adequate resistance to allow the cell to spread and migrate on these materials. Because a lipid tethering approach was pursued, obstructed diffusion acts in favor of allowing cell spreading, by causing a slowdown of diffusion, advantageous for the plating of cells.

5.2 Outlook

Future experiments utilizing the platform established with this research look to analyze interesting properties and allow previously unattainable questions to be answered. With a highly adaptable strategy established, there are several avenues of experimentation that are directly attainable with the current understanding. Experiments that employ different cell adhesion molecules, in addition to N-cadherin, would allow an extension of this work to different cell lines, with different biological implications to be studied. Lipid bilayers fabricated in this work contained DGS-NTA, which is a functional lipid containing a chelator molecule in its head group, potentially any protein with a histidine-tag could be coupled to these membranes. This opens different biologically relevant interactions, even possible would be the presentation of more than one type of cell adhesion molecule, e.g., presenting both N-cadherin and e-cadherin may cause a significant change in cell function for olfactory supporting cells [205]. Cell lines express different cell adhesion molecules, therefore, a platform that can easily present different kinds of proteins would be of interest.

Originally the design for the polymer gel-tethered bilayer, was modeled after a traction force microscopy (TFM) assay [206]. In a traditional TFM assay, fluorescent beads are incorporated into the polymer hydrogel, the hydrogel is functionalized with cell adhesion molecules, cells are plated and allowed to adhere [207, 208]. Once cells are adhered, the stressed deformed hydrogel is imaged, cells cause deformation of the hydrogel due to the traction forces. After the first imaging series, the cells are removed from the substrate, by trypsin or cytochalasin D, now the hydrogel relaxes back, and another set of images are acquired. The PGTB materials fabricated in this study could be optimized for a TFM assays, which would reveal quantitative and localized information about cellular generated forces. Similarly, to investigate the amount of force generated at the cellular adhesions, it would be interesting to incorporate molecular tension probes that would allow the imaging of forces at the cell surface [209]. These methods utilize a probe molecule that is a polymer, oligonucleotide, or protein, this molecule acts as a spring having a known force constant. The probe is functionalized with a fluorescent molecule and a quencher, the fluorophore emits fluorescence that is dependent on the location of the quencher, thus revealing the extended state of the probe. Interesting quantitative data could be acquired with this type of force probe assay.

Previous work has established PTLBs as a viable platform for the incorporation of transmembrane proteins [210, 211], allowing for biophysical investigations into the effects of lipid composition and ligands. These methods for incorporating proteins could be applied to PGTBs, which even more so than PTLB that are ~5 nm uplifted from the solid support, are removed from the solid denaturing substrate. Of particular interest, would be the possibility of incorporating transmembrane proteins that normally have a prohibitively large cytoplasmic domain. In future work, one could envision the possibility to study protein-protein interactions between the incorporated membrane bound protein and the protein used as the linking protein. Due to the presence of an inert polymer, such as polyacrylamide, incorporated proteins should be highly mobile and free from perturbation from any solid materials, which is traditionally the downfall of supported membranes [14].

The final future experiment would be the development of a different architecture for the presentation of cell adhesion molecules. In the current work, DGS-NTA lipid was used as the architecture for attaching the cell adhesion molecules. With a lipid-based linkage, there is the potential that as force is transferred to the substrate only the top leaflet of the membrane could be

dragged, and that inter-leaflet coupling would be overcome due to the presentation of cellular generated forces. Alternative architectures could include molecules such as transmembrane peptides. There are interesting options to pursue for this type of work, thorough biophysical studies have been conducted on transmembrane alpha-helical peptides, meaning that a very well understood molecule could be used. For example, WALP (tryptophan, alanine, leucine Peptide) contains alanine and leucine repeats along the hydrophobic core of the membrane and is flanked by tryptophan, a bulky amino acid that acts to anchor the peptide in the membrane [212]. Studies have been completed to show the desired length of peptide [213], there are established protocols for fluorescent labeling [214], and the terminal carboxylic and amine ends could be functionalized to produce an interesting linker peptide. One strategy would be to add an activated ester molecule to one end of the peptide, incorporate a cysteine residue for easy fluorescent molecule labeling, and on the opposite end of the peptide add a chelating molecule to attach histidine-tagged protein. With this type of hybrid linker, that would be membrane spanning and covalently bound to the underlying substrate, interesting studies about the importance of cell adhesion molecule diffusion could be pursued. A differing strategy would be to not functionalize the WALP to the polymer substrate, and only add a chelating group, in this strategy the WALP would be free to diffuse and be reorganized by cell generated forces. The main goal of this transmembrane cell adhesion molecule presentation would be to modify the way force generated by the cell would be transferred to the tethered membrane and prevent inter-leaflet uncoupling from happening.

REFERENCES

[1] A. J. Engler, et al., Matrix elasticity directs stem cell lineage specification, Cell 126 (2006) 677-689.

[2] S. Willenborg and S. A. Eming, Cellular networks in wound healing, Science 362 (2018) 891-892.

[3] R. J. Pelham, Jr. and Y. Wang, Cell locomotion and focal adhesions are regulated by substrate flexibility, Proceedings of the National Academy of Sciences of the United States of America 94 (1997) 13661-13665.

[4] D. E. Discher, et al., Tissue cells feel and respond to the stiffness of their substrate, Science 310 (2005) 1139-1143.

[5] V. Vogel and M. Sheetz, Local force and geometry sensing regulate cell functions, Nature Reviews Molecular Cell Biology 7 (2006) 265-275.

[6] A. M. Ross, et al., Physical aspects of cell culture substrates: Topography, roughness, and elasticity, Small 8 (2012) 336-355.

[7] L. A. Lautscham, et al., Biomembrane-mimicking lipid bilayer system as a mechanically tunable cell substrate, Biomaterials 35 (2014) 3198-3207.

[8] D. E. Minner, et al., Polymer-tethered lipid multi-bilayers: A biomembrane-mimicking cell substrate to probe cellular mechano-sensing, Soft Matter 10 (2014) 1189-1198.

[9] Y. Ge, et al., N-cadherin-functionalized polymer-tethered multi-bilayer: A cell surface-mimicking substrate to probe cellular mechanosensitivity, Soft Matter 12 (2016) 8274-8284.

[10] M. L. Dustin, et al., Purified lymphocyte function-associated antigen 3 binds to cd2 and mediates t lymphocyte adhesion, Journal of Experimental Medicine 165 (1987) 677-692.

[11] T. A. Springer, Adhesion receptors of the immune system, Nature 346 (1990) 425-434.

[12] C. Wulfing, et al., Visualizing the dynamics of t cell activation: Intracellular adhesion molecule 1 migrates rapidly to the t cell/b cell interface and acts to sustain calcium levels, Proceedings of the National Academy of Sciences of the United States of America 95 (1998) 6302-6307.

[13] A. Grakoui, The immunological synapse: A molecular machine controlling t cell activation, Science 285 (1999) 221-227.

[14] M. Tanaka and E. Sackmann, Polymer-supported membranes as models of the cell surface, Nature 437 (2005) 656-663.

[15] N. F. Hussain, et al., Bilayer asymmetry influences integrin sequestering in raft-mimicking lipid mixtures, Biophysical Journal 104 (2013) 2212-2221.

[16] M. A. Deverall, et al., Membrane lateral mobility obstructed by polymer-tethered lipids studied at the single molecule level, Biophysical Journal 88 (2005) 1875-1886.

[17] Rayleigh, Surface tension, Nature 43 (1891) 437-439.

[18] I. Langmuir, The constitution and fundamental properties of solids and liquids. Ii. Liquids.1, Journal of the American Chemical Society 39 (1917) 1848-1906.

[19] K. B. Blodgett, Films built by depositing successive monomolecular layers on a solid surface, Journal of the American Chemical Society 57 (1935) 1007-1022.

[20] J. S. Allhusen and J. C. Conboy, The ins and outs of lipid flip-flop, Accounts of Chemical Research 50 (2017) 58-65.

[21] I. Langmuir and V. J. Schaefer, Activities of urease and pepsin monolayers, Journal of the American Chemical Society 60 (1938) 1351-1360.

[22] D. Magde, et al., Thermodynamic fluctuations in a reacting system---measurement by fluorescence correlation spectroscopy, Physical Review Letters 29 (1972) 705-708.

[23] D. Magde, et al., Fluorescence correlation spectroscopy. Ii. An experimental realization, Biopolymers 13 (1974) 29-61.

[24] P. Schwille, Fluorescence correlation spectroscopy and its potential for intracellular applications, Cell Biochemistry and Biophysics 34 (2001) 383-408.

[25] T. Jankowski and R. Janka, Confocor 2 — the second generation of fluorescence correlation microscopes, Springer Series in Chemical Physics 65 (2001) 331-345.

[26] Y. Sako and A. Kusumi, Barriers for lateral diffusion of transferrin receptor in the plasma membrane as characterized by receptor dragging by laser tweezers: Fence versus tether, Journal of Cell Biology 129 (1995) 1559-1574.

[27] T. V. Ratto and M. L. Longo, Obstructed diffusion in phase-separated supported lipid bilayers: A combined atomic force microscopy and fluorescence recovery after photobleaching approach, Biophysical Journal 83 (2002) 3380-3392.

[28] D. Axelrod, et al., Mobility measurement by analysis of fluorescence photobleaching recovery kinetics, Biophysical Journal 16 (1976) 1055-1069.

[29] D. M. Soumpasis, Theoretical analysis of fluorescence photobleaching recovery experiments, Biophysical Journal 41 (1983) 95-97.

[30] M. Kang, et al., Simplified equation to extract diffusion coefficients from confocal frap data, Traffic 13 (2012) 1589-1600.

[31] N. Özkaya and M. Nordin (1999). Mechanical properties of biological tissues. Fundamentals of biomechanics, Springer: 195-218.

[32] H. M. Wyss, et al., Oscillatory rheology: Measuring the viscoelastic behaviour of soft materials, G.I.T. Laboratory Journal 3 (2007) 68-70.

[33] T. Boudou, et al., An extended relationship for the characterization of young's modulus and poisson's ratio of tunable polyacrylamide gels, Biorheology 43 (2006) 721-728.

[34] B. D. Hames (1998). Gel electrophoresis of proteins : A practical approach. Oxford ; New York, Oxford University Press.

[35] Y. Zhao, et al., Clinical and histologic evaluation of a new injectable implant:: Hydrophilic polyacrylamide gel, Annals of Plastic Surgery 53 (2004) 267-272.

[36] A. Suzuki, et al., Direct observation of polymer gel surfaces by atomic force microscopy, The Journal of Chemical Physics 104 (1996) 1751-1757.

[37] S. M. Russell and G. Carta, Mesh size of charged polyacrylamide hydrogels from partitioning measurements, Industrial & Engineering Chemistry Research 44 (2005) 8213-8217.

[38] N. C. Stellwagen, Apparent pore size of polyacrylamide gels: Comparison of gels cast and run in tris-acetate-edta and tris-borate-edta buffers, ELECTROPHORESIS 19 (1998) 1542-1547.

[39] J. R. Tse and A. J. Engler, Preparation of hydrogel substrates with tunable mechanical properties, Current Protocols in Cell Biology 47 (2010) 10.16.11-10.16.16.

[40] C. Tribet and F. Vial, Flexible macromolecules attached to lipid bilayers: Impact on fluidity, curvature, permeability and stability of the membranes, Soft Matter 4 (2008) 68-81.

[41] D. Marsh, Elastic constants of polymer-grafted lipid membranes, Biophysical Journal 81 (2001) 2154-2162.

[42] D. Marsh, et al., Lipid membranes with grafted polymers: Physicochemical aspects, Biochimica et Biophysica Acta 1615 (2003) 33-59.

[43] M. Pantusa, et al., Shifts in chain-melting transition temperature of liposomal membranes by polymer-grafted lipids, Biochimica et Biophysica Acta (BBA) - Biomembranes 1614 (2003) 165-170.

[44] C. Hiergeist and R. Lipowsky, Elastic properties of polymer-decorated membranes, Journal de Physique II 6 (1996) 1465-1481.

[45] V. Nikolov, et al., Behavior of giant vesicles with anchored DNA molecules, Biophysical Journal 92 (2007) 4356-4368.

[46] F. Vial, et al., Long-living channels of well defined radius opened in lipid bilayers by polydisperse, hydrophobically-modified polyacrylic acids, Soft Matter 3 (2007) 75-78.

[47] M. Chakrapani, et al., Acrylamide polymerized in the presence of surfactants: Surface analysis using atomic force microscopy, Langmuir 18 (2002) 6449-6452.

[48] C. A. Keller and B. Kasemo, Surface specific kinetics of lipid vesicle adsorption measured with a quartz crystal microbalance, Biophysical Journal 75 (1998) 1397-1402.

[49] M. J. Peel, et al., Rupture of stochastically occurring vesicle clusters limits bilayer formation on alkane-peg-type supports: Uncoupling clustering from surface coverage, Langmuir 31 (2015) 8830-8840.

[50] E. Kalb, et al., Formation of supported planar bilayers by fusion of vesicles to supported phospholipid monolayers, Biochimica et Biophysica Acta (BBA) - Biomembranes 1103 (1992) 307-316.

[51] J. M. Crane, et al., Measuring lipid asymmetry in planar supported bilayers by fluorescence interference contrast microscopy, Langmuir 21 (2005) 1377-1388.

[52] M. L. Wagner and L. K. Tamm, Reconstituted syntaxin1a/snap25 interacts with negatively charged lipids as measured by lateral diffusion in planar supported bilayers, Biophysical Journal 81 (2001) 266-275.

[53] R. O. Hynes, Integrins: Bidirectional, allosteric signaling machines, Cell 110 (2002) 673-687.

[54] E. E. Schneeberger and R. D. Lynch, The tight junction: A multifunctional complex, American Journal of Physiology 286 (2004) C1213-C1228.

[55] A. S. Yap, et al., Molecular and functional analysis of cadherin-based adherens junctions, Annual Review of Cell and Developmental Biology 13 (1997) 119-146.

[56] D. A. Goodenough, et al., Connexins, connexons, and intercellular communication, Annual Review of Biochemistry 65 (1996) 475-502.

[57] E. Zamir and B. Geiger, Molecular complexity and dynamics of cell-matrix adhesions, Journal of Cell Science 114 (2001) 3583-3590.

[58] M. Abercrombie, et al., The locomotion of fibroblasts in culture: Iv. Electron microscopy of the leading lamella, Experimental Cell Research 67 (1971) 359-367.

[59] M. Abercrombie and G. Dunn, Adhesions of fibroblasts to substratum during contact inhibition observed by interference reflection microscopy, Experimental Cell Research 92 (1975) 57-62.

[60] C. Izzard and L. R. Lochner, Cell-to-substrate contacts in living fibroblasts: An interference reflexion study with an evaluation of the technique, Journal of Cell Science 21 (1976) 129-159.

[61] C. S. Izzard and L. R. Lochner, Formation of cell-to-substrate contacts during fibroblast motility: An interference-reflexion study, Journal of Cell Science 42 (1980) 81-116.

[62] B. Geiger, et al., Environmental sensing through focal adhesions, Nature Reviews Molecular Cell Biology 10 (2009) 21-33.

[63] J. Takagi, et al., Global conformational rearrangements in integrin extracellular domains in outside-in and inside-out signaling, Cell 110 (2002) 599-511.

[64] X. Zhang, et al., Talin depletion reveals independence of initial cell spreading from integrin activation and traction, Nature Cell Biology 10 (2008) 1062-1068.

[65] A. R. Gingras, et al., Structural and dynamic characterization of a vinculin binding site in the talin rod, Biochemistry 45 (2006) 1805-1817.

[66] A. del Rio, et al., Stretching single talin rod molecules activates vinculin binding, Science 323 (2009) 638-641.

[67] T. S. Malinova and S. Huveneers, Sensing of cytoskeletal forces by asymmetric adherens junctions, Trends in Cell Biology 28 (2018) 328-341.

[68] F. Twiss and J. de Rooij, Cadherin mechanotransduction in tissue remodeling, Cellular and Molecular Life Sciences 70 (2013) 4101-4116.

[69] A. Kourtidis, et al., A central role for cadherin signaling in cancer, Experimental Cell Research 358 (2017) 78-85.

[70] V. Vasioukhin, et al., Directed actin polymerization is the driving force for epithelial cell–cell adhesion, Cell 100 (2000) 209-219.

[71] C. Bertocchi, et al., Nanoscale architecture of cadherin-based cell adhesions, Nature Cell Biology 19 (2017) 28-37.

[72] A. Angulo-Urarte, et al., Cell-cell junctions as sensors and transducers of mechanical forces, Biochimica et Biophysica Acta (BBA) - Biomembranes 1862 (2020) 183316.

[73] R. Zaidel-Bar, Cadherin adhesome at a glance, Journal of Cell Science 126 (2013) 373-378.

[74] B. Ladoux, et al., The mechanotransduction machinery at work at adherens junctions, Integrative Biology: Quantitative Biosciences from Nano to Macro 7 (2015) 1109-1119.

[75] M. K. L. Han and J. de Rooij, Converging and unique mechanisms of mechanotransduction at adhesion sites, Trends in Cell Biology 26 (2016) 612-623.

[76] C. K. Choi, et al., Actin and alpha-actinin orchestrate the assembly and maturation of nascent adhesions in a myosin ii motor-independent manner, Nature Cell Biology 10 (2008) 1039-1050.

[77] R. Changede, et al., Nascent integrin adhesions form on all matrix rigidities after integrin activation, Developmental Cell 35 (2015) 614-621.

[78] K. H. Biswas, et al., E-cadherin junction formation involves an active kinetic nucleation process, Proceedings of the National Academy of Sciences of the United States of America 112 (2015) 10932-10937.

[79] H. Wolfenson, et al., Tropomyosin controls sarcomere-like contractions for rigidity sensing and suppressing growth on soft matrices, Nature Cell Biology 18 (2016) 33-42.

[80] X. Hu, et al., Cooperative vinculin binding to talin mapped by time-resolved super resolution microscopy, Nano Lett 16 (2016) 4062-4068.

[81] C. Collins, et al., Changes in e-cadherin rigidity sensing regulate cell adhesion, Proceedings of the National Academy of Sciences 114 (2017) E5835-E5844.

[82] C. S. Chen, et al., Geometric control of cell life and death, Science 276 (1997) 1425-1428.

[83] A. Curtis and C. Wilkinson, New depths in cell behaviour: Reactions of cells to nanotopography, Biochemical Society Symposia 65 (1999) 15-26.

[84] R. McBeath, et al., Cell shape, cytoskeletal tension, and rhoa regulate stem cell lineage commitment, Developmental Cell 6 (2004) 483-495.

[85] J. Zimmerberg and S. McLaughlin, Membrane curvature: How bar domains bend bilayers, Current Biology 14 (2004) R250-R252.

[86] M. J. Dalby, et al., Use of nanotopography to study mechanotransduction in fibroblasts--methods and perspectives, European Journal of Cell Biology 83 (2004) 159-169.

[87] E. Martines, et al., A parallel-plate flow chamber to study initial cell adhesion on a nanofeatured surface, IEEE Transactions on NanoBioscience 3 (2004) 90-95.

[88] M. Tamada, et al., Activation of a signaling cascade by cytoskeleton stretch, Developmental Cell 7 (2004) 709-718.

[89] D. Douguet and E. Honoré, Mammalian mechanoelectrical transduction: Structure and function of force-gated ion channels, Cell 179 (2019) 340-354.

[90] J. Wu, et al., Touch, tension, and transduction – the function and regulation of piezo ion channels, Trends in Biochemical Sciences 42 (2017) 57-71.

[91] R. Merkel, et al., Energy landscapes of receptor–ligand bonds explored with dynamic force spectroscopy, Nature 397 (1999) 50-53.

[92] C. Ibar, et al., Tension-dependent regulation of mammalian hippo signaling through limd1, Journal of Cell Science 131 (2018) jcs214700.

[93] N. K. Noren, et al., Cadherin engagement regulates rho family gtpases, Journal of Biological Chemistry 276 (2001) 33305-33308.

[94] W. M. Brieher and A. S. Yap, Cadherin junctions and their cytoskeleton(s), Current Opinion in Cell Biology 25 (2013) 39-46.

[95] H. Wolfenson, et al., Steps in mechanotransduction pathways that control cell morphology, Annual Review of Physiology 81 (2019) 585-605.

[96] N. Jain, et al., Cell geometric constraints induce modular gene-expression patterns via redistribution of hdac3 regulated by actomyosin contractility, Proceedings of the National Academy of Sciences 110 (2013) 11349-11354.

[97] Y. Hou, et al., Surface roughness and substrate stiffness synergize to drive cellular mechanoresponse, Nano Letters 20 (2020) 748-757.

[98] C. M. Lo, et al., Cell movement is guided by the rigidity of the substrate, Biophysical Journal 79 (2000) 144-152.

[99] P. C. Georges and P. A. Janmey, Cell type-specific response to growth on soft materials, J Appl Physiol (1985) 98 (2005) 1547-1553.

[100] T. Yeung, et al., Effects of substrate stiffness on cell morphology, cytoskeletal structure, and adhesion, Cell Motility and the Cytoskeleton 60 (2005) 24-34.

[101] K. Ghosh, et al., Cell adaptation to a physiologically relevant ecm mimic with different viscoelastic properties, Biomaterials 28 (2007) 671-679.

[102] P. Friedl, et al., New dimensions in cell migration, Nature Reviews Molecular Cell Biology 13 (2012) 743-747.

[103] E. Hachet, et al., Design of biomimetic cell-interactive substrates using hyaluronic acid hydrogels with tunable mechanical properties, Biomacromolecules 13 (2012) 1818-1827.

[104] F. Rehfeldt, et al., Hyaluronic acid matrices show matrix stiffness in 2d and 3d dictates cytoskeletal order and myosin-ii phosphorylation within stem cells, Integrative Biology 4 (2012) 422-430.

[105] T. Pompe, et al., Friction-controlled traction force in cell adhesion, Biophysical Journal 101 (2011) 1863-1870.

[106] A. P. Kourouklis, et al., Cell adhesion mechanisms on laterally mobile polymer films, Biomaterials 35 (2014) 4827-4834.

[107] D. Stroumpoulis, et al., Cell adhesion and growth to peptide-patterned supported lipid membranes, Langmuir 23 (2007) 3849-3856.

[108] Y. Kametani and M. Takeichi, Basal-to-apical cadherin flow at cell junctions, Nature Cell Biology 9 (2007) 92-98.

[109] F. Peglion, et al., Adherens junction treadmilling during collective migration, Nature Cell Biology 16 (2014) 639-651.

[110] L. K. Tamm and H. M. McConnell, Supported phospholipid bilayers, Biophysical Journal 47 (1985) 105-113.

[111] E. Sackmann, Supported membranes: Scientific and practical applications, Science 271 (1996) 43-48.

[112] E. T. Castellana and P. S. Cremer, Solid supported lipid bilayers: From biophysical studies to sensor design, Surface Science Reports 61 (2006) 429-444.

[113] A. A. Brian and H. M. McConnell, Allogeneic stimulation of cytotoxic t cells by supported planar membranes, Proceedings of the National Academy of Sciences of the United States of America 81 (1984) 6159-6163.

[114] J. Raedler, et al., Phenomenology and kinetics of lipid bilayer spreading on hydrophilic surfaces, Langmuir 11 (1995) 4539-4548.

[115] S. J. Johnson, et al., Structure of an adsorbed dimyristoylphosphatidylcholine bilayer measured with specular reflection of neutrons, Biophysical Journal 59 (1991) 289-294.

[116] S. Krueger, et al., Neutron reflectivity studies of single lipid bilayers supported on planar substrates, Basic Life Sciences 64 (1996) 205-213.

[117] J. Salafsky, et al., Architecture and function of membrane proteins in planar supported bilayers: A study with photosynthetic reaction centers †, Biochemistry 35 (1996) 14773-14781.

[118] K. Jacobson, Lateral diffusion in membranes, Cell Motility 3 (1983) 367-373.

[119] E. Sackmann, The seventh datta lecture. Membrane bending energy concept of vesicle- and cell-shapes and shape-transitions, FEBS Letters 346 (1994) 3-16.

[120] G. I. Bell, et al., Cell adhesion. Competition between nonspecific repulsion and specific bonding, Biophysical Journal 45 (1984) 1051-1064.

[121] A. Kloboucek, et al., Adhesion-induced receptor segregation and adhesion plaque formation: A model membrane study, Biophysical Journal 77 (1999) 2311-2328.

[122] S. F. Fenz, et al., Inter-membrane adhesion mediated by mobile linkers: Effect of receptor shortage, Soft Matter 7 (2011) 952-962.

[123] A. Albersdorfer, et al., Adhesion-induced domain formation by interplay of long-range repulsion and short-range attraction force: A model membrane study, Biophysical Journal 73 (1997) 245-257.

[124] A. Boulbitch, et al., Kinetics of membrane adhesion mediated by ligand-receptor interaction studied with a biomimetic system, Biophysical Journal 81 (2001) 2743-2751.

[125] L. B. Smilenov, et al., Focal adhesion motility revealed in stationary fibroblasts, Science 286 (1999) 1172-1174.

[126] A. S. Smith, et al., Force-induced growth of adhesion domains is controlled by receptor mobility, Proceedings of the National Academy of Sciences of the United States of America 105 (2008) 6906-6911.

[127] S. F. Fenz, et al., Membrane fluctuations mediate lateral interaction between cadherin bonds, Nat. Phys. 13 (2017) 906-913.

[128] R. Parthasarathy and J. T. Groves, Protein patterns at lipid bilayer junctions, Proceedings of the National Academy of Sciences of the United States of America 101 (2004) 12798-12803.

[129] S. D. Marlin and T. A. Springer, Purified intercellular adhesion molecule-1 (icam-1) is a ligand for lymphocyte function-associated antigen 1 (lfa-1), Cell 51 (1987) 813-819.

[130] M. L. Dustin and T. A. Springer, Lymphocyte function-associated antigen-1 (lfa-1) interaction with intercellular adhesion molecule-1 (icam-1) is one of at least three mechanisms for lymphocyte adhesion to cultured endothelial cells, Journal of Cell Biology 107 (1988) 321-331.

[131] A. Grakoui, et al., The immunological synapse: A molecular machine controlling t cell activation, Science 285 (1999) 221-227.

[132] C. R. Monks, et al., Three-dimensional segregation of supramolecular activation clusters in t cells, Nature 395 (1998) 82-86.

[133] S. Pautot, et al., Neuronal synapse interaction reconstituted between live cells and supported lipid bilayers, Nature Chemical Biology 1 (2005) 283-289.

[134] C. H. Yu, et al., Early integrin binding to arg-gly-asp peptide activates actin polymerization and contractile movement that stimulates outward translocation, Proceedings of the National Academy of Sciences of the United States of America 108 (2011) 20585-20590.

[135] C. H. Yu, et al., Integrin-matrix clusters form podosome-like adhesions in the absence of traction forces, Cell Reports 5 (2013) 1456-1468.

[136] C. J. Hsu, et al., Ligand mobility modulates immunological synapse formation and t cell activation, PloS One 7 (2012) e32398.

[137] J. Tsai and L. C. Kam, Lateral mobility of e-cadherin enhances rac1 response in epithelial cells, Cellular and Molecular Bioengineering 3 (2010) 84-90.

[138] V. P. Ma, et al., Ratiometric tension probes for mapping receptor forces and clustering at intermembrane junctions, Nano Lett 16 (2016) 4552-4559.

[139] C. R. Nowosad, et al., Germinal center b cells recognize antigen through a specialized immune synapse architecture, Nature Immunology 17 (2016) 870-877.

[140] R. Glazier and K. Salaita, Supported lipid bilayer platforms to probe cell mechanobiology, Biochimica et Biophysica Acta 1859 (2017) 1465-1482.

[141] Y. Liu, et al., DNA-based nanoparticle tension sensors reveal that t-cell receptors transmit defined pn forces to their antigens for enhanced fidelity, Proceedings of the National Academy of Sciences of the United States of America 113 (2016) 5610-5615.

[142] Z. Wan, et al., The activation of igm- or isotype-switched igg- and ige-bcr exhibits distinct mechanical force sensitivity and threshold, Elife 4 (2015)

[143] J. T. Groves, et al., Micropatterning fluid lipid bilayers on solid supports, Science 275 (1997) 651-653.

[144] T. D. Perez, et al., E-cadherin tethered to micropatterned supported lipid bilayers as a model for cell adhesion, Langmuir 21 (2005) 11963-11968.

[145] K. D. Mossman, et al., Altered tcr signaling from geometrically repatterned immunological synapses, Science 310 (2005) 1191-1193.

[146] K. Salaita, et al., Restriction of receptor movement alters cellular response: Physical force sensing by epha2, Science 327 (2010) 1380-1385.

[147] R. G. Moulick, et al., Reconstitution of fusion proteins in supported lipid bilayers for the study of cell surface receptor-ligand interactions in cell-cell contact, Langmuir 32 (2016) 3462-3469.

[148] T. Lohmuller, et al., Supported membranes embedded with fixed arrays of gold nanoparticles, Nano Lett 11 (2011) 4912-4918.

[149] F. Pi, et al., Size-tunable organic nanodot arrays: A versatile platform for manipulating and imaging cells, Nano Letters 15 (2015) 5178-5184.

[150] K. H. Biswas, et al., Sustained alpha-catenin activation at e-cadherin junctions in the absence of mechanical force, Biophysical Journal 111 (2016) 1044-1052.

[151] J. Andersson and I. Koper, Tethered and polymer supported bilayer lipid membranes: Structure and function, Membranes 6 (2016)

[152] W. Rawicz, et al., Effect of chain length and unsaturation on elasticity of lipid bilayers, Biophysical Journal 79 (2000) 328-339.

[153] D. Marsh, Elastic curvature constants of lipid monolayers and bilayers, Chemistry and Physics of Lipids 144 (2006) 146-159.

[154] M. Seitz, et al., Long-range interaction forces between polymer-supported lipid bilayer membranes, Langmuir 17 (2001) 4616-4626.

[155] M. Rovira-Bru, et al., Size and structure of spontaneously forming liposomes in lipid/peg-lipid mixtures, Biophysical Journal 83 (2002) 2419-2439.

[156] W. C. Hwang and R. E. Waugh, Energy of dissociation of lipid bilayer from the membrane skeleton of red blood cells, Biophysical Journal 72 (1997) 2669-2678.

[157] R. Simson, et al., Membrane bending modulus and adhesion energy of wild-type and mutant cells of dictyostelium lacking talin or cortexillins, Biophysical Journal 74 (1998) 514-522.

[158] I. Bivas, et al., Mechanical properties of lipid bilayers containing grafted lipids, Perspect. Supramol. Chem. 6 (2000) 207-219.

[159] A. P. Siegel, et al., Compartmentalizing a lipid bilayer by tuning lateral stress in a physisorbed polymer-tethered membrane, Soft Matter 6 (2010) 2723-2732.

[160] A. P. Siegel, et al., Metric between buckling structures and elastic properties in physisorbed polymer-tethered lipid monolayers, Soft Matter 8 (2012) 5873-5880.

[161] H. Colognato, et al., Laminin polymerization induces a receptor-cytoskeleton network, Journal of Cell Biology 145 (1999) 619-631.

[162] L. Woiterski, Claudepierre, T., Luxenhofer, R., Jordan, R., Kas, J., Stages of neuronal network formation, New Journal of Physics 17 (2013)

[163] O. Purrucker, et al., Control of frictional coupling of transmembrane cell receptors in model cell membranes with linear polymer spacers, Physical Review Letters 98 (2007)

[164] P. G. Saffman and M. Delbruck, Brownian motion in biological membranes, Proceedings of the National Academy of Sciences of the United States of America 72 (1975) 3111-3113.

[165] O. Purrucker, et al., Supported membranes with well-defined polymer tethers-incorporation of cell receptors, Chemphyschem 5 (2004) 327-335.

[166] M. A. Deverall, et al., Transbilayer coupling of obstructed lipid diffusion in polymer-tethered phospholipid bilayers, Soft Matter 4 (2008) 1899-1908.

[167] R. Bruinsma, et al., Self-assembly of membrane junctions, Biophysical Journal 67 (1994) 746-750.

[168] D. Zuckerman and R. Bruinsma, Statistical mechanics of membrane adhesion by reversible molecular bonds, Physical Review Letters 74 (1995) 3900-3903.

[169] N. Gov, et al., Cytoskeleton confinement and tension of red blood cell membranes, Physical Review Letters 90 (2003) 228101.

[170] N. Gov and S. A. Safran, Pinning of fluid membranes by periodic harmonic potentials, Physical Review. E: Statistical, Nonlinear, and Soft Matter Physics 69 (2004) 011101.

[171] A. Nicolas and S. A. Safran, Elastic deformations of grafted layers with surface stress, Physical Review. E: Statistical, Nonlinear, and Soft Matter Physics 69 (2004) 051902.

[172] L. Zhang and S. Granick, Interleaflet diffusion coupling when polymer adsorbs onto one sole leaflet of a supported phospholipid bilayer, Macromolecules 40 (2007) 1366-1368.

[173] L. Zhang and S. Granick, Slaved diffusion in phospholipid bilayers, Proceedings of the National Academy of Sciences of the United States of America 102 (2005) 9118-9121.

[174] M. A. Deverall, et al., Transbilayer coupling of obstructed lipid diffusion in polymer-tethered phospholipid bilayers, Soft Matter 4 (2008) 1899-1908.

[175] R. R. Bhat, et al., Tailoring cell adhesion using surface-grafted polymer gradient assemblies, Advanced Materials 17 (2005) 2802-+.

[176] B. D. Gates, et al., New approaches to nanofabrication: Molding, printing, and other techniques, Chemical Reviews 105 (2005) 1171-1196.

[177] R. A. Segalman, Patterning with block copolymer thin films, Materials Science & Engineering R-Reports 48 (2005) 191-226.

[178] T. Okazaki, et al., Polymerized lipid bilayers on a solid substrate: Morphologies and obstruction of lateral diffusion, Langmuir 25 (2009) 345-351.

[179] Y. H. Lin, et al., Physisorbed polymer-tethered lipid bilayer with lipopolymer gradient, Materials 5 (2012) 2243-2257.

[180] O. Purrucker, et al., Confinement of transmembrane cell receptors in tunable stripe micropatterns, Journal of the American Chemical Society 127 (2005) 1258-1264.

[181] K. Morigaki, et al., Micropatterned composite membranes of polymerized and fluid lipid bilayers, Langmuir 20 (2004) 7729-7735.

[182] C. K. Yee, et al., Direct photochemical patterning and refunctionalization of supported phospholipid bilayers, Journal of the American Chemical Society 126 (2004) 13962-13972.

[183] S. Waichman, et al., Diffusion and interaction dynamics of individual membrane protein complexes confined in micropatterned polymer-supported membranes, Small 9 (2013) 570-577.

[184] Y. Kaizuka and J. T. Groves, Structure and dynamics of supported intermembrane junctions, Biophysical Journal 86 (2004) 905-912.

[185] S. R. Tabaei, et al., Self-assembly formation of multiple DNA-tethered lipid bilayers, Journal of Structural Biology 168 (2009) 200-206.

[186] M. Chung, et al., DNA-tethered membranes formed by giant vesicle rupture, Journal of Structural Biology 168 (2009) 190-199.

[187] D. H. Murray, et al., Supported double membranes, Journal of Structural Biology 168 (2009) 183-189.

[188] X. Han, et al., A self-assembly route for double bilayer lipid membrane formation, Chemphyschem 11 (2010) 569-574.

[189] D. E. Minner, et al., Iterative layer-by-layer assembly of polymer-tethered multi-bilayers using maleimide-thiol coupling chemistry, Soft Matter 9 (2013) 9643-9650.

[190] G. Decher, Fuzzy nanoassemblies: Toward layered polymeric multicomposites, Science (Washington, D. C.) 277 (1997) 1232-1237.

[191] L. Tayebi, et al., Long-range interlayer alignment of intralayer domains in stacked lipid bilayers, Nat Mater 11 (2012) 1074-1080.

[192] H. E. Warriner, et al., Lamellar biogels: Fluid-membrane-based hydrogels containing polymer lipids, Science 271 (1996) 969-973.

[193] R. Merkel, et al., Molecular friction and epitactic coupling between monolayers in supported bilayers, J. Phys. (Paris) 50 (1989) 1535-1555.

[194] P. Mascalchi, et al., Probing the influence of the particle in single particle tracking measurements of lipid diffusion, Soft Matter 8 (2012) 4462-4470.

[195] A. Engler, et al., Substrate compliance versus ligand density in cell on gel responses, Biophysical Journal 86 (2004) 617-628.

[196] A. Buxboim, et al., How deeply cells feel: Methods for thin gels, J Phys Condens Matter 22 (2010) 194116.

[197] A. K. Denisin and B. L. Pruitt, Tuning the range of polyacrylamide gel stiffness for mechanobiology applications, ACS Applied Materials & Interfaces 8 (2016) 21893-21902.

[198] N. M. Green, Avidin. 1. The use of (14-c)biotin for kinetic studies and for assay, The Biochemical journal 89 (1963) 585-591.

[199] M. Kühner, et al., Lipid mono- and bilayer supported on polymer films: Composite polymer-lipid films on solid substrates, Biophysical Journal 67 (1994) 217-226.

[200] T. Shoaib, et al., Assembly, morphology, diffusivity, and indentation of hydrogel-supported lipid bilayers, Langmuir 33 (2017) 7105-7117.

[201] T. Fujiwara , et al., Phospholipids undergo hop diffusion in compartmentalized cell membrane, Journal of Cell Biology 157 (2002) 1071-1082.

[202] R. Peters and K. Beck, Translational diffusion in phospholipid monolayers measured by fluorescence microphotolysis, Proceedings of the National Academy of Sciences of the United States of America 80 (1983) 7183-7187.

[203] F. Pincet and J. Husson, The solution to the streptavidin-biotin paradox: The influence of history on the strength of single molecular bonds, Biophysical Journal 89 (2005) 4374-4381.

[204] K. Shilts and C. A. Naumann, Tunable cell-surface mimetics as engineered cell substrates, Biochimica Et Biophysica Acta-Biomembranes 1860 (2018) 2076-2093.

[205] S. Katsunuma, et al., Synergistic action of nectins and cadherins generates the mosaic cellular pattern of the olfactory epithelium, The Journal of cell biology 212 (2016) 561-575.

[206] A. J. S. Ribeiro, et al., For whom the cells pull: Hydrogel and micropost devices for measuring traction forces, Methods 94 (2016) 51-64.

[207] J. P. Butler, et al., Traction fields, moments, and strain energy that cells exert on their surroundings, American Journal of Physiology-Cell Physiology 282 (2002) C595-C605.

[208] U. S. Schwarz and J. R. D. Soiné, Traction force microscopy on soft elastic substrates: A guide to recent computational advances, Biochimica et Biophysica Acta (BBA) - Molecular Cell Research 1853 (2015) 3095-3104.

[209] Y. Liu, et al., Molecular tension probes for imaging forces at the cell surface, Accounts of Chemical Research 50 (2017) 2915-2924.

[210] M. L. Wagner and L. K. Tamm, Tethered polymer-supported planar lipid bilayers for reconstitution of integral membrane proteins: Silane-polyethyleneglycol-lipid as a cushion and covalent linker, Biophysical Journal 79 (2000) 1400-1414.

[211] Y. Ge, et al., Two forms of opa1 cooperate to complete mitochondria inner membrane fusion, Biophysical Journal 118 (2020) 553a.

[212] J. A. Killian and T. K. Nyholm, Peptides in lipid bilayers: The power of simple models, Current Opinion in Structural Biology 16 (2006) 473-479.

[213] S. Morein, et al., Characterization of the thermotropic behavior and lateral organization of lipid-peptide mixtures by a combined experimental and theoretical approach: Effects of hydrophobic mismatch and role of flanking residues, Biophysical Journal 82 (2002) 1405-1417.

[214] A. Holt, et al., Tilt and rotation angles of a transmembrane model peptide as studied by fluorescence spectroscopy, Biophysical Journal 97 (2009) 2258-2266.